Investigating how peripheral myelin-specific antibodies contribute to central nervous system demyelination – implications for future therapeutical approaches

Dissertation

for the award of the degree

„Doctor rerum naturalium“

of the Georg-August University Göttingen

within the doctoral program „Molecular Medicine“

of the Georg-August University School of Science (GAUSS)

submitted by

Marie Freier

born in Leipzig

Göttingen, May 2022

Members of the Thesis Committee

1st member – Prof. Dr. Martin Sebastian Weber
Department of Neuropathology
University Medical Center, Georg-August University Göttingen

2nd member – Prof. Dr. Holger Reichardt
Institute for Cellular and Molecular Immunology
University Medical Center, Georg-August University Göttingen

3rd member – Dr. Sebastian Kügler
Department of Neurology
University Medical Center, Georg-August University Göttingen

Further members of the Examination Board

Prof. Dr. Jutta Gärtner
Department of Pediatrics and Adolescent Medicine
University Medical Center, Georg-August University Göttingen

Prof. Dr. Michael Werner Sereda
Translational Neurogenetics
Max Planck Institute for Multidisciplinary Sciences

Prof. Dr. Jürgen Wienands
Institute for Cellular and Molecular Immunology
University Medical Center, Georg-August University Göttingen

Date of oral examination: 20.06.2022

Für all die Menschen, die mich so liebevoll unterstützt haben

TABLE OF CONTENTS

LIST OF FIGURES

LIST OF TABLES

ABBREVIATIONS

Abbreviations, SI units and chemicals which can be found in the dictionary are not listed.

α	Anti
Ab	Antibody
ADCC	Antibody-dependent cellular cytotoxicity
ADEM	Acute demyelinating encephalomyelitis
APC	Antigen-presenting cells
APS	Ammonium persulfate
AQP4	Aquaporin-4
BBB	Blood-brain barrier
BSA	Bovine serum albumin
BTK	Bruton's tyrosine kinase
CBA	Cell-based assay
CD	Cluster of differentiation
CDC	Complement-dependent cytotoxicity
CNS	Central nervous system
CSF	Cerebrospinal fluid
DAB	3,3'-Diaminobenzidine
DC	Dendritic cell
DL650	DyLight 650
DMEM	Dulbecco's Modified Eagle Medium
DMSO	Dimethyl sulfoxide
EAE	Experimental autoimmune encephalomyelitis
EDTA	Ethylenediaminetetraacetic acid
EGFP	Enhanced green fluorescent protein
ELISA	Enzyme-linked immunosorbent assay
EmGFP	Emerald green fluorescent protein
Fab	Antigen-binding fragment
FACS	Fluorescence-activated cell sorting
FBS	Fetal bovine serum
Fc	Crystallizable fragment
FcγR	Fc gamma receptor
FCS	Fetal calf serum
FITC	Fluorescein isothiocyanate
GM-CSF	Granulocyte macrophage colony-stimulating factor
H_2O_2	Hydrogen peroxide
h8.18C5	humanized 8.18C5
HCl	Hydrochloric acid
HE	Hematoxylin and eosin

HEK293-A	Human embryonic kidney 293-A
IFN	Interferon
Ig	Immunoglobulin
IL	Interleukin
ITAM	Immunoreceptor tyrosine-based activation motif
ITIM	Immunoreceptor tyrosine-based inhibitory motif
IVIg	Intravenous immunoglobulins
LB	Lysogeny broth
LFB	Luxol fast blue
LETM	Longitudinally extensive transverse myelitis
MACS	Magnetic-activated cell sorting
M-CSF	Macrophage colony-stimulating factor
mDC	Myeloid dendritic cell
MFI	Mean fluorescence intensity
MHC	Major histocompatibility complex
MOG	Myelin oligodendrocyte glycoprotein
MOGAD	Myelin oligodendrocyte glycoprotein antibody-associated disease
MRI	Magnetic resonance imaging
MS	Multiple sclerosis
Na_2CO_3	Sodium carbonate
NaCl	Sodium chloride
NaH_2PO_4	Anhydrous monobasic sodium phosphate
$NaHCO_3$	Sodium hydrogen carbonate
NaOH	Sodium hydroxide
NEAA	Non-essential amino acids
$(NH_4)_2SO_4$	Ammonium sulfate
NMO	Neuromyelitis optica
NMOSD	Neuromyelitis optica spectrum disorders
ON	Optic neuritis
OVA	Ovalbumin
PAS	Periodic acid schiff
PBMC	Peripheral blood mononuclear cell
PBS	Phosphate buffered saline
PCR	Polymerase chain reaction
pDC	Plasmacytoid dendritic cell
PFA	Paraformaldehyde
PGE_2	Prostaglandin E_2
PPMS	Primary progressive multiple sclerosis
rpm	Revolutions per minute
RPMI	Roswell Park Memorial Institute
RRMS	Relapsing-remitting multiple sclerosis
RT	Room temperature

SDS	Sodium dodecyl sulfate
SDS-PAGE	Sodium dodecyl sulfate polyacrylamide gel electrophoresis
SEM	Standard error of the mean
SPMS	Secondary progressive multiple sclerosis
TEMED	Tetramethylethylenediamine
TLR	Toll-like receptor
TMB	3,3’,5,5’-Tetramethylbenzidine
TNF	Tumor necrosis factor
Tris	Tris(hydroxymethyl)aminomethane
XLA	X-linked agammaglobulinemia
WT	Wildtype

ABSTRACT

The discovery of peripheral autoantibodies against myelin oligodendrocyte glycoprotein (MOG) allowed the delineation of MOG antibody-associated disease (MOGAD) from other central nervous system (CNS) demyelinating disorders, such as multiple sclerosis. Although the mechanisms and site of disease initiation are unknown in MOGAD, rising evidence indicates that peripheral MOG-specific antibodies may harbor pathogenic functions. In this regard, anti-MOG antibody-mediated opsonization of endogenous MOG was previously suggested to trigger inflammatory CNS demyelination in mice. However, it remains elusive if this can also occur in MOGAD patients. Hence, the first project of the present study focused on investigating the opsonizing capacity of MOG-reactive antibodies isolated from MOGAD patients. Using an *in vitro* setting with human myeloid antigen-presenting cells, the study on hand demonstrated that patient-derived anti-MOG antibodies opsonized soluble and membrane-bound MOG, thus facilitating antigen recognition and uptake by *in vitro* differentiated antigen-presenting cells presumable via Fcγ receptor (FcγR) III. These findings support the hypothesis that anti-MOG antibody-mediated opsonization represents a disease-triggering mechanism in MOGAD patients.

Based on this, targeting peripheral anti-MOG antibodies and their effector mechanisms may be an efficient strategy for the treatment of MOGAD. Since Bruton's tyrosine kinase (BTK) is crucially involved in FcγR signaling in myeloid cells, its inhibition may prevent activation of myeloid cells induced by anti-MOG antibody-mediated opsonization. Thus, the second project of the study addressed the therapeutic potential of BTK inhibitor evobrutinib in anti-MOG antibody-triggered CNS demyelination. In a set of *in vivo* experiments, it was first observed that evobrutinib did not affect the phenotype of myeloid cells in the absence of inflammation. In anti-MOG antibody-induced CNS inflammation however, evobrutinib was found to prevent the clinical manifestation of experimental autoimmune encephalomyelitis (EAE) by significantly reducing inflammatory CNS demyelination in the spinal cord. Analysis of immune cells in secondary lymphoid organs showed that BTK inhibition diminished the expression of FcγRs on monocytes and macrophages, but did not alter the phenotype of T cells in the chronic phase of EAE. Taken together, these results indicate that BTK inhibition by evobrutinib can be a promising strategy to counteract anti-MOG antibody-mediated CNS demyelination. However, the underlying immunological mechanisms need to be further investigated.

1 INTRODUCTION

1.1 Inflammatory demyelinating disorders of the central nervous system

Demyelination in the central nervous system (CNS) occurs when the myelin sheath of neurons is damaged, resulting in neurological dysfunctions such as vision impairment or weakness. It can be caused by different environmental factors, including viruses and toxins, but also by inflammatory autoimmune reactions. The heterogenous group of inflammatory CNS demyelinating diseases comprises a variety of disorders, including multiple sclerosis (MS), neuromyelitis optica spectrum disorders (NMOSD) and myelin oligodendrocyte glycoprotein antibody-associated disease (MOGAD). Although these disorders share clinical and pathological similarities, intensive investigations of their pathomechanisms have resulted in their delineation as distinct disease entities.

1.1.1 Multiple sclerosis

1.1.1.1 Clinical features

With around 2.8 million affected people worldwide, MS is the most common chronic inflammatory demyelinating disease of the CNS. First clinical symptoms typically develop between the age of 20 to 40 years with females twice as likely to be affected than males (Walton et al. 2020). Depending on the affected CNS region, patients can present a broad range of symptoms including partial or complete vision loss, ataxia and limb weakness. With disease progression, most patients experience bladder dysfunction, fatigue, muscle spasms as well as cognitive deficits (Hauser and Oksenberg 2006). Based on the clinical course, MS can be divided into 3 main subtypes. The most common form is relapsing-remitting MS (RRMS), which affects approximately 85 % of MS patients. This subtype is characterized by recurrent acute periods of neurologic dysfunction (relapses), followed by episodes of partial or full recovery. Over time, around 65 % of these patients transition to a progressive disease with incomplete recovery after relapses and disability accumulation, termed secondary progressive MS (SPMS). 15 % of MS patients are diagnosed with primary progressive MS (PPMS) and experience gradual worsening from disease onset without remission (Hauser and Oksenberg 2006; Lublin et al. 2014).

1.1.1.2 Pathology and immunopathogenesis

A pathological hallmark for the diagnosis of MS are multifocal lesions in the white and grey matter of the CNS, which can be observed by magnetic resonance imaging (MRI). MS lesions can be formed anywhere in the CNS but they are mainly detected in the brain stem, spinal cord, optic nerve and periventricular areas (Gilmore et al. 2009; Green et al. 2010). They are characterized by rounded, demyelinated areas with variable axonal loss and reactive gliosis (Stadelmann et al. 2011). Although the immunopathology of lesions varies among MS patients, they mainly consist of $CD8^+$ T lymphocytes and activated microglia and macrophages, with smaller infiltrations of $CD4^+$ T cells, B lymphocytes and plasma cells. Furthermore, they can contain antibody and complement deposits as well as myelin-loaded macrophages (Kuhlmann et al. 2017; Lassmann 2018; Lucchinetti et al. 2000).

To date, the cause of MS has not been identified but the disease pathogenesis is increasingly elucidated. It is currently assumed that autoreactive T cells trigger an inflammatory response that results in CNS demyelination. In detail, myelin-specific T lymphocytes are believed to become activated in the periphery by antigen-presenting cells (APCs) and to upregulate adhesion molecules, allowing them to migrate across the blood-brain barrier (BBB). After entering the CNS, these T cells can be reactivated by local APCs, provoking the release of pro-inflammatory cytokines such as interferon (IFN)-γ and tumor necrosis factor (TNF)-α. The secreted cytokines, in turn, induce the activation of CNS-resident microglia and the recruitment of peripheral immune cells, resulting in additional waves of inflammation (Hauser and Oksenberg 2006; Hemmer et al. 2002; Sospedra and Martin 2005).

Besides T cells, B lymphocytes and their products are believed to be crucial determinants in the immunopathogenesis of MS. This hypothesis is particularly supported by the remarkable efficiency of B cell-depleting therapies with monoclonal anti-CD20 antibodies, e.g. Rituximab, in MS patients (Hauser et al. 2008). Another indicator for the crucial involvement of B cells is the presence of oligoclonal immunoglobulins (Ig), termed oligoclonal bands, in the cerebrospinal fluid (CSF) of many MS patients, which originate from locally supported plasma cells (Obermeier et al. 2008; von Budingen et al. 2010). Furthermore, antibody deposits are found on myelin structures in the area of ongoing CNS demyelination, which underlines the potential involvement of autoantibodies in the destruction of myelin in MS lesions (Genain et al. 1999).

1.1.1.3 Treatment strategies

1.1.1.3.1 Approved therapies

MS medications are applied to treat acute attacks, ameliorate symptoms and slow disease progression through disease-modifying therapies. These therapies suppress or modulate different immune mechanisms in MS patients, resulting in a reduced relapse rate and accumulation of MRI lesions. In recent years, a variety of disease-modifying therapies has been developed, which can be grouped into 4 categories based on their mode of action (Hauser and Cree 2020; Weber et al. 2012):

(1) Modulation of immune cell functions – e.g. interferons and dimethyl fumarate
(2) Inhibition of immune cell trafficking – e.g. natalizumab and fingolimod
(3) Reduction of cell proliferation – e.g. mitoxantrone and teriflunomide
(4) Depletion of immune cell subsets – e.g. rituximab and ocrelizumab

Since MS has been considered to be a T cell-driven disease for many years, the first approved therapies focused on these lymphocytes. However, it is now understood that B cells also play a pivotal role in the pathogenesis of MS, which led to the development of new disease-modifying therapies targeting B lymphocytes, including the monoclonal anti-CD20 antibody ocrelizumab (Hauser et al. 2017).

1.1.1.3.2 Inhibition of Bruton's tyrosine kinase

A new therapeutic strategy to control pathogenic B cells in MS patients is the inhibition of Bruton's tyrosine kinase (BTK). Belonging to the family of TEC kinases, BTK is a cytoplasmic non-receptor tyrosine kinase, which is expressed in cells of hematopoietic origin including B lymphocytes and myeloid cells, but not plasma cells (Hendriks et al. 2014). It is known for its essential role in B cell receptor signaling, a critical step for B cell activation, maturation and proliferation. The absence of BTK, e.g. in X-linked agammaglobulinemia (XLA) patients, causes a strong deficit of peripheral B and plasma cells, resulting in very low levels of circulating Igs (Conley et al. 2000). Furthermore, BTK is required for the signaling pathways of Fc, cytokine, chemokine and toll-like receptors in myeloid cells and B lymphocytes (Hendriks et al. 2014; Lopez-Herrera et al. 2014). Upon activation of the respective signaling cascade, BTK is phosphorylated by Lyn or Syk kinases, followed by BTK autophosphorylation. Subsequently, active BTK can phosphorylate phospholipase Cγ2, which triggers calcium influx and activation of several transcription factors, such as nuclear factor (NF)-κB (Neys et al. 2021).

Due to the involvement of BTK in different signaling pathways of many cell types, inhibition of BTK represents a promising mechanism to target inflammatory processes in MS patients. Currently, several BTK inhibitors are in the clinical development for MS, including evobrutinib. Evobrutinib is an irreversible inhibitor of BTK with high kinase selectivity, which forms a covalent bond with the amino acid residue Cys481 in the ATP binding site of BTK (Carnero Contentti and Correale 2020). Besides its capacity to significantly reduce disease severity in animal models of rheumatoid arthritis and systemic lupus erythematosus, evobrutinib has also shown a high therapeutic efficiency in the MS animal model experimental autoimmune encephalomyelitis (EAE) (Caldwell et al. 2019; Park et al. 2016; Torke et al. 2020). In detail, the administration of evobrutinib inhibited the activation and maturation of B cells as well as the release of pro-inflammatory cytokines, resulting in a reduced clinical and histological severity (Torke et al. 2020). In humans, evobrutinib has been recently tested as a monotherapy for RRMS in a phase II trial. Patients receiving evobrutinib showed a significantly reduced number of gadolinium-enhancing lesions compared to the placebo group, but no significant differences in the disability progression (Montalban et al. 2019).

1.1.2 Neuromyelitis optica spectrum disorders

1.1.2.1 Clinical course and diagnosis

NMOSD, previously known as neuromyelitis optica (NMO), was first described by Eugene Devic and his student Fernand Gault in 1894 (Jarius and Wildemann 2013). It is a group of chronic demyelinating diseases characterized by inflammation processes in the spinal cord and optic nerves. Between 0.5 and 4 people per 100 000 inhabitants are diagnosed with NMOSD and females are 9 times more affected than men (Etemadifar et al. 2015; Gold SM et al. 2019). Compared to MS, NMOSD patients show more frequent and severe relapses and recovery is often incomplete, resulting in a quick deterioration. Although some patients have brain or brainstem involvement, most of them exhibit optic neuritis (ON, unilateral or bilateral) or longitudinally extensive transverse myelitis (LETM). Depending on the site of inflammation, NMOSD patients can experience various symptoms. When the spinal cord is involved, limb weakness, bladder dysfunction and sensorimotor problems occur in most patients. Whereas when the optic nerve is affected, patients experience blurry vision or visual loss (Carnero Contentti and Correale 2021; Morrow and Wingerchuk 2012).

Since NMOSD shares some clinical and radiological features with MS, it was erroneously considered as a variant of MS for many years. But with the discovery of IgG antibodies against the water channel aquaporin-4 (AQP4) in the serum of NMOSD patients, a crucial diagnostic tool was defined and NMOSD was differentiated from MS (Lennon et al. 2004). Based on the diagnostic criteria defined by Wingerchuk and colleagues in 2007 and 2015 (Wingerchuk et al. 2007; Wingerchuk et al. 2015), NMOSD patients can be divided into AQP4 antibody-positive or AQP4 antibody-negative, with the former making up between 60 and 70 % of NMOSD cases (Sato et al. 2014). Diagnosis of NMOSD further requires the occurrence of at least one of the following clinical criteria: ON, LETM, area postrema syndrome, acute brainstem syndrome or NMOSD-typical brain lesions with diencephalic clinical syndrome (Wingerchuk et al. 2015). However, if the patients AQP4-IgG serology is unknown or negative, at least two of the aforementioned characteristics are needed for the diagnosis of NMOSD.

1.1.2.2 Pathology and immunopathogenesis

The pathology of NMOSD lesions is characterized by the binding of pathogenic autoantibodies to AQP4 expressed on the endfeet of astrocytes (Lennon et al. 2005; Lennon et al. 2004). The highest concentrations of AQP4 are found on astrocytes surrounding endothelial cells as well as in ependymal cell membranes (Hinson et al. 2012). Binding of anti-AQP4 antibodies to AQP4 triggers the activation of the classical complement cascade, resulting in granulocyte, macrophage and lymphocyte infiltration and subsequent astrocyte damage. As a consequence, astrocytes can no longer support the surrounding CNS cells, which causes oligodendrocyte and neuronal loss. However, the exact mechanism of oligodendrocyte and neuron destruction remains unclear (Carnero Contentti and Correale 2021; Hinson et al. 2012). This observation led to the conclusion that NMOSD is an astrocytopathy and demyelination only occurs as a result of a primary astrocyte destruction. The preferential occurrence of NMOSD lesions in the spinal cord and optic nerves may be due to the higher expression of AQP4 in these regions compared to the brain (Matiello et al. 2013).

Although the process of disease initiation is still unknown, growing evidence points towards a peripherally initiated immune response in NMOSD. The first indication for this hypothesis is the rare presence of intrathecally produced anti-AQP4 antibodies in the CSF, suggesting that these antibodies are mainly generated in the periphery (Bennett et al. 2009). In this regard, AQP4 antibody-plasmablasts are found to be selectively elevated in the blood of NMOSD patients, and maintenance of these plasmablasts is facilitated by increased levels of

interleukin 6 (IL-6) (Chihara et al. 2011). In addition, Hillebrand and colleagues demonstrated in rats that systemically injected anti-AQP4 antibodies can enter the CNS via circumventricular organs and meningeal or parenchymal blood vessels, initiating the formation of NMOSD-like lesions with AQP4 loss. This effect was further enhanced in the presence of encephalitogenic T-cells (Hillebrand et al. 2019). Although the processes of CNS infiltration by AQP4-reactive antibodies have not been completely deciphered yet, the mechanisms of anti-AQP4 antibody pathogenesis in the CNS have been extensively studied through functional assays in animals and human tissues. It was revealed that serum-derived IgG from NMOSD patients binds to astrocytes and increases the permeability of a human *in vitro* BBB model (Vincent et al. 2008). Furthermore, the binding of AQP4-specific antibodies to astrocytes can cause astrocytopathy, secondary oligodendrocytopathy and demyelination through complement-dependent cytotoxicity (CDC) and antibody-dependent cellular cytotoxicity (ADCC) (Alexopoulos et al. 2015; Phuan et al. 2012; Vincent et al. 2008).

While the role of antibodies in NMOSD is well-characterized, the functions of T cells are widely unknown. In contrast to the predominance of $CD8^+$ T lymphocytes in MS patients, activated $CD4^+$ T cells are primarily found in NMOSD patients. However, NMOSD lesions are characterized by a low number of infiltrated T lymphocytes, suggesting that they are not directly involved in lesion formation. Instead, T cells may act in the peripheral immune response by disrupting tolerance or contributing to anti-AQP4 antibody production (Papadopoulos and Verkman 2012).

1.1.2.3 Therapy options

Currently, NMOSD treatment is subdivided into treatment of acute inflammatory attacks and long-term relapse prevention. First-line treatment during acute relapses includes intravenous application of high-dose methylprednisolone, followed by tapered oral steroids (Songthammawat et al. 2020). If the patient's response is insufficient, plasma exchange can be performed to remove pathogenic antibodies (Bonnan et al. 2009; Roesner et al. 2012).

To prevent further relapses and minimalize disability, long-term immunosuppressive therapies including azathioprine and rituximab are used. Over the last years however, monoclonal antibodies against the complement protein C5 (eculizumab), the IL-6 receptor (satralizumab) or CD19 (inebilizumab) have expanded the list of drugs for the treatment of NMOSD (Carnero Contentti and Correale 2021).

1.1.3 Myelin oligodendrocyte glycoprotein antibody-associated disease

1.1.3.1 Myelin oligodendrocyte glycoprotein

Myelin oligodendrocyte glycoprotein (MOG) is a transmembrane protein, which is expressed in the CNS on oligodendrocyte membranes and the outer lamella of the myelin sheath. The precise function of MOG remains elusive but it is thought to be involved in maintenance of the myelin sheath and in cell-cell communication (Johns and Bernard 1999; Peschl et al. 2017a). Belonging to the immunoglobulin superfamily, MOG consists of an extracellular immunoglobulin variable domain, a hydrophobic transmembrane domain, a short cytoplasmic loop, a second hydrophobic transmembrane region and a cytoplasmic end (Kroepfl et al. 1996). Although MOG only accounts for a quantitatively minor component (~0.05 %) within myelin, the distinct structure and its outer location on myelin sheaths make MOG a potential target for pathogenic autoantibodies and T lymphocytes (Johns and Bernard 1999).

1.1.3.2 Clinical characteristics and diagnosis

MOGAD is a recently defined demyelinating disease of the CNS, which is characterized by the occurrence of antibodies against MOG in the serum of patients. Approximately 1 – 6 % of adult patients with CNS demyelinating disorders are diagnosed with MOGAD, whereas children exhibit an anti-MOG antibody seropositivity frequency of about 40 % during a first inflammatory demyelinating syndrome (Marignier et al. 2021). Females are 2 – 3 times more affected than males and first clinical symptoms appear between the age of 30 and 40 years (Weber et al. 2018). The clinical spectrum of MOGAD includes various phenotypes such as LETM, ON, cortical encephalitis and acute demyelinating encephalomyelitis (ADEM), and disease courses can be monophasic or relapsing (Jarius et al. 2018). In adults, LETM and ON are the most frequent phenotypes and patients show rather a relapsing disease course. Depending on the site of inflammation, patients with LETM or ON experience similar symptoms as NMOSD patients, including dysesthesia, bladder dysfunction, limb paresis (LETM) or vision loss (ON). Children mostly suffer from ADEM, which is usually a one-time incident. In ADEM, most patients have headache, nausea, malaise and vomiting, but ataxia, hemiparesis and vision impairment can also occur (Ambrosius et al. 2020).

Since MOGAD has been just recently defined, determination of consensus diagnostic criteria is still ongoing. The above mentioned clinical features of MOGAD can be also observed in MS or NMOSD patients, which makes it difficult to diagnose MOGAD on the basis of clinical or neuroimaging findings. Therefore, the detection of anti-MOG antibodies in the blood of

patients is essential for a proper diagnosis. In the beginning, MOG-specific antibodies were detected by peptide-based enzyme-linked immunosorbent assay (ELISA) or Western blotting. However, these methods only have a low specificity, resulting in misdiagnoses of MS patients being anti-MOG antibody seropositive (Berger et al. 2003). Today, the gold standard method for detecting MOG-reactive autoantibodies in patient's blood is the live cell-based assay (CBA), which involves full-length human MOG expressed on the cell surface of eukaryotic cell lines (Ambrosius et al. 2020). It is recommended to test patients during or right after acute attacks as antibody titers fluctuate and can decrease over time (Waters et al. 2020).

1.1.3.3 Pathology and immunopathogenesis

Pathological studies of lesions in MOGAD patients are still rare. Based on a study of two autopsies and 22 brain biopsies of confirmed MOGAD cases, Höftberger and colleagues demonstrated that lesions are characterized by perivenous and confluent white matter demyelination. They further contain complement deposition and immune cell infiltrates consisting mainly of $CD4^+$ T cells and granulocytes. In contrast to lesions of NMOSD patients, AQP4 on astrocytes is preserved, revealing that MOGAD is not an astrocytopathy (Hoftberger et al. 2020).

Although several findings indicate that MOG-specific antibodies may have a pathogenic role in MOGAD patients, the precise function of anti-MOG antibodies and the site of disease initiation remain unknown. In rodents, intrathecally applied, patient-derived anti-MOG antibodies were able to induce clinical disease by enhancing CNS infiltration of intravenously injected MOG-specific T cells (Spadaro et al. 2018). In this context, Flach et al. further revealed that peripherally administered anti-MOG antibodies can enter the CNS and facilitate recognition of MOG to resident antigen-presenting phagocytes, resulting in an accelerated tissue destruction by T lymphocytes (Flach et al. 2016). Kinzel and colleagues propose a model in which the peripheral immune response against MOG plays an important, disease-driving role. They observed that in mice containing MOG-reactive T cells, the peripheral injection of anti-MOG antibodies triggered the proliferation and pro-inflammatory differentiation of peripheral T cells, which subsequently entered the CNS and caused EAE (Kinzel et al. 2016).

1.1.3.4 Treatment options

Since MOGAD is a relatively newly defined disease with low prevalence, no large treatment trials have been conducted yet. Therefore, MOGAD patients are treated similarly to NMOSD

patients. The drug of choice for the treatment of an acute attack is high-dose intravenous methylprednisolone. A second-line treatment strategy is warranted for patients with severe attacks or who do not improve sufficiently after methylprednisolone and consists of plasma exchange (five exchanges on alternative days), immunoadsorption or intravenous immunoglobulins (IVIg) (Marignier et al. 2021).

To prevent further relapses and thus hinder disability progression of MOGAD patients, immunomodulating and immunosuppressive therapies are applied. These include azathioprine, rituximab, oral corticosteroids, methotrexate, mycophenolate mofetil and repeated cycles of IVIg (Ambrosius et al. 2020). A retrospective multicenter study on 70 MOGAD patients revealed that IVIg-treated patients exhibit the lowest relapse rate (20 %), followed by azathioprine (59 %), rituximab (61 %) and mycophenolate mofetil (74 %) (Chen et al. 2020). However, since 70 % of pediatric patients with MOGAD have a monophasic disease course (Waters et al. 2020), it is recommended to start long-time treatment in children only after a second event.

1.1.4 Experimental autoimmune encephalomyelitis

Many mechanisms in the immunopathogenesis of CNS demyelination disorders were deciphered in the animal model EAE, which reproduces specific immunological and neuropathological features of these diseases. In rodents, EAE can be induced by different methods but the most common one is the active immunization with myelin-derived proteins or peptides emulsified in complete Freund's adjuvant and co-administration of pertussis toxin. This triggers the activation of myelin-specific $CD4^+$ T cells in the periphery, which subsequently enter the CNS and initiate a cascade of inflammatory processes, resulting in demyelination and axonal damage (Fletcher et al. 2010; Gold R et al. 2006). This leads to the manifestation of an ascending paralysis starting at the tail, followed by the hind and fore limbs.

Although EAE is considered to be primarily mediated by T cells, B lymphocytes and their products become increasingly important. In this context, Kinzel and colleagues recently established an anti-MOG antibody-driven EAE model. The repetitive peripheral injection of the anti-MOG antibody clone 8.18C5 into MOG-specific T cell receptor transgenic mice (2D2 mice) was sufficient to induce clinical EAE in approximately 20 % of 2D2 mice. Furthermore, around 55 % of mice receiving 8.18C5 antibody developed histological EAE. It was revealed that anti-MOG antibodies triggered the activation and pro-inflammatory

differentiation of peripheral MOG-reactive T cells, which subsequently entered the CNS and caused EAE (Kinzel et al. 2016). This newly established EAE model represents a useful tool to study the pathomechanisms as well as potential therapeutic targets in anti-MOG antibody-induced CNS demyelination.

1.2 Myeloid antigen-presenting cells

Dendritic cells (DCs) and macrophages are known as professional APCs, which link the innate and adaptive immune system by recognizing and internalizing foreign antigens and subsequently presenting the processed antigens to $CD4^+$ T cells in the context of major histocompatibility complex (MHC) class II molecules (Murphy 2012). For this purpose, they constitutively express MHCII and upregulate co-stimulatory molecules, such as CD40 and CD86, upon activation (Kambayashi and Laufer 2014).

1.2.1 Dendritic cells

DCs originate from hematopoietic bone marrow precursor cells and are found in blood, lymphoid tissues and epithelia. In the steady state, immature DCs reside in peripheral tissues and continuously capture antigens. Upon activation by antigen encounter and/or inflammatory cytokines, DCs become mature, upregulate co-stimulatory molecules and migrate to lymphoid organs. Subsequently, mature DCs present the processed antigen to $CD4^+$ T cells, which in turn regulate other immune effectors, such a B lymphocytes and macrophages (Banchereau et al. 2000; Steinman 1991).

DCs can be divided into two major subsets, termed plasmacytoid DCs (pDCs) and myeloid DCs (mDCs) (Geissmann et al. 2010). In humans, pDCs are characterized by the expression of CD303 and CD304 and can produce large amounts of type I interferons in response to viral infections (Collin et al. 2013; Colonna et al. 2004). MDCs express typical myeloid marker, including CD11c and CD13, and can be further split into $CD1c^+$ and $CD141^+$ subsets. A third fraction of $CD11c^+$ mDCs exhibits monocyte-related features and expresses CD14 on the cell surface (Collin et al. 2013).

1.2.2 Macrophages

Macrophages originate from circulating monocytes and differentiate upon entry into lymphoid and non-lymphoid tissues. Although they have the ability to present antigens to T cells, macrophages are primarily specialized in pathogen clearance and inflammation

regulation (Geissmann et al. 2010). They display a variety of pathogen recognition receptors and can be activated by a broad range of pathogens. Based on the activation state and function, macrophages are often divided into M1- and M2-type macrophages. M1 macrophages, also termed classically activated macrophages, can be polarized by interferon (IFN)-γ and combat pathogens by secreting pro-inflammatory cytokines, such as IL-12 and IL-1β. By contrast, IL-4 induces alternatively activated macrophages (M2), which produce anti-inflammatory cytokines, including IL-10, and participate in tissue repair (Ambarus et al. 2012). However, due to the rising number of functions and external stimuli of macrophages, the M1/M2 model is still under debate.

1.2.3 Fcγ receptors on myeloid antigen-presenting cells

DCs and macrophages express various Fcγ receptors (FcγRs) which mediate their interaction with monomeric and aggregated IgG. FcγRs can be divided into type I and II, with each type displaying distinct structures and functions. However, only FcγR type I will be further described. In humans, type I FcγRs comprise FcγR I, FcγR IIa, FcγR IIb, FcγR IIc, FcγR IIIa and Fcγ RIIIb, whereas mice express FcγR I, FcγR IIb, FcγR III and FcγR IV (Bournazos and Ravetch 2017; Bruhns 2012). According to their function, these receptors can be subdivided into activating (FcγR I, FcγR IIa, FcγR IIc, FcγR IIIa, FcγR IIIb, FcγR IV) and inhibitory (FcγR IIb) receptors. Activating FcγRs transmit signals via an intracellular immunoreceptor tyrosine-based activation motif (ITAM), whereas the inhibitory receptor exhibits an immunoreceptor tyrosine-based inhibitory motif (ITIM). Binding of IgG immune complexes to activating FcγRs triggers the recruitment and interaction of several kinases, including Syk, Src and BTK, which subsequently leads to a variety of pro-inflammatory responses, including calcium influx, cytokine release and up-regulation of pro-inflammatory genes. This signaling pathway is tightly regulated by the inhibitory FcγR IIb. ITIMs induce the recruitment of SHIP family phosphatases, which inhibit the recruitment and activation of Src, resulting in blockage of the activating pathway (Bournazos and Ravetch 2017; Joller et al. 2011).

Several groups have investigated the expression of FcγRs on myeloid APCs, revealing that the expression levels vary between DCs and macrophages, but also between different DC subsets. In human peripheral blood, $CD1c^+$ and $CD141^+$ mDCs express the activating FcγR I and FcγR IIa as well as the inhibitory FcγR IIb, but not FcγR III. PDCs, however, exhibit minimal or no

expression of FcγRs on their surface (Boruchov et al. 2005; Fanger et al. 1996). By contrast, monocyte-related mDCs and macrophages express all FcγRs (Guilliams et al. 2014).
In mice, splenic mDCs as well as macrophages were found to express FcγR I, FcγR IIb, FcγR III and FcγR IV, whereas pDCs exclusively express the inhibitory FcγR IIb (Flores et al. 2009; Junker et al. 2020; Lehmann et al. 2017).

1.2.4 Bruton's tyrosine kinase in myeloid cells

Although BTK was initially thought to be only essential for B cell development, rising evidence indicates that BTK also plays a pivotal role in myeloid cells. In this regard, it has been revealed that BTK is required in the signaling of Fc, cytokine, chemokine and toll-like receptors (Hendriks et al. 2014; Lopez-Herrera et al. 2014). Pharmacological modulation of BTK was shown to inhibit FcγR signaling in monocytes by impeding the activation of NF-κB (Haselmayer et al. 2019). This can result in suppressed production of TNF-α, IL-1β or IL-6 (Bame et al. 2021; Chang et al. 2011; Ren et al. 2016). Moreover, inhibition of BTK expression can reduce FcγR-mediated phagocytosis in macrophages (Jongstra-Bilen et al. 2008). It was further demonstrated that BTK is activated downstream of the granulocyte macrophage colony-stimulating factor (GM-CSF) receptor in macrophages and thus regulates their inflammatory differentiation (Alankus et al. 2018). BTK is also crucially involved in toll-like receptor (TLR) signaling. Monocytes from XLA patients, which have mutations in the BTK gene (Lopez-Herrera et al. 2014), were found to be impaired in the production of pro-inflammatory cytokines, such as IL-1β and TNF-α, upon stimulation of TLR4 or TLR2 (Horwood et al. 2003; Horwood et al. 2006). In BTK-deficient mice however, bone marrow-derived macrophages produced enhanced levels of the pro-inflammatory cytokine IL-6 and decreased levels of the anti-inflammatory cytokine IL-10 in comparison to wildtype (WT) cells upon activation of different TLRs (Schmidt et al. 2006). Thus, BTK may differently regulate TLR signaling in human and murine myeloid cells.

1.3 The role of antibodies in CNS demyelinating disorders

The discovery of peripheral antibodies against AQP4 and MOG, respectively, represents a key element for the delineation of NMOSD and MOGAD as distinct disease entities. Although initially introduced as diagnostic markers, rising evidence points towards a pathogenic role of anti-AQP4 and anti-MOG antibodies in these disorders.

1.3.1 Antibody structure and function

Antibodies are pivotal determinants in the armamentarium of immune defense. First identified by von Behring and Kitasato in 1890, antibodies are secreted by plasma cells and can be found in blood and tissue fluids. They are large Y-shaped proteins and consist of two identical heavy and two light polypeptide chains (Fig. 1). The upper part, called Fab region (Fab = antigen-binding fragment), consists of one constant and one variable domain from each heavy and light chain and harbors the antigen-binding site. The variable domain can be composed of an extremely large variety of different amino acid sequences, thus enabling antibodies to recognize millions of different antigens. The lower part of an antibody, termed Fc region (Fc = crystallizable fragment), comprises two constant domains of the heavy chains. It specifies the effector function as well as the isotype of an antibody. Five different antibody isotypes can be classified: IgA, IgD, IgE, IgG and IgM. IgG antibodies can be further subdivided into four subclasses – humans possess IgG1, IgG2, IgG3 and IgG4, whereas in mice they are termed IgG1, IgG2a, IgG2b and IgG3 (Kapingidza et al. 2020; Schroeder and Cavacini 2010).

Antibodies can fulfill a number of functions to protect the host but there are three major mechanisms to be mentioned. First, coating of a pathogen by antibodies can lead to its neutralization. This function is essential for a potent immune response against viruses as well as for the vaccine-mediated resistance against tetanus and pertussis toxin. Furthermore, antibodies can bind to pathogens and subsequently activate the classical complement cascade, resulting in the lysis of the pathogens. Finally, antibodies can bind pathogenic antigens and facilitate their recognition and uptake by phagocytic cells, a process termed opsonization (Forthal 2014; Joller et al. 2011).

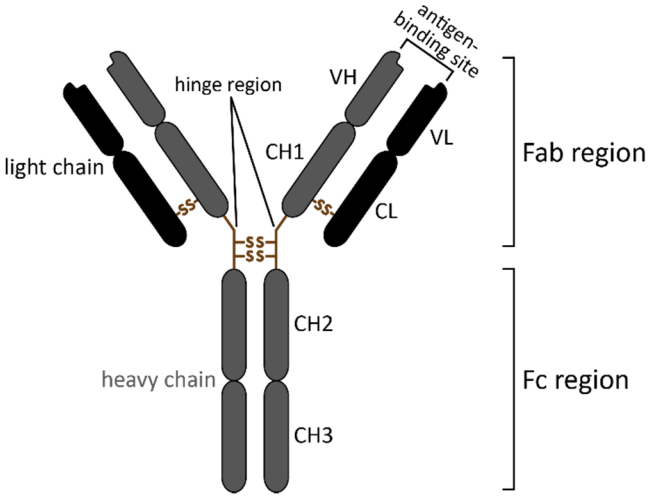

Figure 1: Antibody structure of IgG. Heavy chains are depicted in grey, light chains in black. Fab = antigen-binding fragment, Fc = crystallizable fragment, CH = constant domain of the heavy chain, CL = constant domain of the light chain, VH = variable domain of the heavy chain, VL = variable domain of the light chain

1.3.2 Autoantibodies in CNS demyelinating disorders

As antibodies represent a pivotal weapon in the body's immune response, it is not surprising that autoantibodies, i.e. antibodies directed against structures of the own body, can cause great damage, resulting in severe diseases. Every part of the body can be affected, also the CNS. In NMOSD patients, autoantibodies against the water channel AQP4 specifically target AQP4 expressed on astrocytes, causing their destruction and subsequent demyelination (Hinson et al. 2012; Lennon et al. 2005; Lennon et al. 2004). The pathomechanisms of AQP4-reactive antibodies have been intensively studied, revealing that they induce CDC, ADCC, microglial activation and AQP4 degradation (Hinson et al. 2007; Phuan et al. 2012; Vincent et al. 2008). In addition, clinical observations show that anti-AQP4 antibody seropositivity correlates with disease activity and the presence of AQP4-specific antibodies may predict further relapses in NMOSD patients (Carnero Contentti and Correale 2021).

In contrast, the pathogenesis and the site of action of MOG-reactive antibodies in MOGAD patients are still unknown. Several studies suggest that these antibodies may directly bind to MOG within the CNS and cause inflammatory demyelination by enhancing T cell infiltration (Flach et al. 2016; Peschl et al. 2017b; Spadaro et al. 2018). The work of Kinzel and colleagues, which is the basis for the present study, indicates that peripheral anti-MOG antibodies are capable of triggering CNS demyelination without entering the CNS. They demonstrated in a transgenic mouse model that the peripheral administration of anti-MOG antibodies initiated the activation and proliferation of peripheral MOG-specific T cells, which subsequently

infiltrated the CNS and caused EAE. The underlying mechanism was evaluated in a set of *in vitro* experiments, showing that anti-MOG antibodies opsonized MOG und thus promoted its uptake by myeloid APCs. This process was strictly FcγR-dependent, as the use of APCs from FcγR knockout mice abolished the enhancing effect. The internalized MOG was further processed and presented to naïve T lymphocytes, which differentiated in an encephalitogenic manner (Kinzel et al. 2016). In conjunction, these findings suggest that anti-MOG antibody-mediated opsonization of endogenous MOG may act as a disease-driving mechanism in CNS demyelination disorders.

1.4 Aims of the study

1.4.1 Aim 1: Investigation of the opsonizing capacity of patient-derived anti-MOG antibodies

While it has been proposed that anti-MOG antibody-mediated opsonization of endogenous CNS antigen can trigger inflammatory CNS demyelination in mice (Kinzel et al. 2016), it remains elusive if this may likewise occur in MOGAD patients. The first project therefore aimed to assess the capacity of patient-derived anti-MOG antibodies to opsonize human MOG. Using *in vitro* differentiated human myeloid APCs, it was investigated how IgG and serum samples from MOGAD patients affect the internalization of MOG by human phagocytes. Furthermore, the effect of anti-MOG antibody-mediated opsonization on the expression of FcγRs and markers involved in antigen presentation on human APCs was evaluated. In a last set of experiments, the opsonizing activity of patient-derived anti-AQP4 antibodies was analyzed.

1.4.2 Aim 2: Inhibition of Bruton's tyrosine kinase as a therapeutic strategy for anti-MOG antibody-mediated CNS demyelination

Since BTK is crucially involved in FcγR signaling in myeloid cells (Koprulu and Ellmeier 2009; Lopez-Herrera et al. 2014), its inhibition may prevent activation of myeloid cells triggered by MOG-specific antibodies and thus counteract anti-MOG antibody-induced CNS demyelination. Hence, in the second part of the study, the effect of BTK inhibitor evobrutinib on myeloid cells activated by anti-MOG antibody-mediated opsonization was investigated *in vitro* and *in vivo*. *In vivo*, it was first analyzed how BTK inhibition affects the phenotype of immune cells in the absence of inflammation. In a second experimental setup, the impact of evobrutinib on clinical and histological severity as well as on immunological features in anti-MOG antibody-driven EAE was examined.

2 MATERIALS AND METHODS

2.1 Materials

2.1.1 Reagents and kits

Table 1: Reagents

Reagent	Manufacturer
Acetic acid	Merck, Millipore, Germany
Acrylamide, 30 %	Carl Roth, Germany
Agar-Agar	Carl Roth, Germany
Agarose	Starlab Gmbh, Germany
AIM V medium	Thermo Fisher Scientific, USA
Ammonium persulfate (APS)	Carl Roth, Germany
Ammonium sulfate ($(NH_4)_2SO_4$)	Carl Roth, Germany
Anhydrous monobasic sodium phosphate (NaH_2PO_4)	Sigma-Aldrich, USA
Anti-mouse IgG biotin antibody	Sigma-Aldrich, USA
Bacto™ tryptone	Thermo Fisher Scientific, USA
Bacto™ yeast extract	Thermo Fisher Scientific, USA
β-Mercaptoethanol	Sigma-Aldrich, USA
BD FACS Clean™	BD Biosciences, USA
BD FACS Flow™	BD Biosciences, USA
BD FACS Rinse™	BD Biosciences, USA
BD Phosflow™ Perm/Wash buffer I, 10x	BD Biosciences, USA
BD Phosflow™ Lyse/Fix, 5x	BD Biosciences, USA
Biocoll® separating solution	Bio&SELL, Germany
Bovine serum albumin (BSA)	Carl Roth, Germany
Bromophenol blue	Sigma-Aldrich, USA
CellGenix® GMP DC medium	CellGenix, Germany
CD14 MicroBeads	Miltenyi Biotec, Germany
Chloral hydrate	Merck Millipore, Germany
Citric acid	Merck Millipore, Germany
Citric acid monohydrate	Merck Millipore, Germany
Coomassie Brilliant Blue G250 dye	Thermo Fisher Scientific, USA
DePeX mounting medium	SERVA Electrophoresis GmbH, Germany
3,3'-Diaminobenzidine tetrachloride (DAB)	Sigma-Aldrich Chemie GmbH, Germany
Dimethyl sulfoxide (DMSO)	Sigma-Aldrich, USA
Disodium hydrogen phosphate ($Na_2HPO_4x7H_20$)	Carl Roth, Germany
Dream Taq® PCR mix, 2x	Thermo Fisher Scientific, USA

Dulbecco's Modified Eagle's Medium (DMEM)	PAN Biotech, Germany
Ethanol, 100 %	Merck Millipore, Germany
Ethylenediaminetetraacetic acid (EDTA)	Carl Roth, Germany
EDTA disodium salt dihydrate (EDTA-$Na_2 \cdot 2H_2O$)	Sigma-Aldrich, USA
Evobrutinib (BTK inhibitor)	Merck Serono, Germany
Fetal bovine serum (FBS), ultra-low IgG	Thermo Fisher Scientific, USA
Fetal calf serum (FCS)	Sigma-Aldrich, USA
Fixable Viability Stain 520	BD Biosciences, USA
FuGENE® HD transfection reagent	Promega, USA
Fungin™	InvivoGen, USA
GelRed	Biotium, Inc., Fremont, USA
GeneRuler 1 kb DNA ladder	Thermo Fisher Scientific, USA
Glycerol, 100 %	Carl Roth, Germany
Glycine	Carl Roth, Germany
Hoechst 33342	Thermo Fisher Scientific, USA
Human MOG_{1-125} protein	GenScript Biotech, Netherlands
Human serum, heat inactivated	Sigma-Aldrich, USA
Human or mouse TruStain FcX™ Fc block	BioLegend, USA
Hydrochloric acid (HCl)	Merck Millipore, Germany
Hydrogen peroxide (H_2O_2), 30 %	Merck Millipore, Germany
HyperLadder™ 50 bp	Meridian Bioscience, BioCat GmbH, Germany
Kleptose	Merck Serono, Germany
L-Glutamine, 200 mM	Sigma-Aldrich, USA
Lithium carbonate solution, 0.05 %	Dianova, Germany
Luxol® Fast Blue solution	Sigma-Aldrich, USA
Mayer’s hemalum	Merck Millipore, Germany
Methanol, 100 %	Carl Roth, Germany
Murine MOG_{1-117} protein	GenScript Biotech, Netherlands
NEBuffer™ r3.1, 10x	New England Biolabs, USA
Non-essential amino acids (NEAA)	Thermo Fisher Scientific, USA
OVA-FITC	Thermo Fisher Scientific, USA
Paraffin oil	Carl Roth, Germany
Paraformaldehyde (PFA), powder	Merck Millipore, Germany
Penicillin/streptomycin	Thermo Fisher Scientific, USA
Phosphate-buffered saline (PBS), 1x	Thermo Fisher Scientific, USA
Phosphate-buffered saline (PBS), 10x	Lonza Bioscience, Switzerland
Plasmocin® Prophylactic	InvivoGen, USA
Polyethylenimine	Sigma-Aldrich, USA
Precision Plus Protein Dual Color ladder	Bio-Rad, Germany
Propan-2-ol (isopropyl alcohol)	Th. Geyer GmbH & Co. KG, Germany

rCutSmart™ buffer, 10x	New England Biolabs, USA
Roswell Park Memorial Institute (RPMI) 1640	Sigma-Aldrich, USA
Sodium carbonate (Na_2CO_3)	Merck Millipore, Germany
Sodium chloride (NaCl)	Carl Roth, Germany
Sodium hydrogen carbonate ($NaHCO_3$)	Merck Millipore, Germany
Sodium hydroxide (NaOH)	Carl Roth, Germany
Sodium dodecyl sulfate (SDS), 10 %	Carl Roth, Germany
Sodium pyruvate, 100 mM	Sigma-Aldrich, USA
Streptavidin-HRP	R&D Systems, USA
Subcloning Efficiency™ DH5α competent cells	Thermo Fisher Scientific, USA
Sulfuric acid (H_2SO_4)	Carl Roth, Germany
3,3',5,5'-Tetramethylbenzidine (TMB)	Moss Inc., Maryland, USA
Tetramethylethylenediamine (TEMED)	Thermo Fisher Scientific, USA
Tris(hydroxymethyl)aminomethane (Tris)	Carl Roth, Germany
Trisodium citrate dihydrate	Merck Millipore, Germany
Trypan blue	Sigma-Aldrich, USA
Trypsin/EDTA, 0.05 %	PAN Biotech, Germany
Tween® 20	Merck Millipore, Germany
Xylene	Th. Geyer GmbH & Co. KG, Germany

Table 2: Kits

Kit	Manufacturer
DyLight™ 650 Antibody Labeling kit	Thermo Fisher Scientific, USA
GraviTrap™ Ab buffer kit	Merck Millipore, Germany
LIVE/DEAD™ Fixable AQUA or NIR Dead Cell Stain kit	Thermo Fisher Scientific, USA
NucleoBond® Xtra Midi Plus DNA Purification kit	Macherey-Nagel
Periodic Acid Schiff (PAS) Staining kit	Carl Roth, Germany
QIAprep Spin Miniprep kit	Qiagen, Netherlands

2.1.2 Solutions, buffers and media

Table 3: Solutions, buffers and media

Solution/buffer/medium	Composition
APS, 10 %	50 mg APS 500 µl distilled water
Blocking buffer for immunohistochemistry	PBS 10 % FCS
Chloral hydrate, 14 %	14 % chloral hydrate distilled water

Citrate buffer, 10 mM	2.1 g citric acid 1 l distilled water pH 6
Coating buffer	8.4 g $NaHCO_3$ 3.5 g Na_2CO_3 1 l distilled water pH 9.5, sterile-filtered
Coomassie Brilliant Blue G250	0.625 g Coomassie Brilliant Blue G250 106.25 ml ethanol 12.5 ml methanol 25 ml acetic acid 106.25 ml distilled water
Cryo medium	20 % DMSO 80 % FCS
DAB working solution	PBS 0.5 mg/ml DAB 20 µl 30 % H_2O_2 per 50 ml DAB
Destain solution	30 % methanol 10 % acetic acid
Dialysis binding buffer	5.42 g NaH_2PO_4 16.36 g $Na_2HPO_4x7H_20$ 5 l distilled water pH 7.0
ELISA washing buffer	1 ml Tween® 20 1.8 l distilled water 200 ml 10x PBS
ELISA stop solution	2 N H_2SO_4 solution
Eosin, 1 %	70 % isopropyl alcohol 1 % eosin G 0.5 % acetic acid added before use sterile-filtered
Fluorescence-activated cell sorting (FACS) buffer	PBS, sterile 2 % FCS
HCl-alcohol, 1 %	1 % HCl absolute 99 % ethanol absolute
Human embryonic kidney (HEK) 293-A cells medium	DMEM 1 % NEAA 10 % FCS 1 % penicillin/streptomycin 5 µg plasmocin
Kleptose buffer, 20 %	3.45 g citric acid monohydrate 1.06 g trisodium citrate dihydrate 40 g Kleptose distilled water, *ad* 200 ml pH 3.0

Lysis buffer (for genotyping)	0.5 g NaOH 37.2 mg EDTA-$Na_2 \cdot 2H_2O$ 500 ml distilled water pH 12.0
Lysogeny broth (LB) medium	10 g tryptone 5 g yeast extract 5 g NaCl distilled water, *ad* 1 l ph 7.0 for agar plates: 15 g agar-agar
Magnetic-activated cell sorting (MACS) buffer	PBS, sterile 0.5 % FCS 2 mM EDTA pH 7.2
Neutralization buffer (for genotyping)	3.152 g Tris 500 ml distilled water pH 5.0
PBS, 10x	95.5 g PBS 1 l distilled water
RD1 buffer (ELISA blocking buffer)	200 ml 10x PBS 20 g BSA 1.8 l distilled water
RPMI complete	RPMI-1640 10 % FCS 1 mM sodium pyruvate 50 µM β-mercaptoethanol 1 % penicillin/streptomycin 2 mM L-glutamine
SDS-polyacrylamide gel electrophoresis (SDS-PAGE) loading buffer	50 mM tris 12 % SDS 30 % glycerol 0.02 % bromophenol blue distilled water pH 6.8
SDS-PAGE running buffer	0.025 M tris 1.5 % glycine 0.1 % SDS distilled water pH 8.3
SDS-PAGE separating gel buffer	1.5 M tris distilled water pH 8.8
SDS-PAGE stacking gel buffer	0.5 M tris distilled water pH 6.8

TAE (tris, acetic acid, EDTA) buffer, 50x	40 mM tris 20 mM acetic acid 1 mM EDTA 1 l distilled water pH 8.0

2.1.3 Plasmids, antibiotics and restriction endonucleases

Table 4: Plasmids for transfection

Plasmid	Resistance	Characteristic	Source of supply
pcDNA6.2-hAQP4-EmGFP	Ampicillin	Encodes isoforms M-1 and M-23 of human AQP4 fused C-terminally to emerald green fluorescent protein (EmGFP)	Prof. Markus Reindl, Medical University Innsbruck, Austria
pEGFP-N1-hMOG	Kanamycin	Encodes isoform α-1 of human MOG fused to enhanced green fluorescent protein (EGFP)	Prof. Markus Reindl
pFUSE-CHIg-hIG1-8.18C5	Zeocin	Encodes the variable region of the mouse 8.18C5-specific kappa heavy chain fused to the constant region of the human kappa heavy chain	Prof. Markus Reindl
pFUSE2-CLIg-8.18C5	Blasticidin	Encodes the variable region of the mouse 8.18C5-specific kappa light chain fused to the constant region of the human kappa light chain	Prof. Markus Reindl

Table 5: Antibiotics

Antibiotic	Final concentration in medium	Manufacturer
Ampicillin	50 µg/ml	Carl Roth, Germany
Blasticidin	100 µg/ml	InvivoGen, USA
Kanamycin	25 µg/ml	Carl Roth, Germany
Zeocin	100 µg/ml	Thermo Fisher Scientific, USA

Table 6: Restriction endonucleases

Restriction endonuclease	Corresponding buffer	Manufacturer
*BamH*I	NEBuffer™ r3.1	New England Biolabs, USA
*Bpm*I	Buffer B	Thermo Fisher Scientific, USA
*BseY*I	NEBuffer™ r3.1	New England Biolabs, USA
*Sal*I	NEBuffer™ r3.1	New England Biolabs, USA
*Stu*I	rCutSmart™ Buffer	New England Biolabs, USA

2.1.4 Antibodies, cytokines and inhibitors

Table 7: Monoclonal antibodies for flow cytometry

Specificity	Reactivity	Fluorochrome	Clone	Dilution	Manufacturer
BTK	Human	PE	53/BTK	1:10	BD Biosciences, USA
CD1c	Human	BV421	L161	1:100	BioLegend, USA
CD11c	Human	PE-Cy5.5	BU15	1:100	Thermo Fisher Scientific, USA
CD11c	Human	PE	3.9	1:50	BioLegend, USA
CD13	Human	PE-Cy7	WM15	1:100	BioLegend, USA
CD14	Human	FITC	M5E2	1:100	BD Biosciences, USA
CD14	Human	APC	M5E2	1:100	BioLegend, USA
CD14	Human	BV421	MφP9	1:100	BD Biosciences, USA
CD14	Human	PE-CF594	MφP9	1:100	BD Biosciences, USA
CD16	Human	AF700	3G8	1:100	BD Biosciences, USA
CD32	Human	PE	FUN-2	1:100	BioLegend, USA
CD40	Human	PE	5C3	1:100	BioLegend, USA
CD64	Human	BV421	10.1	1:100	BioLegend, USA
CD69	Human	BV785	FN50	1:100	BioLegend, USA
CD80	Human	PE-Cy7	L307.4	1:100	BD Biosciences, USA
CD80	Human	BUV395	L307.4	1:100	BD Biosciences, USA
CD86	Human	BV421	FUN-1	1:100	BD Biosciences, USA
CD141	Human	PE	AD5-14H12	1:100	Miltenyi Biotec, Germany
CD163	Human	FITC	GHI/61	1:100	BioLegend, USA
CD206	Human	BV421	15-2	1:50	BioLegend, USA
CD303	Human	FITC	AC144	1:100	Miltenyi Biotec, Germany
CD304	Human	APC	AD5-17F6	1:100	Miltenyi Biotec, Germany
MHCII	Human	APC	Tü36	1:100	BioLegend, USA
Mouse IgG2a isotype control	-	PE	-	1:10	BD Biosciences, USA
B220	Mouse	PE-Cy7	RA3-6B2	1:100	BD Biosciences, USA
CD3	Mouse	BUV395	145-2C11	1:100	BD Biosciences, USA
CD3	Mouse	PE	145-2C11	1:100	BioLegend, USA
CD4	Mouse	BV510	GK1.5	1:100	BioLegend, USA
CD8	Mouse	FITC	53-6.7	1:100	BioLegend, USA
CD11b	Mouse	FITC	M1/70	1:100	BioLegend, USA
CD11b	Mouse	Pacific Blue	M1/70	1:100	BioLegend, USA
CD11b	Mouse	PE-Cy7	M1/70	1:100	BD Biosciences, USA
CD11c	Mouse	FITC	N418	1:100	BioLegend, USA
CD16	Mouse	AF700	275003	1:100	R&D Systems, USA

CD19	Mouse	PerCP-Cy5.5	1D3/CD19	1:100	BioLegend, USA
CD21	Mouse	BV510	7G6	1:100	BD Biosciences, USA
CD23	Mouse	APC	B3B4	1:100	BioLegend, USA
CD25	Mouse	PE	PC61.5	1:100	Invitrogen, USA
CD32	Mouse	FITC	917012B	1:100	BioLegend, USA
CD44	Mouse	APC	IM7	1:100	BioLegend, USA
CD64	Mouse	PE	X54-5/7.1	1:100	BioLegend, USA
CD69	Mouse	PE-Cy7	H1.2F3	1:100	BioLegend, USA
CD69	Mouse	PerCP-Cy5.5	H1.2F3	mouse	BioLegend, USA
CD80	Mouse	PE	16-10A1	1:100	BD Biosciences, USA
CD86	Mouse	BV605	GL1	1:100	BD Biosciences, USA
CD93	Mouse	PE	AA4.1	1:100	BioLegend, USA
CD95	Mouse	BV421	Jo2	1:100	BD Biosciences, USA
IgD	Mouse	BV421	11-26c.2a	1:100	BioLegend, USA
IgMb	Mouse	FITC	AF6-78	1:100	BD Biosciences, USA
Ly-6C	Mouse	BV421	HK1.4	1:100	BioLegend, USA
Ly-6G	Mouse	APC	1A8	1:100	BioLegend, USA
MHCII	Mouse	Pacific Blue	AF6-120.1	1:100	BioLegend, USA
Siglec-F	Mouse	PE-CF594	E50-2440	1:100	BD Biosciences, USA

Table 8: Antibodies, cytokines and inhibitors for cell culture and *in vivo* experiments

Antibody/cytokine/inhibitor	**Manufacturer**
Goat anti-human IgG APC antibody	Jackson ImmunoResearch, USA
Imipramine-HCl (macropinocytosis inhibitor)	Sigma-Aldrich, USA
*InVivo*MAb human IgG1 isotype control	Bio X Cell, USA
*InVivo*MAb mouse IgG1 isotype control, clone MOPC-21	Bio X Cell, USA
Latrunculin A (phagocytosis inhibitor)	Thermo Fisher Scientific, USA
Prostaglandin E_2 (PGE_2)	Sigma-Aldrich, USA
Recombinant human granulocyte macrophage colony-stimulating factor (GM-CSF)	Miltenyi Biotec, Germany
Recombinant human interleukin (IL)-1β	Thermo Fisher Scientific, USA
Recombinant human IL-4	Thermo Fisher Scientific, USA
Recombinant human IL-6	BioLegend, USA
Recombinant human interferon-γ	BioLegend, USA
Recombinant human macrophage colony-stimulating factor (M-CSF)	Sigma-Aldrich, USA
Recombinant human tumor necrosis factor (TNF)-α	Thermo Fisher Scientific, USA

Table 9: Primary antibodies for immunohistochemical staining

Specificity	Clone	Species	Antigen retrieval	Dilution	Manufacturer
CD3	SP7	Rabbit	Citrate buffer	1:50	DCS, Germany
MAC-3	M3/84	Rat	Citrate buffer	1:200	BD Pharmingen, USA

Table 10: Secondary antibodies for immunohistochemical staining

Specificity	Dilution	Manufacturer
Anti-rabbit IgG, biotinylated	1:250	Jackson ImmunoResearch, USA
Anti-rat IgG, biotinylated	1:500	DCS, Germany

2.1.5 Consumables

Table 11: Consumables

Consumable	Manufacturer
Amicon® Pro Purification filter, 50 kDa	Merck Millipore, Germany
Bottle top filter, 0.2 µM	Sarstedt, Germany
Cell cultures dishes, 10 cm	Sarstedt, Germany
Cell culture flasks (75 cm^2, 175 cm^2)	Greiner Bio-One, Austria
Cell culture plates, flat bottom (6-well, 96-well)	Greiner Bio-One, Austria
Cell culture plates, round bottom (96-well)	Sarstedt, Germany
Cell strainer, 70 µm	Greiner Bio-One, Austria
FACS tube	Sarstedt, Germany
LS columns (MACS)	Miltenyi Biotec, Germany
Needles	BD Biosciences, USA
Nunc™ cell culture flasks, 300 cm^2	Thermo Scientific, USA
Nunc™ Maxisorp® 96-well ELISA plate	Thermo Scientific, USA
Pipette tips (10 µl, 20 µl, 200 µl, 1000 µl)	Sarstedt, Germany
Pre-separation filters, 30 µm	Miltenyi Biotec, Germany
rProtein A/Protein G GraviTrap™ column	Sigma-Aldrich, USA
Serological pipettes (5 ml, 10 ml, 25 ml)	Sarstedt, Germany
Serum gel micro sample tube	Sarstedt, Germany
Servapor® dialysis tubes, MWCO 12000 – 14000	SERVA Electrophoresis GmbH, Germany
S-Monovette® K3 EDTA tubes	Sarstedt, Germany

Syringes (1 ml, 3 ml, 10 ml)	BD Biosciences, USA
Tubes (0.5 ml, 1 ml, 2 ml)	Eppendorf, Germany
Tubes (10 ml, 15 ml, 50 ml)	Sarstedt, Germany

2.1.6 Technical devices

Table 12: Technical devices

Device	Manufacturer
BD™ LSR II flow cytometer	BD Biosciences, USA
Centrifuge J6-HC	Beckman Coulter, USA
Centrifuge 5804 R	Eppendorf, Germany
Electrophoresis power supply EC 135-90	Thermo Scientific, USA
iMark™ microplate reader	Bio-Rad, Germany
Microcentrifuge 5415 R	Eppendorf, Germany
Microscope	Olympus, Germany
Microtome	Leica, Germany
Microwave	Bosch, Germany
Mini-PROTEAN® Tetra handcast kit	Bio-Rad, Germany
NanoDrop 3300	Thermo Scientific, USA
Neubauer chamber	Carl Roth, Germany
Olympus microscope BX63	Olympus, Germany
Orbital shaker Thermoshake	Gerhardt Analytical Systems, Germany
QuadroMACS™ separator	Miltenyi Biotec, Germany
Sub-Cell GT Cell electrophoresis system	Bio-Rad, Germany
Thermocycler T3	Biometra, Germany
Thermo shaker TS-100	VWR, USA
Ultraviolet (UV) table	Vilber, Germany

2.1.7 Software

Table 13: Software

Software	Application	Manufacturer
FACS DIVA software 8.02	Data acquisition flow cytometry	BD Biosciences, USA
FlowJo v10.8.0	Data analysis flow cytometry	Tree Star Inc., USA
GraphPad Prism 6	Graphs and statistical analysis	GraphPad software Ins., USA
ImageJ 1.47d	Data analysis histology and fluorescence microscopy	National Institutes of Health, USA
OMERO	Data analysis histology	Glencoe Software Inc., USA

2.2 Blood, plasma und serum samples

For the generation of human antigen-presenting cells, peripheral blood mononuclear cells (PBMCs) were collected from healthy donors. The protocol was approved by the Ethic Committee of the University Medical Center Göttingen (approval number 3/4/14). Plasma and serum samples from MOGAD and NMOSD patients were kindly provided by Prof. Markus Reindl (Medical University Innsbruck), Prof. Klemens Ruprecht (Charité Berlin), Dr. Albert Saiz (Hospital Clinic Barcelona) and Dr. Marius Ringelstein (University Medical Center Düsseldorf). Plasma from a Sjogren's syndrome patient was tested negative for anti-MOG and anti-AQP4 antibodies and served as negative control. For serum samples, a mixture of sera from 3 healthy donors served as negative control. The use of the patient's material was approved by the Ethic Committees of the Hospital Clinic Barcelona, the Charité Berlin, the University Medical Center Düsseldorf and the University Medical Center Göttingen, written consent was obtained.

Table 14: Overview of plasma and serum samples from MOGAD, NMOSD and Sjogren's syndrome patients

Diagnosis	Number of patients	Sample type	CBA: normalized median fluorescence intensity (range)[a]	Sex (female/male)	Age at sampling (mean ± SD, in years)
MOGAD	3	Plasma	MOG: 4.6 – 376.8	3/0	45 ± 23
MOGAD	6	Serum	MOG: 2.7 – 96.4	3/3	48 ± 7
NMOSD	3	Plasma	AQP4: 127.0 – 808.4	3/0	52 ± 14
NMOSD	3	Serum	AQP4: 92.1 – 244.2	3/0	24 ± 8
Sjogren's syndrome	1	Plasma	MOG: 0.98 AQP4: 1.2	0/1	58

[a] Plasma and serum samples were analyzed for anti-MOG and anti-AQP4 antibodies using CBA (see methods). The measured MOG or AQP4 median fluorescence intensities were normalized by a control vector (ratio of MOG or AQP4 median versus control median).

2.3 Animals

Transgenic 2D2 mice were generated, characterized and kindly provided by Dr. Bettelli and Dr. Kuchroo (Boston, USA). In these mice, the majority of $CD4^+$ T cells express a MOG_{35-55}-specific T cell receptor composed of Vα3.2 and Vβ11 (Bettelli et al. 2003). Animals were bred and housed under standard laboratory conditions at the Central Animal Facility of the University Medical Center Göttingen. Mice had access to water and food *ad libitum* and a 12 h/12 h light/dark cycle under specific-pathogen-free conditions. All experiments were carried out as approved by the government of Lower Saxony (protocol number 33.9-42502-04-17/2745).

2.4 Methods – experiments with prokaryotic cells

2.4.1 Cultivation, maintenance and cryopreservation of prokaryotic cells

After transformation, DH5α *Escherichia coli* (*E. coli)* cells were grown in LB medium supplemented with antibiotics for selection listed in table 5. Liquid *E. coli* cultures were cultivated in sterile Erlenmeyer flasks or 10 ml tubes on an orbital shaker at 175 rpm and 37 °C for 14 – 16 h. Thereafter, cells were harvested by centrifugation and plasmid deoxyribonucleic acid (DNA) was isolated with mini and midi preparation kits, respectively.

For maintenance of the *E. coli* strain, cells were plated onto LB agar plates that contained the appropriate antibiotic (selection agar plates). The inoculated plates were aerobically incubated at 37 °C overnight and subsequently stored at 4 °C for four weeks at most.

For cryopreservation, *E. coli* cells were cultured in LB medium and the appropriate antibiotic at 37 °C for 14 – 16 h. Afterwards, 750 µl liquid culture were mixed with 250 µl of 100 % glycerol and immediately frozen at -80 °C.

2.4.2 Transformation

Transformation describes the uptake of exogenous DNA by bacterial cells resulting in a genetic alteration of the cells. Plasmid DNA was mixed with 50 µl of chemically competent DH5α *E. coli* cells and incubated on ice for 20 min. After a heat shock at 42 °C for 45 s, cells were placed on ice for 3 min. Subsequently, 400 µl of pre-warmed LB medium were added and cells were incubated shaking vigorously at 37 °C for 45 min. 50 µl of the mixture were spread onto a selection agar plate and *E. coli* were aerobically cultivated at 37 °C overnight.

2.4.3 Isolation of DNA

2.4.3.1 Mini preparation

3 ml LB medium containing the appropriate antibiotic were inoculated with a single colony picked from a selection agar plate and incubated shaking at 37 °C for 14 – 16 h. The next day, *E. coli* cells were pelletized by centrifugation at 10 000 rpm and room temperature (RT) in a microcentrifuge for 3 min. For the isolation of plasmid DNA, the QIAprep Spin Miniprep kit was used following the instructions of the manufacturer. Purified plasmid DNA was eluted in 50 µl sterile double-distilled water and DNA concentration was determined using NanoDrop.

2.4.3.2 Midi preparation

Larger amounts of plasmid DNA were isolated with the NucleoBond® Xtra Midi Plus DNA Purification kit. For this purpose, *E. coli* cells were cultured in 100 ml LB medium supplemented with the appropriate antibiotic and harvested by centrifugation at 5000 rpm, RT for 10 min. The isolation of DNA was conducted according to the protocol of the manufacturer. Plasmid DNA was eluted in 400 µl sterile double-distilled water and solved for 1 h on ice. DNA concentration was measured by NanoDrop.

2.4.4 Restriction digestion of plasmid DNA

To verify the integrity of the plasmids, purified DNA was digested using restriction endonucleases (listed in table 6). Each digestion reaction was carried out in a total volume of 20 µl and contained 500 – 800 ng DNA, 2 µl of the appropriate digestion buffer, 1 unit restriction enzyme and sterile double-distilled water. Restriction digestions were incubated at 37 °C for 3 h and subsequently visualized by agarose gel electrophoresis.

2.4.5 Agarose gel electrophoresis

This method was used for separating DNA by size for visualization of restriction digestions and polymerase chain reaction (PCR) products. Depending on the length of DNA fragments, the agarose concentration varied between 1 % (w/v) and 2 % (w/v). Agarose powder was mixed with 100 ml 1X TAE buffer and dissolved in a microwave for 2 – 3 min. After a short cooling period, 3 µl GelRed were added and the liquid agarose was poured into a gel tray. 2 µl of digestion reactions and 5 µl of PCR samples were mixed with loading dye and loaded into the gel. For determining the size of DNA fragments, the HyperLadder™ 50 bp (fragment sizes: 50, 100, 200, 300, 400, 500, 600, 700, 800, 1000, 1200, 1400, 1600, 1800, 2000 basepairs (bp)) or GeneRuler 1 kb DNA ladder (fragment sizes: 250, 500, 750, 1000, 1500, 2000, 2500, 3000,

3500, 4000, 5000, 6000, 8000, 10000 bp) was applied. Gel electrophoresis was conducted at 120 V until DNA fragments were sufficiently separated. Subsequently, the separated DNA fragments were visualized by UV light.

2.5 Methods – experiments with eukaryotic cells

2.5.1 Cultivation and cryopreservation of human embryonic kidney 293-A cells

Human embryonic kidney (HEK) 293-A cells were kindly provided by Prof. Markus Reindl (Medical University Innsbruck) and cultured in HEK293-A medium at 37 °C, 95 % humidity and 5 % CO_2. For passaging the cell line, medium was removed and cells were washed with 10 ml PBS. HEK293-A cells were subsequently covered with 4 ml of 0.05 % trypsin/EDTA and incubated for 3 min. After detaching the cells from the flask by rinsing the bottom with 10 ml HEK293-A medium for several times, cells were collected and centrifuged at 1250 rpm, 4 °C for 10 min. Finally, cells were counted with a Neubauer chamber and $4 \cdot 10^5$ – $6 \cdot 10^5$ cells were seeded in 15 ml fresh HEK293-A medium into 75 cm^2 flasks. Cell splitting was carried out twice a week until passage 35.

For cryopreservation, $2 \cdot 10^6$ HEK293-A cells were resuspended in 500 µl HEK293-A medium, mixed with 500 µl cryo medium and immediately frozen at -80 °C. After 48 h, frozen cells were transferred to liquid nitrogen.

2.5.2 Cultivation and cryopreservation of hybridoma cells

Hybridoma cells were kindly provided by Prof. Linington (University of Glasgow, UK) and cultured in RPMI complete medium with 50 µg/ml fungin at 37 °C, 95 % humidity and 5 % CO_2. The suspension cells were passaged every 3 – 4 days by splitting them 1:5 in 20 ml fresh medium into 75 cm^2 cell culture bottles. After expanding the cell line to 40x 75 cm^2 bottles, cells were split into 80x 175 cm^2 flasks for 8.18C5 antibody production.

For cryopreservation of hybridoma cells, $1 \cdot 10^6$ cells were resuspended in 750 µl FCS, mixed with 750 µl cryo medium and immediately frozen at -80 °C. After 48 h, frozen cells were transferred to liquid nitrogen.

2.5.3 Isolation of peripheral blood mononuclear cells

For isolation of PBMCs, 100 – 150 ml blood from healthy donors were collected in EDTA tubes. 20 – 25 ml of the collected blood were layered on top of 15 – 20 ml Biocoll® separating solution in each 50 ml tube. Blood components were separated by density gradient centrifugation at

1500 rpm, RT, with slow acceleration and break off for 35 min. Mononuclear cells were collected at the interphase between the plasma and the Biocoll® solution layer. The isolated cells were washed with PBS and centrifuged at 1250 rpm, 4 °C, 10 min twice, and the cell number was determined using a Neubauer chamber. Finally, the collected PBMCs were resuspended in MACS buffer and it was proceeded with isolation of $CD14^+$ cells.

2.5.4 *In vitro* generation of human antigen-presenting cells

To differentiate human APCs *in vitro*, PBMCs were isolated from blood of healthy donors. Afterwards, $CD14^+$ cells were isolated by magnetic-activated cell sorting (MACS). For this purpose, human anti-CD14 beads were used and isolation of $CD14^+$ cells was conducted according to the protocol of the manufacturer. $1 \cdot 10^7$ $CD14^+$ cells were seeded into 10 cm cell culture dishes and cultivated in the following media at 37 °C, 95 % humidity, 5 % CO_2 for 5 days:

Table 15: Cultivation media for generation of dendritic-like and macrophage-like cells

Dendritic-like cells	Macrophage-like cells
10 ml CellGenix® GMP DC medium	9 ml AIM V medium
1 % penicillin/streptomycin	10 % human serum
800 units/ml human GM-CSF	1 % penicillin/streptomycin
40 ng/ml human IL-4	50 ng/ml human M-CSF

On day 3 post seeding (p.s), cultivation media were renewed by collecting and centrifugating the cell suspensions at 1250 rpm, 4 °C for 10 min. 5 days after seeding, cells were stimulated with the following media for two days:

Table 16: Stimulation media for generation of dendritic-like and macrophage-like cells

Dendritic-like cells	Macrophage-like cells
10 ml CellGenix® GMP DC medium	9 ml AIM V medium
1 % penicillin/streptomycin	10 % human serum
800 units/ml human GM-CSF	1 % penicillin/streptomycin
40 ng/ml human IL-4	10 ng/ml human IFN-γ
2 ng/ml human IL-1β	
10 ng/ml human IL-6	
10 ng/ml human TNF-α	
1 µg/ml PGE_2	

On day 7 p.s., attached and suspension cells were harvested, centrifugated at 1250 rpm, 4 °C for 10 min and washed with DMEM once. After determining the cell number, dendritic-like and macrophage-like cells were seeded for various experiments.

2.5.5 DyLight 650 labeling of human MOG

To be able to quantify the internalization of soluble MOG by the generated APCs, human MOG_{1-125} protein was fluorescently labeled with the DyLight™ 650 Antibody Labeling kit. 1 mg human MOG was labeled as instructed by the manufacturer and the degree of labeling was determined by NanoDrop.

2.5.6 Nonliposomal transfection of plasmid DNA

For experiments with cell-bound human MOG or AQP4, HEK293-A cells were transfected with plasmid DNA encoding for the respective protein (listed in table 4). Transfection is the process of introducing foreign DNA or ribonucleic acid (RNA) into eukaryotic cells using physical or chemical methods. The day before transfection, HEK293-A cells were harvested and counted as described in section 2.5.1. Depending on the size of the cell culture plates, appropriate cell numbers were seeded (see table 17), resulting in a cell confluency of 70 – 80 % on the next day. 24 h later, purified pEGFP-N1-hMOG or pcDNA6.2-hAQP4-EmGFP DNA was mixed with the nonliposomal transfection reagent FuGENE® HD and DMEM. After incubation for 5 min at RT, the transfection mixture was added to the seeded HEK293-A cells. 48 h post transfection, the transfection efficiency was analyzed by fluorescence microscopy and cells were harvested for phagocytosis experiments.

Table 17: Overview of transfection properties per well

Final experiment	Cell culture plate	Total volume per well	Seeded cell number	Volume of seeded cells	Amount of plasmid DNA	Volume of FuGENE® HD reagent	Total volume of transfection reaction
Microscopic analysis	96-well (flat)	100 µl	$0.1 \cdot 10^5$ cells	100 µl	200 ng	0.72 µl	5 µl
Phagocytosis assay	6-well	3 ml	$2 \cdot 10^5$ cells	3 ml	6 µg	21.8 µl	150 µl

2.5.7 Phagocytosis assay

To assess the phagocytic capacity of *in vitro* differentiated APCs, $5 \cdot 10^4$ dendritic-like and macrophage-like cells were seeded in a 96-well round bottom plate and rested for 1 h at 37 °C. If indicated, the inhibitors imipramine (macropinocytosis), latrunculin A (phagocytosis) or evobrutinib (BTK) and their appropriate control solutions were added to the seeded cells, followed by an incubation of 1 h. Subsequently, soluble human MOG-DL650 and transfected HEK293-A cells, respectively, were added. MOG-DL650 was used at final concentrations of

0 – 8 µg/ml. To harvest transfected HEK293-A cells, they were washed with PBS, detached using trypsin and counted. HEK293-A cells were applied at final concentrations of 0 – $128 \cdot 10^3$ cells per well. Where indicated, purified humanized 8.18C5 (c_{final} = 15 µg/ml), human IgG (c_{final} = 100 µg/ml) or serum samples (c_{final} = 1 mg/ml) were added to the wells. After incubating the reaction mixtures for 2 h or 18 h at 37 °C, cell supernatants were collected for ELISA analysis. Cells were washed with PBS once and further processed for flow cytometry analysis.

2.5.8 Flow cytometry analysis

To quantify the uptake of soluble or membrane-bound protein by APCs and to analyze the expression of surface markers on human and murine cells, flow cytometry analysis (also called „FACS“) was conducted. If not otherwise specified, the staining protocol was performed in a 96-well round well plate at 4 °C in the dark and all washing steps included the addition of 160 µl FACS buffer to the wells followed by centrifugation at 1250 rpm, 4 °C for 7 min.

In detail, cells were washed with 160 µl PBS and centrifuged. To stain necrotic cells, 30 µl of the LIVE/DEAD™ Fixable AQUA or NIR Dead Cell Stain kit diluted 1:500 in PBS were added and cells were incubated in the dark at RT for 10 min. Afterwards, 30 µl of human or mouse TruStain FcX™ Fc block diluted 1:50 in FACS buffer were added to block unspecific binding of antibodies to Fc receptors of the cells. After an incubation for 10 min, cells were washed with FACS buffer. To stain molecules on the cell surface, 30 µl of fluorophore-conjugated antibodies (listed in table 7) diluted as indicated in FACS buffer were added and cells were incubated for 15 min. Human cells were subsequently washed with FACS buffer twice, resuspended in 100 µl FACS buffer, transferred to FACS tubes and analyzed by the FACS DIVA software 8.02 at the BD™ LSR II flow cytometer. Murine cells were washed with FACS buffer once and subsequently fixed by incubating them with 100 µl 2 % PFA in PBS for 30 min. After two washing steps, cells were resuspended in 80 µl FACS buffer, transferred to FACS tubes and analyzed by the FACS DIVA software 8.02 at the BD™ LSR II flow cytometer. Further analysis of the measured data was conducted using FlowJo v10.8.0.

2.5.9 Phosflow

The BD Phosflow technology was used to analyze the intracellular expression of BTK by the generated dendritic-like and macrophage-like cells. If not otherwise indicated, all protocol steps were performed in the dark and cells were centrifuged at 2500 rpm, RT for 7 min.

In detail, the *in vitro* differentiated cells were harvested on day 7 p.s. and centrifuged at 1250 rpm, 4 °C for 10 min. After resuspending the cells in pre-warmed PBS, $2.5 \cdot 10^5$ cells were transferred to each 10 ml tube and centrifuged. To stain necrotic cells, 250 µl of the Fixable Viability Stain 520 dye diluted 1:5000 in pre-warmed PBS were added and cells were incubated at 37 °C for 8 min. Thereafter, 2 ml PBS were added and cells were centrifuged. To lyse and fix the generated APCs, they were incubated with 500 µl of pre-warmed BD Phosflow™ Lyse/Fix diluted 1:5 in double-distilled water at 37 °C for 10 min. Cells were centrifuged and subsequently permeabilized by resuspending them in 1 ml ice-cold BD Phosflow™ Perm/Wash buffer I diluted 1:10 in double-distilled water. After an incubation step of 15 min at RT, cells were centrifuged, washed with 1 ml ice-cold Perm/Wash buffer and centrifuged again. To intracellularly stain BTK, cells were resuspended in 100 µl Perm/Wash buffer and 10 µl of the PE-conjugated BTK antibody or the appropriate isotype control (listed in table 7) were added. Cells were incubated at RT for 1 h, washed with 3 ml Perm/Wash buffer and centrifuged. After resuspending the cells in 100 µl Perm/Wash buffer, they were transferred to FACS tubes and analyzed by flow cytometry.

2.5.10 Production of 8.18C5

The murine monoclonal anti-MOG IgG1 antibody clone 8.18C5 was produced using hybridoma cells, which were cultivated as described in section 2.5.2. For optimal production of 8.18C5, hybridoma cells were cultured for 7 days in 80x 175 cm^2 flasks containing 50 ml RPMI medium supplemented with 5 % FCS, 1 mM sodium pyruvate, 50 µM β-mercaptoethanol, 1 % penicillin/streptomycin and 2 mM L-glutamine. Afterwards, the cell supernatant containing the secreted antibody was harvested by centrifugation at 2000 rpm, 4 °C for 10 min. For purification of the monoclonal antibody, the protein was first precipitated by adding ammonium sulfate to the supernatant and incubating the mixture at 4 °C overnight, constantly mixing. On the next day, the precipitated protein was pelletized in a Beckman Coulter J6-HC centrifuge at 10 000 rpm, 4 °C for 30 min and subsequently solved in 10x PBS. Afterwards, the anti-MOG antibody was purified as described in chapter 2.5.13 and eventually analyzed by NanoDrop, SDS-PAGE and MOG ELISA.

2.5.11 Production of humanized 8.18C5

A humanized form of the anti-MOG antibody clone 8.18C5 (h8.18C5) was produced in HEK293-A cells to serve as positive control for anti-MOG antibody positive IgG and serum samples in

phagocytosis experiments. HEK293-A cells were cultured at 37 °C, 5 % CO_2 in 9x 75 cm^2 flasks containing 15 ml HEK293-A medium supplemented with 5 % ultra-low IgG FCS instead of 10 % normal FCS. The day before transfection, cells were harvested as described in section 2.5.1 and seeded into 6x 300 cm^2 Nunc™ cell culture bottles, resulting in a cell confluency of 70 – 80 % on the next day. For transient expression of the humanized antibody, HEK293-A cells were transfected with the transfection reagent polyethylenimine and 2 plasmid constructs which either encode the variable region of the mouse 8.18C5-specific kappa heavy chain fused to the constant region of the human kappa heavy chain (pFUSE-CHIg-hIG1-8.18C5) or the variable region of the mouse 8.18C5-specific kappa light chain fused to the constant region of the human kappa light chain (pFUSE2-CLIg-8.18C5, listed in table 4). In detail, 40 µg pFUSE-CHIg-hIG1-8.18C5 DNA and 60 µg pFUSE2-CLIg-8.18C5 DNA were mixed with 500 µl of 1 mg/ml polyethylenimine and filled up with DMEM to 5 ml. After pre-incubating the transfection mixture at RT for 10 min, it was added to the seeded cells cultured in 80 ml 5 % FCS HEK293-A medium. Transfected HEK293-A cells were cultivated at 37 °C for 8 days and the secreted antibody was subsequently harvested by collecting the supernatant. To remove cells, the supernatant was centrifuged at 1250 rpm, 4 °C for 10 min. Finally, the humanized antibody was purified as described in chapter 2.5.13 and analyzed by NanoDrop, SDS-PAGE, MOG ELISA and CBA.

2.5.12 Purification of whole immunoglobulin G from human plasma

Human plasma samples were obtained from Sjogren's syndrome, MOGAD and NMOSD patients by plasmapheresis. Whole IgG was purified from 50 ml human plasma as described in section 2.5.13. Subsequently, the purified IgG was analyzed by NanoDrop, MOG ELISA and CBA.

2.5.13 Purification of immunoglobulin G

To purify the murine and humanized 8.18C5 antibody as well as human whole IgG, their solvents were first exchanged into binding buffer (see table 3) by dialysis. For this purpose, the protein solution was transferred into Servapor® dialysis tubes (MWCO 12000 – 14000) and dialysis was performed in 5 L binding buffer at 4 °C overnight. The next day, the binding buffer was replaced by fresh buffer and dialysis was conducted for additional 5 h. Thereafter, the protein solution was collected from the dialysis tubes, sterile-filtered and stored at 4 °C until further processing.

For purification of IgG, rProtein A/Protein G GraviTrap™ columns and the GraviTrap™ Ab buffer kit were used. The purification was conducted according to the instructions of the manufacturer and the purified 8.18C5 was collected in elution/neutralizing buffer. Finally, the buffer was exchanged into 1x PBS by centrifugation using 50 kDa Amicon® Pro Purification filters. Centrifugation steps were performed at 4000 rpm, 4 °C, 30 min until the buffer was completely exchanged. The purified antibody was sterile-filtered and further analyzed.

2.5.14 Sodium dodecyl sulfate polyacrylamide gel electrophoresis

To examine the integrity and purity of the murine and humanized 8.18C5 antibody, sodium dodecyl sulfate polyacrylamide gel electrophoresis (SDS-PAGE) was used, which allows the separation of proteins by size. For this purpose, the discontinuous gel system based on Laemmli (Laemmli 1970) was applied and gel equipment from the Mini-PROTEAN® Tetra handcast kit was used.

After assembling the gel glass plates, the following separating gel solutions were poured into the glass plates and overlaid with isopropyl alcohol:

Table 18: Composition of 6 % and 12 % separating gels

Solution	6 % gel (for non-reducing conditions)	12 % gel (for reducing conditions)
Acrylamide, 30 %	6 %	12 %
Separating gel buffer	0.375 M	0.375 M
SDS, 10 %	0.1 %	0.1 %
Double-distilled water	*ad* 7.5 ml	*ad* 7.5 ml
APS, 10 %	0.05 %	0.05 %
TEMED	0.16 %	0.16 %

Gels were left to set for 1 h and the overlayed isopropyl alcohol was subsequently removed. For the stacking gel, the following solution was poured into the glass plates and combs were immediately inserted:

Table 19: Composition of the stacking gel

Solution	Stacking gel
Acrylamide, 30 %	5 %
Stacking gel buffer	0.125 M
SDS, 10 %	0.1 %
Double-distilled water	*ad* 7.5 ml
APS, 10 %	0.05 %

TEMED	0.16 %

Gels were allowed to set for 30 min. In the meantime, protein samples were prepared by mixing 10 µg of the purified antibody with loading buffer. For reducing conditions, β-mercaptoethanol (100 %) was added to a final concentration of 0.5 %. To disrupt the secondary and tertiary structure of the antibody, the mixtures were subsequently heated at 70 °C for non-reducing and 95 °C for reducing conditions for 5 min. After loading the denatured protein samples and the Precision Plus Protein Dual Color ladder (fragment sizes: 10, 15, 20, 25, 37, 50, 75, 100, 150, 250 kDa) into the gels, antibody samples were separated in SDS-PAGE running buffer at 40 – 60 mA for 40 – 50 min.

To visualize the resolved proteins, gels were stained with Coomassie Brilliant Blue G250. For this purpose, gels were washed with double-distilled water for 5 min twice and subsequently stained with Coomassie Brilliant Blue G250 solution for 25 min. Afterwards, gels were washed with double-distilled water 3 times for 5 min each and decolorized with destain solution overnight.

2.5.15 MOG enzyme-linked immunosorbent assay

The MOG binding capacity of the murine and humanized 8.18C5 and anti-MOG antibody$^+$ IgG samples was determined by MOG ELISA. If not otherwise specified, incubation steps were carried out on a shaker at RT and washing included 3 washing steps with 150 µl ELISA wash buffer. A Nunc™ Maxisorp® 96-well ELISA plate was coated with 100 µl of 10 µg/ml murine or human MOG protein and incubated at 4 °C overnight. The next day, the plate was washed, blocked with 200 µl RD1 buffer for 1 h and washed again. Antibody samples and controls were diluted 1:500, 1:1500, 1:4500, 1:13500 and 1:40500 in RD1 buffer and 100 µl of the dilutions were applied onto the plate. After an incubation of 2 h, the plate was washed and subsequently incubated with 100 µl anti-mouse or anti-human IgG-biotin detection antibody diluted 1:6000 and streptavidin-HRP diluted 1:40 in RD1 buffer for 1 h in the dark. The plate was washed four times and 100 µl TMB were applied. After a maximal incubation of 20 min in the dark, 100 µl ELISA stop solution were added and the OD was subsequently measured at 450 nm with 540 nm wavelength correction using the iMark™ microplate reader.

2.5.16 Cell-based assay

Human IgG and serum samples were analyzed for MOG- or AQP4-specific antibodies using cell-based assay (CBA). All experiments were performed by Dr. Stefan Nessler (Department of

Neuropathology, University Medical Center Göttingen). Briefly, HEK293-A cells which stably expressed human MOG isoform α-1, human AQP4 isoform M23 or the appropriate control vectors (CV) on the surface were incubated with IgG or serum samples diluted 1:50 in the growth medium for 15 min on ice. Cells were subsequently washed 3 times with FACS buffer and APC-labeled goat anti-human IgG antibody was added. After an incubation of 15 min on ice, cells were washed twice, transferred to FACS tubes and analyzed by flow cytometry. The median fluorescence intensity was measured and the median ratio of HEK-MOG versus HEK-CV or HEK-AQP4 versus HEK-CV was calculated.

2.6 Methods – *in vivo* experiments

2.6.1 Genotyping of 2D2 mice

The genotype of 2D2 mice was determined using PCR. All genotyping experiments were conducted by Katja Grondey and Julian Koch (Department of Neuropathology, University Medical Center Göttingen). For the isolation of DNA from tail biopsies of 2D2 mice, the tissue was digested in 100 µl lysis buffer at 99 °C for 30 min and 100 µl neutralization buffer were subsequently added. PCR reactions contained 1 µl of the isolated DNA, 10 µl 2x Dream Taq® PCR mix, 7 µl nuclease-free water and 1 µl of each primer:

primer 1: 5'-CCC GGG CAA GGC TCA GCC ATG CTC CTG-3'
primer 2: 5'-GCG GCC GCA ATT CCC AGA GAC ATC CCT CC-3'

Reactions were run in the T3 thermocycler at the following cycling conditions:

94 °C	2 min	initial denaturation
94 °C	1 min	denaturation
58 °C	1 min	annealing
72 °C	1 min	extension
72 °C	1 min	final extension
4 °C	∞	storage

Finally, PCR products were visualized by agarose gel electrophoresis as described in section 2.4.5.

2.6.2 EAE induction

To induce antibody-driven EAE, the anti-MOG antibody clone 8.18C5 was repetitively injected into the tail vein of 2D2 mice. 150 µg 8.18C5 antibody or isotype control antibody (*InVivo*MAb

mouse IgG1, clone MOPC-21) were injected twice a week up to a total of ten injections and clinical signs of EAE were evaluated daily as follows: 0 = no clinical signs; 1.0 = tail paralysis; 2.0 = hind limb paresis; 3.0 = severe hind limb paresis; 4.0 = paralysis of both hind limbs; 4.5 = hind limb paralysis and beginning forelimb paresis, 5.0 = moribund or dead. To monitor the antibody titer in the blood of 2D2 mice, serum was analyzed after the fifth and the last antibody injection. For this purpose, blood from the *vena facialis* was collected into serum gel micro sample tubes and centrifuged at 13 000 rpm, RT for 5 min. Serum samples were subsequently analyzed by MOG ELISA.

2.6.3 Evobrutinib treatment

Evobrutinib was dissolved in 20 % Kleptose buffer (listed in table 3). The compound was administered daily by oral gavage at a concentration of 3 mg/kg bodyweight, starting 3 days before the first 8.18C5 antibody injection. Control mice received 20 % kleptose buffer.

2.6.4 *Ex vivo* isolation of immune cells and histology

At the end of each experiment, immune cells were analyzed by flow cytometry and histological analysis of the brain and spinal cord was performed. For *ex vivo* analysis of immune cells via flow cytometry, spleen, cervical and inguinal lymph nodes were collected and passed through a 70 µM cell strainer. After two washing steps with PBS and centrifugation at 1250 rpm, 4 °C for 10 min, cells were seeded in 96-well round bottom plates and further processed for flow cytometry analysis.

To perform histological analysis, animals were transcardially perfused with PBS followed by 4 % PFA in PBS. Brain, spinal cord, liver and spleen were isolated, stored in 4 % PFA at 4 °C for 2 – 3 days and subsequently transferred to PBS. For paraffin embedding of the tissues, the brain was dissected into 2 – 3 mm coronal slices and the spinal cord was cut into 8 – 10 sections. Spleen and liver slices were utilized as positive and negative control, respectively, for histochemical stainings. The tissues were subsequently washed in water and dehydrated by a graded alcohol/xylene/paraffin series using an automated tissue processor. Finally, tissue sections were embedded in paraffin and processed for immunohistochemistry.

2.6.5 Histochemistry and immunohistochemistry

For histochemical and immunohistochemical stainings, paraffin blocks were sliced into 1 µm sections using a microtome and slices were mounted on glass slides. To deparaffinize and

rehydrate the tissue slices, they were incubated at 60 °C for 60 min and subsequently treated as follows:

4x	10 min	xylene
1x	5 min	xylene/isopropyl alcohol
2x	5 min	100 % isopropyl alcohol
1x	5 min	90 % isopropyl alcohol
1x	5 min	70 % isopropyl alcohol
1x	5 min	50 % isopropyl alcohol
∞		distilled water

After histochemical or immunohistochemical stainings, tissue sections were dehydrated by performing the xylene/isopropyl alcohol series described above in reverse, incubating every step for 3 min. Finally, the stained slices were mounted with DePeX mounting medium.

2.6.5.1 Hematoxylin and eosin staining

Histological sections were stained with hematoxylin and eosin (HE) to obtain a general overview of the tissue. Hematoxylin stains cell nuclei in a blue-purple color, whereas eosin marks the cytoplasm and extracellular matrix in pink. For the staining, slices were deparaffinized and rehydrated as described above. Subsequently, they were incubated in Mayer's hemalum for 5 min and rinsed with distilled water. After differentiating the sections by shortly immersing them into 1 % HCl-alcohol, slices were blued by rising them in flowing tap water for 10 min. Tissue sections were then incubated with 1 % eosin for 5 min and rinsed with distilled water. Finally, the stained sections were dehydrated and mounted with DePeX medium.

2.6.5.2 Luxol fast blue – periodic acid-Schiff staining

To evaluate myelin loss in the brain and spinal cord, sections were stained with luxol fast blue (LFB) and periodic acid-Schiff (PAS). Myelin is stained blue by LFB and PAS marks demyelinated parenchyma and grey matter in pink. After deparaffinizing the sections up to the 90 % isopropyl alcohol step, they were incubated with LFB solution at 60 °C overnight. The next day, slides were washed in 90 % isopropyl alcohol and subsequently differentiated by shortly immersing them into 0.05 % lithium carbonate solution, followed by 70 % isopropyl alcohol and distilled water. Sections were then incubated with 1 % periodic acid for 10 min and rinsed in flowing tap water for 5 min. After washing the slides with distilled water twice, they were incubated in Schiff's solution for 40 min and subsequently washed in flowing tap water for

20 min. To stain cell nuclei, sections were incubated in Mayer's hemalum for 5 min and shortly rinsed with distilled water. After differentiating the sections by shortly immersing them into 1 % HCl-alcohol, slices were blued by rinsing them in flowing tap water for 10 min. Finally, the stained sections were dehydrated and mounted with DePeX medium.

2.6.5.3 Immunohistochemical staining

For determining the infiltration of immune cells into the brain and spinal cord, immunohistochemical stainings with antibodies against CD3 (T cells) and MAC-3 (macrophages) were performed. If not otherwise indicated, all washing steps included washing with PBS for 3 times. Sections were first deparaffinized and rehydrated as described in section 2.6.5. To expose antigenic sites in the tissues, an antigen retrieval was conducted by heating the slides in citrate buffer in a steamer for 45 min. Sections were then washed with PBS and incubated with 3 % H_2O_2 at 4 °C for 10 min to block the endogenous peroxidase and reduce unspecific signals. After washing the slides with PBS, they were incubated with 10 % FCS in a humidified chamber at RT for 30 min to prevent unspecific antibody binding. Sections were subsequently incubated with 100 µl anti-CD3 or anti-MAC-3 antibody diluted in 10 % FCS (antibodies listed in table 9) in a humidified chamber at 4 °C overnight. The next day, slides were rinsed with PBS and incubated with the corresponding biotin-conjugated secondary antibody listed in table 10 (diluted in 10 % FCS) in a humidified chamber at RT for 1 h. After washing the slides with PBS, they were incubated with 0.1 % peroxidase-conjugated streptavidin (diluted in 10 % FCS) in a humidified chamber at RT for 1 h. Sections were subsequently rinsed with PBS and developed in DAB solution for several minutes, while the staining reaction was controlled under the microscope. DAB acts as a substrate of the peroxidase, resulting in a dark brown staining. After rinsing the slides with distilled water twice, cell nuclei were counterstained with Mayer's hemalum for 10 sec. Slides were then rinsed with distilled water and differentiated by shortly dipping the slides into 1 % HCl-alcohol. Finally, slices were blued by rinsing them in flowing tap water for 5 min, dehydrated and mounted with DePeX medium.

2.7 Statistical analysis

All statistical analyses were calculated using the software GraphPad Prism 6. Data are depicted as mean ± SEM (standard error of the mean). *In vitro* phagocytosis assays with inhibitors (Fig. 4) or h8.18C5 (Fig. 6) as well as cell surface stainings after phagocytosis assays (Fig. 12 –

14) were analyzed by a two-sided *t* test. Phagocytosis assays with human IgG and serum samples (Fig. 7 – 11) were analyzed using a one-way ANOVA followed by Dunnett's multiple comparison test, comparing antibody negative IgG/serum to antibody positive samples. For BTK inhibition in WT mice (Fig. 13, 14), the Mann-Whitney U test was used. The Kaplan-Meier curve of treated transgenic 2D2 mice was analyzed by the Mantel-Cox logrank test (Fig. 17). Histological and flow cytometry data from experiments with transgenic 2D2 mice (Fig. 18 – 23) were analyzed using the Kruskal-Wallis test followed by Dunn's test for multiple comparison. P-values of statistical differences correspond to:

$p > 0.05$ - not significant
$p \leq 0.05$ - *
$p \leq 0.01$ - **
$p \leq 0.001$ - ***
$p \leq 0.0001$ - ****

3 RESULTS

3.1 Project 1: Investigation of the opsonizing capacity of patient-derived anti-MOG antibodies

Kinzel and colleagues previously suggested that opsonization of CNS antigen by MOG-reactive antibodies may act as a disease-triggering process in mice. They showed that the peripheral administration of anti-MOG antibodies induced the activation and proliferation of MOG-specific T cells, which subsequently entered the CNS and caused EAE (Kinzel et al. 2016). In MOGAD patients however, the mechanisms of disease induction and progression have not been deciphered yet. It is also uncertain if human anti-MOG antibodies harbor pathogenic functions. Hence, the first project of the present study addressed the potential pathogenic role of patient-derived anti-MOG antibodies. Using *in vitro* differentiated human myeloid APCs, it was investigated if peripheral autoantibodies from MOGAD patients have the ability to opsonize human MOG, thus mediating antigen recognition and internalization by myeloid APCs.

3.1.1 *In vitro* differentiated human antigen-presenting cells exhibit specific phenotypes

To assess the opsonizing capacity of patient-derived anti-MOG antibodies, an *in vitro* setting with human myeloid APCs was established. For this purpose, $CD14^+$ myeloid cells were isolated from peripheral blood mononuclear cells of healthy donors and cultured in the presence of distinct cytokines for 7 days (Fig. 2A). In the presence of GM-CSF, IL-4, IL-1β, IL-6, TNF-α and PGE_2, myeloid cells were differentiated into cells which resembled human DCs (therefore termed dendritic-like cells). To generate macrophage-like cells, $CD14^+$ cells were cultured under the influence of M-CSF, IFN-γ and human serum. In the course of differentiation, immature dendritic-like cells were characterized by a branched morphology, whereas mature dendritic-like cells displayed a round shape and were detached from the cell culture plate. Macrophage-like cells attached to the plate during cultivation, exhibiting an oblong or rounded shape at the end (Fig. 2B). Flow cytometry analysis of the differentiated cells revealed that both cell types highly expressed CD11c, but they differed in the expression of CD14 (Fig. 2C, 3C, D).

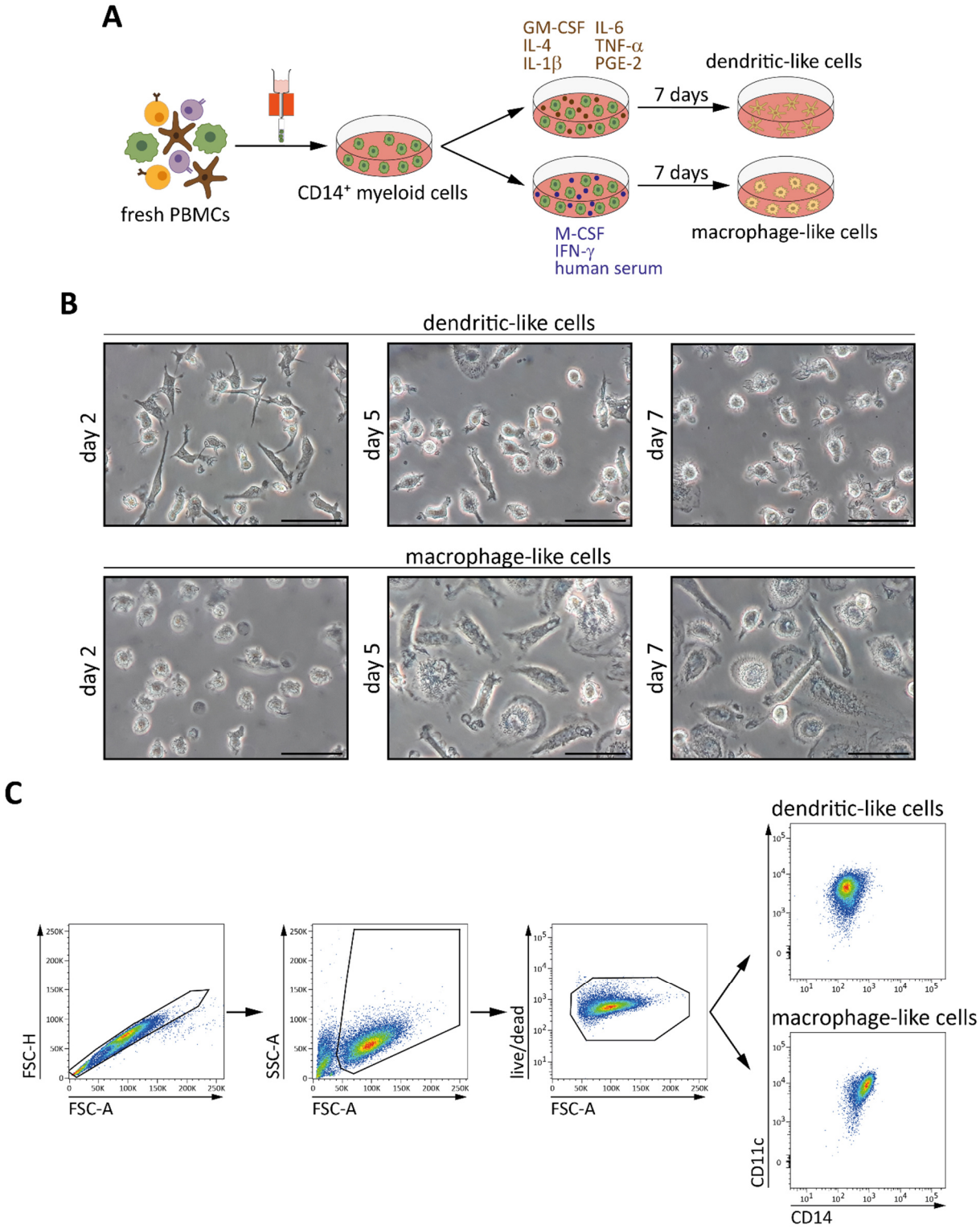

Figure 2: *In vitro* differentiation of human myeloid APCs. $CD14^+$ myeloid cells were isolated from human peripheral blood mononuclear cells (PBMCs) of healthy donors by magnetic-activated cell sorting and cultured in the presence of the in **(A)** indicated cytokines. 7 days post seeding, mature dendritic-like and macrophage-like cells were harvested. **A)** Illustration of the generation process. **B)** Morphologic development of human APCs in the course of differentiation; scale bar = 20 µm. **C)** Gating strategy for flow cytometry analysis of the generated cells. After excluding doublets and dead cells, dendritic-like and macrophage-like cells were stained for CD11c and CD14.

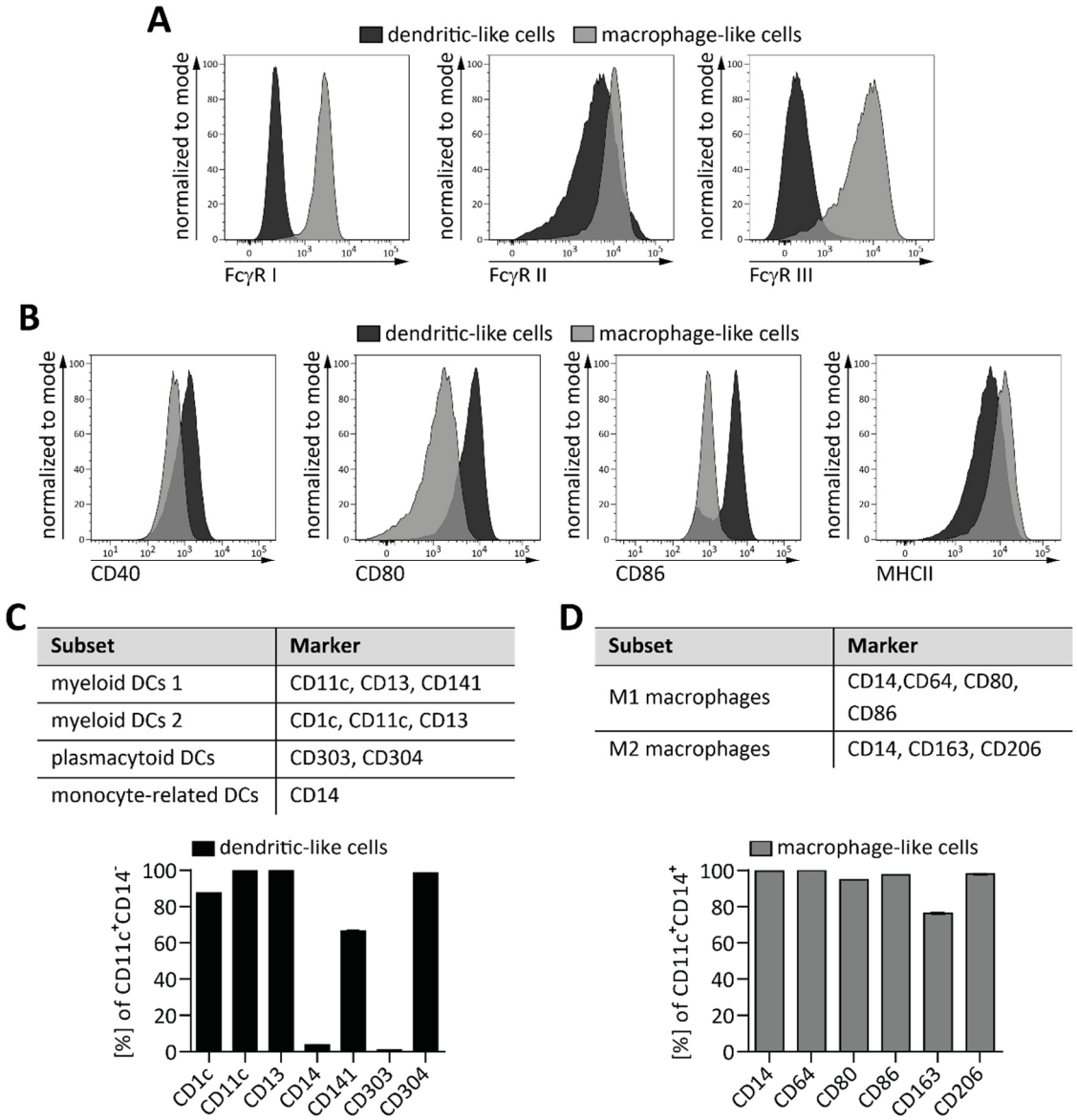

Subset	Marker
myeloid DCs 1	CD11c, CD13, CD141
myeloid DCs 2	CD1c, CD11c, CD13
plasmacytoid DCs	CD303, CD304
monocyte-related DCs	CD14

Subset	Marker
M1 macrophages	CD14,CD64, CD80, CD86
M2 macrophages	CD14, CD163, CD206

Figure 3: The generated APCs display different profiles of cell surface markers. Dendritic-like and macrophage-like cells were analyzed for the expression of **(A)** FcγRs, **(B)** molecules involved in antigen presentation and markers specific for **(C)** dendritic cell (DC) subsets or **(D)** macrophage subsets using flow cytometry. **A, B)** Representative histograms of 5 independent experiments. **C, D)** Tables with a selection of markers characteristic for DC subsets (Collin et al. 2013) or macrophage subsets (Ambarus et al. 2012). Mean frequency of the indicated markers ± SEM gated on intact $CD11c^{+}CD14^{-}$ dendritic-like cells or $CD11c^{+}CD14^{+}$ macrophage-like cells; n = 3; representative data of 2 independent experiments.

Since FcγRs are required for the effector functions of myeloid APCs, their expression on dendritic-like and macrophage-like cells was examined by flow cytometry. Macrophage-like cells expressed FcγRs I, II and III, whereas dendritic-like cells only showed high expression of FcγR II, which comprises an activating (FcγR IIa) and an inhibitory (FcγR IIb) receptor (Fig. 3A). Furthermore, the expression of molecules involved in antigen presentation was determined, showing that both cell types expressed CD40, CD80, CD86 and MHCII, with dendritic-like cells mostly displaying higher expression levels than macrophage-like cells (Fig. 3B). To evaluate

whether *in vitro* differentiated human APCs share similar features with DCs and macrophages occurring in the human body, the expression of markers specific for subsets of DCs or macrophages was analyzed. The generated dendritic-like cells expressed molecules specific for myeloid and plasmacytoid but not for monocyte-related DCs (Fig. 3C). Macrophage-like cells presented high expression levels of M1 and M2 markers (Fig. 3D), suggesting that *in vitro* differentiated cells cannot be assigned to distinct subsets of myeloid APCs. Taken together, these results indicate that *in vitro* differentiated dendritic-like and macrophage-like cells are characterized by particular morphologies and cell surface marker profiles. Both cell types express common features of APCs and are thus suitable to examine the opsonizing capacity of MOG-specific antibodies.

3.1.2 Human antigen-presenting cells are capable of internalizing soluble and membrane-bound protein

A crucial prerequisite for investigating the opsonizing capacity of patient-derived anti-MOG antibodies is the ability of the differentiated cells to internalize human MOG. To assess this function, dendritic-like and macrophage-like cells were incubated with fluorescently labeled, soluble MOG (MOG-DL650) for 2 h and protein uptake was determined by flow cytometry. As depicted in Fig. 4A, both cell types internalized soluble MOG in a concentration-dependent manner. To specify the endocytosis mechanism, inhibitors targeting macropinocytosis or phagocytosis were applied. Addition of the macropinocytosis inhibitor imipramine resulted in a significantly decreased MOG-DL650 uptake by dendritic-like or macrophage-like cells (Fig. 4B). A similar effect was observed in the presence of the phagocytosis inhibitor latrunculin A, although the reduction of MOG internalization was less efficient (Fig. 4C). A mixture of imipramine and latrunculin A potently diminished but did not completely inhibit protein uptake by human APCs (Fig. 4D). These observations indicate that soluble human MOG is mainly internalized by macropinocytosis followed by phagocytosis, but other mechanisms of endocytosis may be additionally involved.

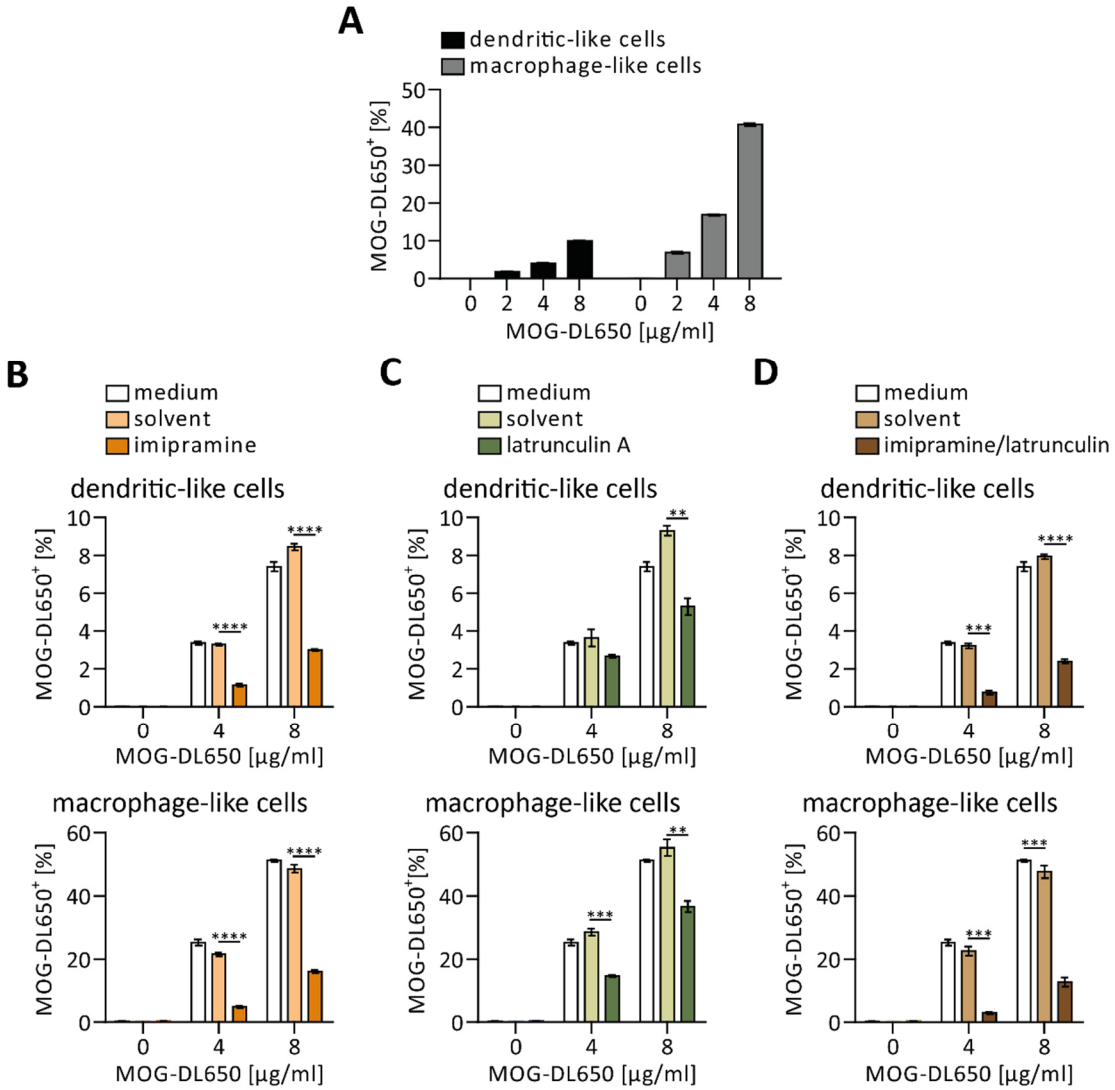

Figure 4: Dendritic-like and macrophage-like cells internalize soluble human MOG by macropinocytosis and phagocytosis. *In vitro* differentiated APCs were incubated with fluorescent-labeled soluble MOG (MOG-DL650) for 2 h. The MOG uptake was quantified by flow cytometry. **A)** Frequency of MOG-DL650$^+$ cells ± SEM gated on intact CD11c$^+$CD14$^-$ dendritic-like cells or CD11c$^+$CD14$^+$ macrophage-like cells; n = 3; representative data of 5 independent experiments. **B – D)** To investigate the mechanism of internalization, human APCs were pre-incubated with **(B)** imipramine (macropinocytosis inhibitor, solved in methanol), **(C)** latrunculin (phagocytosis inhibitor, solved in DMSO) or **(D)** both for 30 min, and fluorescently labeled MOG was subsequently added. Mean frequency of MOG-DL650$^+$ cells ± SEM gated on intact CD11c$^+$CD14$^-$ dendritic-like cells or CD11c$^+$CD14$^+$ macrophage-like cells; n = 3; representative data of 2 – 3 independent experiments; two-sided *t* test of solvent vs. inhibitor.

Since MOG physiologically occurs as a transmembrane protein, it was further investigated whether the generated APCs are capable of internalizing membrane-bound MOG. For this purpose, HEK293-A cells were transfected with pEGFP-N1-hMOG, which encodes isoform α-1 of human MOG fused to enhanced green fluorescent protein (EGFP). The expression of MOG-EGFP on the membrane of HEK293-A cells was visualized by fluorescence microscopy 48 h post transfection and is shown as a greenish staining (Fig. 5A). To analyze the ingestion of membrane-bound MOG by human APCs, HEK293-A cells were harvested 48 h post

transfection and incubated with dendritic-like or macrophage-like cells for 2 h. Both cell types internalized human MOG-EGFP expressed by HEK293-A cells in a concentration-dependent manner (Fig. 5B). To determine the opsonizing capacity of patient-derived anti-AQP4 antibodies in subsequent experimental approaches, AQP4 protein expressed on the cell surface was required. HEK293-A cells were therefore transfected with pcDNA6.2-hAQP4-EmGFP, which encodes isoforms M-1 and M-23 of human AQP4 fused C-terminally to emerald green fluorescent protein (EmGFP). 48 h post transfection, the expression of AQP4-EmGFP on HEK293-A cells was visualized by fluorescence microscopy (Fig. 5C). Subsequently, cells were harvested and incubated with human APCs. Similar to membrane-bound MOG, dendritic-like and macrophage-like cells ingested membrane-bound AQP4-EmGFP (Fig. 5D). In summary, these finding demonstrate that *in vitro* differentiated APCs are capable of ingesting soluble as well as membrane-bound protein.

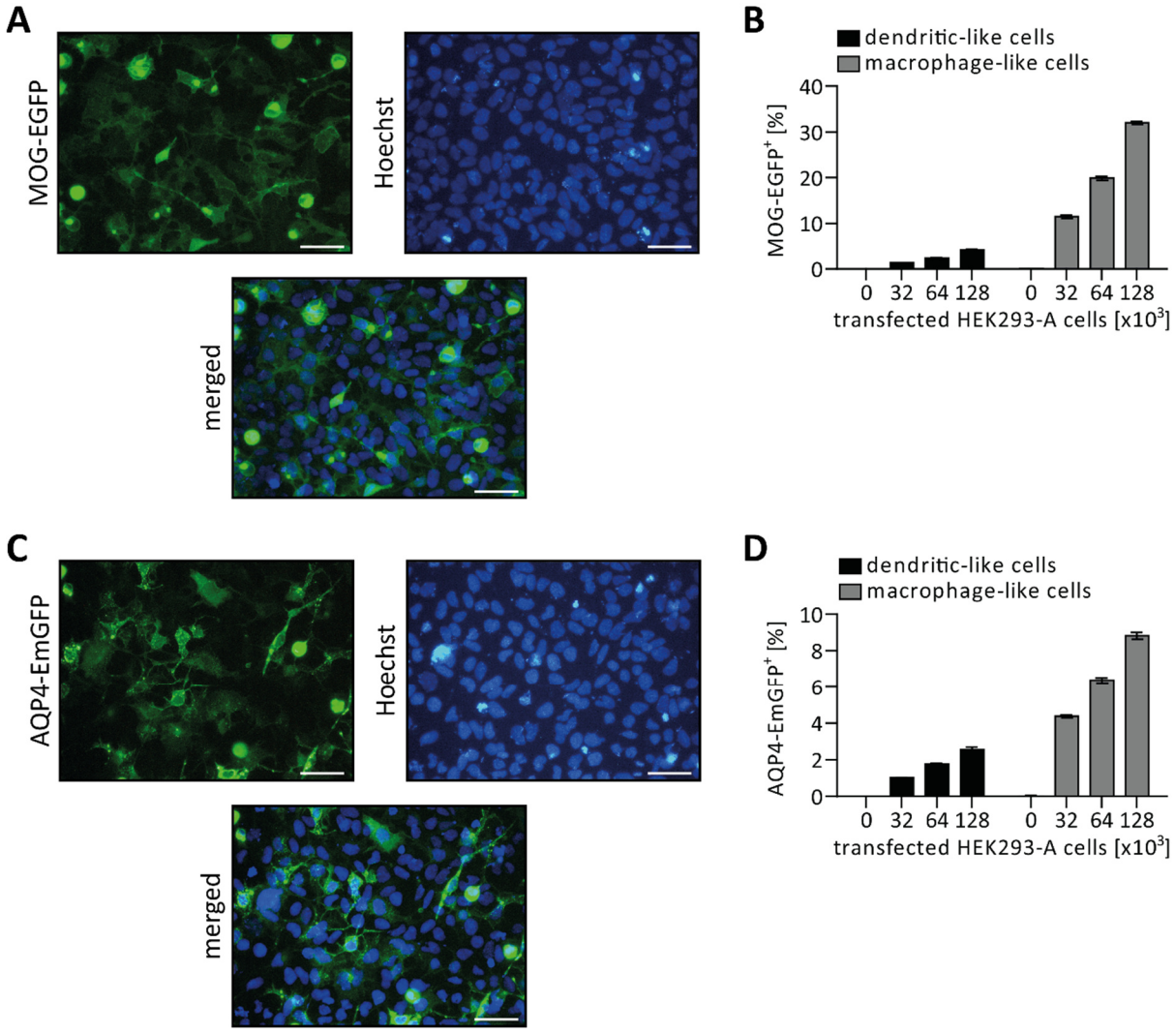

Figure 5: The differentiated APCs are capable of internalizing membrane-bound human MOG and AQP4. To obtain membrane-bound human MOG or AQP4, HEK293-A cells were transiently transfected with either **(A, B)** pEGFP-N1-hMOG (MOG-EGFP) or **(C, D)** pcDNA6.2-hAQP4-EmGFP (AQP4-EmGFP). **A, C)** 48 h post transfection, transfected cells were counterstained with Hoechst 33342 and visualized by fluorescence microscopy; scale bar = 50 µm. **B, D)** Transfected HEK293-A cells were harvested 48 h post transfection and incubated with dendritic-like or macrophage-like cells for 2 h. Mean frequency of **(B)** MOG-EGFP$^+$ or **(D)** AQP4-EmGFP$^+$ cells ± SEM gated on intact CD11c$^+$CD14$^-$ dendritic-like cells or CD11c$^+$CD14$^+$ macrophage-like cells; n = 3; representative data of 3 independent experiments.

3.1.3 Humanized anti-MOG antibody 8.18C5 enhances the uptake of membrane-bound MOG by *in vitro* differentiated phagocytes

Next, it was examined whether *in vitro* differentiated APCs are generally capable of recognizing and internalizing opsonized protein. For this purpose, a humanized form of the anti-MOG antibody clone 8.18C5 (h8.18C5) was produced by HEK293-A cells for 8 days and its functional integrity was verified by MOG ELISA and CBA. H8.18C5 antibody was able to bind soluble (Fig. 6A) and membrane-bound human MOG (Fig. 6B). To analyze the opsonization capacity of the monoclonal antibody, human APCs were incubated with soluble MOG (MOG-

DL650) or HEK293-A cells expressing MOG-EGFP in the presence of h8.18C5 or human IgG1 isotype antibody. As depicted in Fig. 6C, the addition of h8.18C5 antibody did not alter the internalization of soluble MOG-DL650 by dendritic-like or macrophage-like cells. In contrast, the frequency of APCs containing membrane-bound MOG-EGFP was strongly increased in the presence of h8.18C5 antibody (Fig. 6D). These results indicate that humanized anti-MOG antibody 8.18C5 opsonizes membrane-bound but not soluble MOG, thus promoting the ingestion of membrane-bound MOG by human APCs.

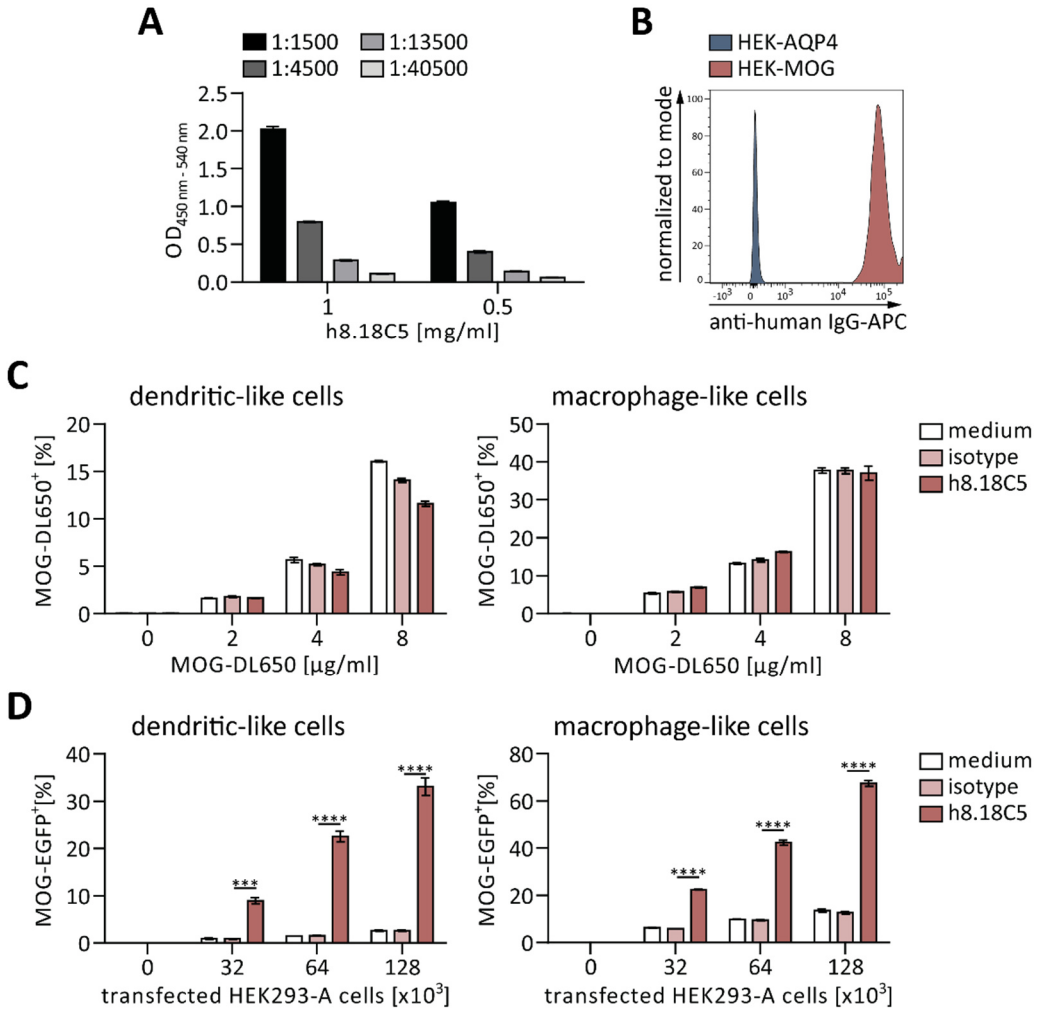

Figure 6: The uptake of membrane-bound but not of soluble MOG can be fostered by humanized 8.18C5 antibody. A) Detection of the in HEK293-A cells produced, humanized 8.18C5 (h8.18C5) antibody by MOG ELISA. The ELISA plate was coated with human MOG_{1-125} and 1:1500, 1:4500, 1:13500 and 1:40500 dilutions of 0.5 mg/ml and 1 mg/ml h8.18C5 were applied; OD = optical density; mean ± SEM; n = 2. **B)** Analysis of the binding capacity of h8.18C5 to membrane-bound MOG using CBA. HEK293-A cells, which stably expressed human MOG (HEK-MOG) or AQP4 (HEK-AQP4) on the cell surface, were incubated with h8.18C5 and bound h8.18C5 antibody was detected with APC-labeled anti-human IgG antibody. **C, D)** Dendritic-like and macrophage like cells were incubated with **(C)** soluble human MOG (MOG-DL650) or **(D)** HEK293-A cells expressing MOG-EGFP in the presence of hIgG1 isotype control or h8.18C5 for 2 h. The frequency of $MOG\text{-}DL650^+$ and $MOG\text{-}EGFP^+$ cells, respectively, was quantified by flow cytometry; mean [%] ± SEM gated on intact $CD11c^+CD14^-$ dendritic-like cells or $CD11c^+CD14^+$ macrophage-like cells; n = 3; representative data of 2 independent experiments; two-sided *t* test of isotype vs. h8.18C5.

3.1.4 Patient-derived anti-MOG antibodies opsonize human MOG

After demonstrating that *in vitro* differentiated APCs are capable of internalizing MOG and recognizing opsonized membrane-bound MOG, the opsonizing capacity of human anti-MOG antibodies was investigated. For this purpose, the effect of IgG and serum samples from MOGAD patients on the phagocytosis activity of dendritic-like and macrophage-like cells was analyzed.

3.1.4.1 IgG isolated from MOGAD patients facilitate MOG recognition to human antigen-presenting cells

In the first experimental approach, whole IgG isolated from a Sjogren's syndrome patient, which served as negative control, and 3 different MOGAD patients (Fig. 7A, 8A) were tested for their ability to opsonize human MOG. Anti-MOG antibody seropositivity of the purified IgG samples was verified by CBA, revealing that anti-MOG antibody positive IgG #1 and #3 exhibited the highest antibody levels (Fig. 7B). Since previous experiments showed that opsonization of membrane-bound but not of soluble MOG resulted in an increased protein uptake by human phagocytes (see section 3.1.3), *in vitro* differentiated APCs were first incubated with HEK293-A cells expressing MOG-EGFP in the presence of purified IgG. As indicated in Fig. 7C and D, all anti-MOG antibody positive IgG samples significantly enhanced the uptake of MOG-EGFP by dendritic-like and macrophage-like cells, whereas anti-MOG antibody negative IgG had no impact on the ingestion rate. Reflecting the findings of the CBA, anti-MOG antibody positive IgG #2 exhibited the lowest efficiency in promoting protein internalization (Fig. 7D). To prove that the observed ingestion increase is specific for human MOG, the aforementioned experimental setup was repeated with HEK293-A cells expressing human AQP4-EmGFP instead of human MOG-EGFP. Neither anti-MOG antibody negative nor anti-MOG antibody positive IgG enhanced the uptake of membrane-bound AQP4 by human phagocytes (Fig. 7E). These results show that human anti-MOG antibodies can specifically opsonize membrane-bound human MOG, fostering its internalization by antigen-presenting cells.

A

α-MOG Ab$^{-/+}$ IgG	Patient's clinical key feature
MOG Ab$^-$ IgG	Sjogren's syndrome
MOG Ab$^+$ IgG #1	LETM
MOG Ab$^+$ IgG #2	bilateral ON
MOG Ab$^+$ IgG #3	bilateral ON

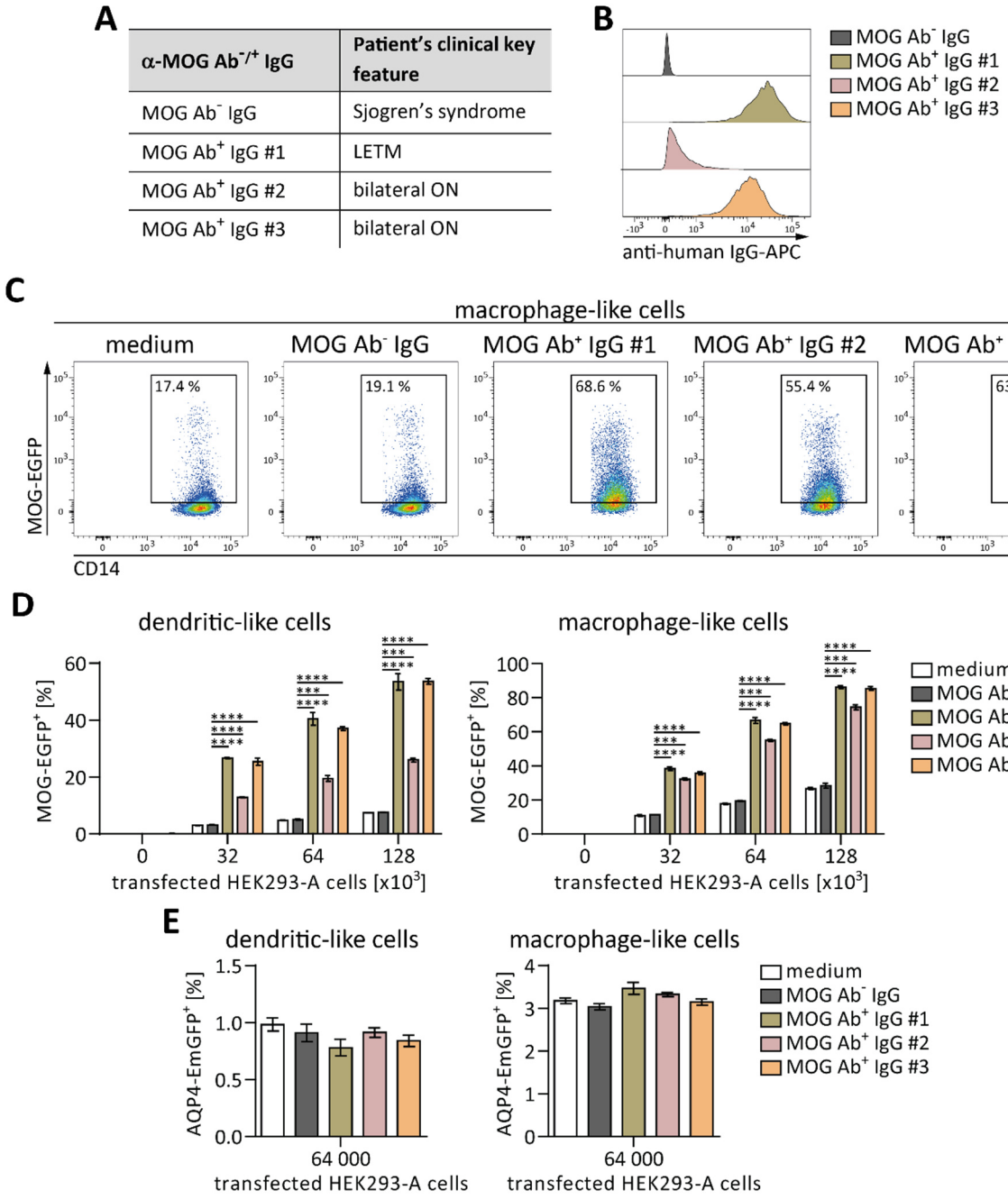

Figure 7: Whole IgG isolated from MOGAD patients significantly increase the internalization of membrane-bound MOG by human phagocytes. A) Overview of the purified whole IgG samples from anti-MOG antibody (Ab) negative/positive patients and the corresponding clinical features. **B)** Anti-MOG antibody positivity of the isolated IgG samples was determined using CBA. HEK293-A cells stably expressing human MOG on the cell surface were incubated with whole IgG and bound anti-MOG antibodies were detected with APC-labeled anti-human IgG antibody. **C, D)** Generated APCs were incubated with HEK293-A cells transiently expressing MOG-EGFP in the presence of anti-MOG antibody negative or positive whole IgG for 2 h. **(C)** Representative flow cytometry plots of macrophage-like cells. **(D)** Mean frequency of MOG-EGFP$^+$ cells ± SEM gated on intact CD11c$^+$CD14$^-$ dendritic-like cells or CD11c$^+$CD14$^+$ macrophage-like cells; n = 3; representative data of 3 independent experiments; one-way ANOVA with Dunnett's multiple comparison test of MOG Ab$^-$ IgG vs. MOG Ab$^+$ IgG samples. **E)** Dendritic-like and macrophage-like cells were incubated with HEK293-A cells transiently expressing AQP4-EmGFP on the surface and anti-MOG antibody negative/positive whole IgG for 2 h. Mean [%] of AQP4-EmGFP$^+$ cells ± SEM gated on intact CD11c$^+$CD14$^-$ dendritic-like cells or CD11c$^+$CD14$^+$ macrophage-like cells; n = 3; representative data of 2 independent experiments; one-way ANOVA with Dunnett's multiple comparison test of MOG Ab$^-$ IgG vs. MOG Ab$^+$ IgG samples.

Although opsonization of soluble MOG mediated by humanized 8.18C5 antibody did not affect the phagocytosis rate of *in vitro* differentiated APCs (see section 3.1.3), it was still examined whether patient-derived anti-MOG antibodies can opsonize soluble human MOG. To assess the ability to bind soluble MOG, anti-MOG antibody negative and positive IgG samples were analyzed by MOG ELISA. Anti-MOG antibody positive IgG #2 and #3 recognized soluble human MOG with IgG #3 exhibiting a higher binding affinity than IgG #2 (Fig. 8B). However, only anti-MOG antibody positive IgG #2 facilitated antigen recognition to dendritic-like and macrophage-like cells, resulting in an increased uptake of soluble human MOG (Fig. 8C, D). This effect was specific for MOG, as the replacement of human MOG by ovalbumin protein nullified the observed ingestion enhancement (Fig. 8E). Taken together, these findings indicate that some patient-derived anti-MOG antibodies are also capable of opsonizing soluble human MOG, thus promoting its uptake by human phagocytes.

A

α-MOG Ab$^{-/+}$ IgG	Patient's clinical key feature
MOG Ab$^-$ IgG	Sjogren's syndrome
MOG Ab$^+$ IgG #1	LETM
MOG Ab$^+$ IgG #2	bilateral ON
MOG Ab$^+$ IgG #3	bilateral ON

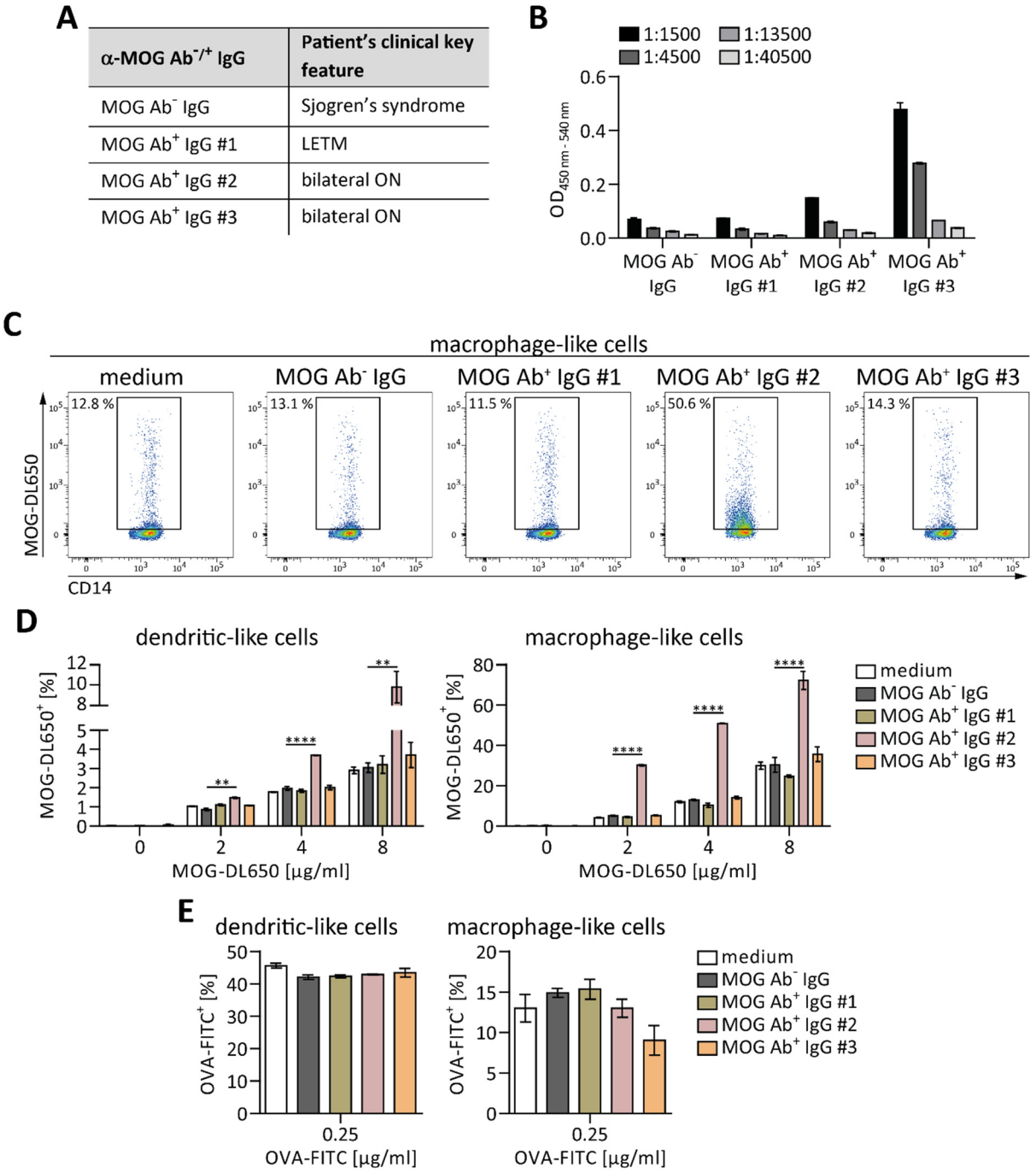

Figure 8: Patient-derived anti-MOG antibody positive IgG partially facilitate the uptake of soluble MOG by human APCs. A) Overview of the purified whole IgG samples from anti-MOG antibody (Ab) negative/positive patients and the corresponding clinical features. **B)** Analysis of the soluble MOG-binding capacity of the isolated IgG samples using MOG ELISA. 1:1500, 1:4500, 1:13500 and 1:40500 dilutions of whole IgG were applied; OD = optical density; mean ± SEM; n = 2. **C, D)** Dendritic-like and macrophage-like cells were incubated with soluble human MOG (MOG-DL650) in the presence of anti-MOG antibody negative or positive whole IgG for 2 h. **C)** Representative flow cytometry plots of macrophage-like cells. **D)** Mean frequency of MOG-DL650$^+$ cells ± SEM gated on intact CD11c$^+$CD14$^-$ dendritic-like cells or CD11c$^+$CD14$^+$ macrophage-like cells; n = 3; representative data of 3 independent experiments; one-way ANOVA with Dunnett's multiple comparison test of MOG Ab$^-$ IgG vs. MOG Ab$^+$ IgG samples. **E)** Generated phagocytes were incubated with FITC-labeled ovalbumin (OVA-FITC) and anti-MOG antibody negative/positive whole IgG for 2 h. Mean frequency ± SEM gated on intact CD11c$^+$CD14$^-$ dendritic-like cells or CD11c$^+$CD14$^+$ macrophage-like cells; n = 3; representative data of 2 independent experiments; one-way ANOVA with Dunnett's multiple comparison test of MOG Ab$^-$ IgG vs. MOG Ab$^+$ IgG samples.

3.1.4.2 Anti-MOG antibody positive serum enhances the ingestion of human MOG by myeloid antigen-presenting cells

To achieve more physiological conditions, the isolated IgG samples, which possessed concentrated anti-MOG antibody levels due to purification, were substituted by patient-derived serum samples. Blood sera from 6 MOGAD patients were collected and anti-MOG antibody seropositivity was verified using CBA (Fig. 9A, B). As negative control, sera from 3 healthy controls were mixed and anti-MOG antibody seronegativity was confirmed by CBA (Fig. 9B). The opsonizing capacity of the serum samples was assessed by incubating them with HEK293-A cells expressing MOG-EGFP and dendritic-like or macrophage-like cells. All anti-MOG antibody positive sera significantly increased the MOG uptake by human APCs compared to anti-MOG antibody negative serum, with serum #1 and #5 exhibiting the greatest impact (Fig. 9C). The observed enhancement was specific for human MOG as serum containing MOG-specific antibodies did not promote the internalization of human AQP4 expressed on HEK293-A cells (Fig. 9D). These results further emphasize the ability of patient-derived anti-MOG antibodies to opsonize human MOG, thus fostering antigen recognition by human APCs.

A

α-MOG Ab$^{-/+}$ serum	Patient's clinical key feature
MOG Ab$^-$ serum	healthy controls
MOG Ab$^+$ serum #1	LETM
MOG Ab$^+$ serum #2	LETM
MOG Ab$^+$ serum #3	LETM
MOG Ab$^+$ serum #4	LETM
MOG Ab$^+$ serum #5	LETM
MOG Ab$^+$ serum #6	LETM

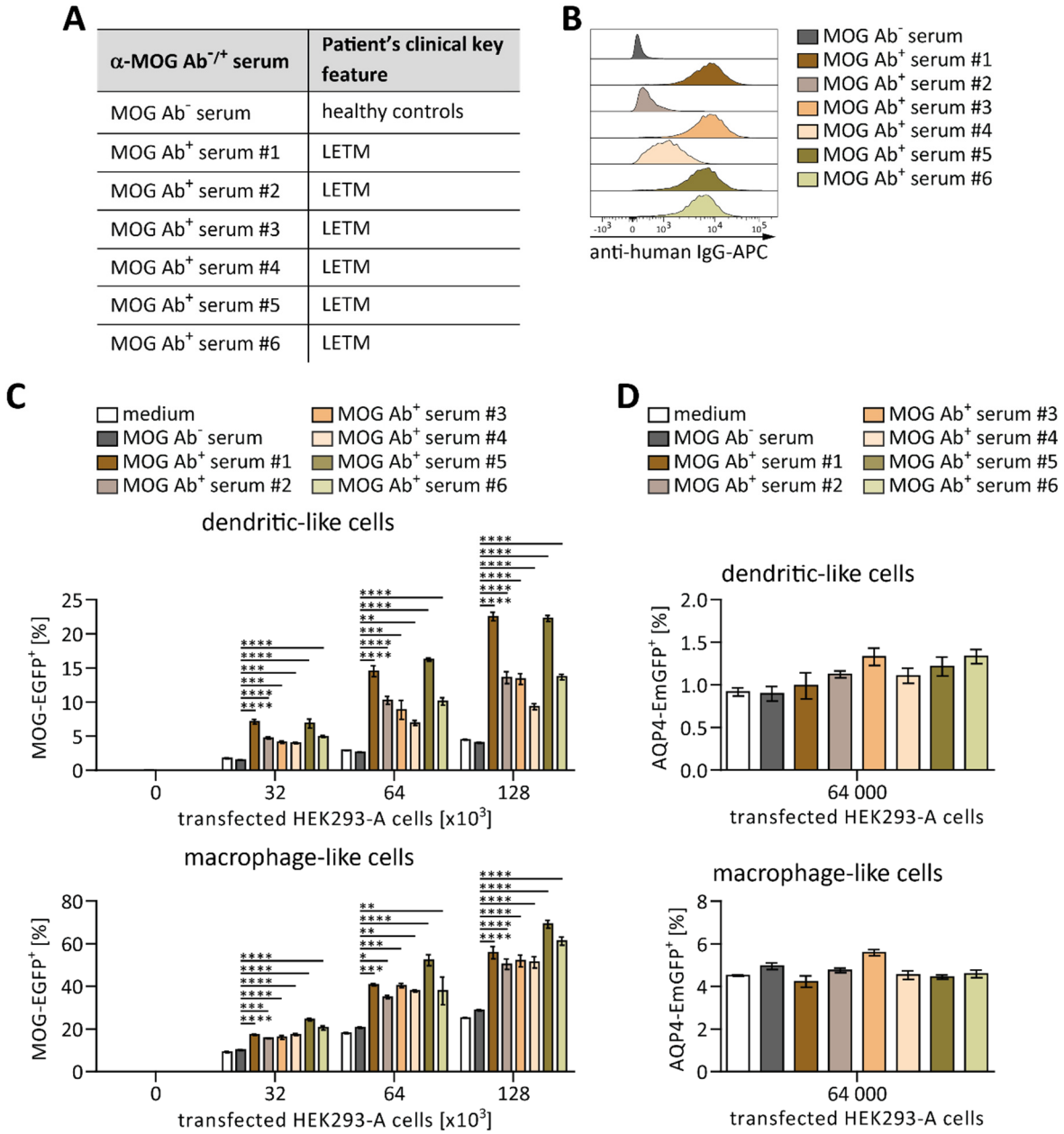

Figure 9: Human anti-MOG antibody positive serum strongly promotes the recognition of membrane-bound MOG by APCs. A) Overview of serum samples from healthy controls and anti-MOG antibody (Ab) positive patients with the corresponding clinical features. **B)** Anti-MOG antibody seropositivity of the isolated serum samples was determined using CBA. HEK293-A cells stably expressing human MOG on the cell surface were incubated with serum and bound anti-MOG antibodies were detected with APC-labeled anti-human IgG antibody. **C)** Generated phagocytes were incubated with HEK293-A cells expressing MOG-EGFP on the surface in the presence of anti-MOG antibody negative or positive serum for 2 h. The frequency of MOG-EGFP$^+$ cells was quantified by flow cytometry and is indicated as mean ± SEM, gated on intact CD11c$^+$CD14$^-$ dendritic-like cells or CD11c$^+$CD14$^+$ macrophage-like cells; n = 3; representative data of 3 independent experiments; one-way ANOVA with Dunnett's multiple comparison test of MOG Ab$^-$ serum vs. MOG Ab$^+$ serum samples. **D)** Dendritic-like and macrophage-like cells were incubated with HEK293-A cells transiently expressing AQP4-EmGFP and anti-MOG antibody negative/positive serum for 2 h. Mean frequency of AQP4-EmGFP$^+$ cells ± SEM gated on intact CD11c$^+$CD14$^-$ dendritic-like cells or CD11c$^+$CD14$^+$ macrophage-like cells; n = 3; representative data of 2 independent experiments; one-way ANOVA with Dunnett's multiple comparison test of MOG Ab$^-$ serum vs. MOG Ab$^+$ serum samples.

3.1.5 MOG-specific antibodies potentially mediate antigen recognition to macrophage-like cells via Fcγ receptor III

After demonstrating that patient-derived anti-MOG antibodies foster protein uptake by *in vitro* differentiated phagocytes, it was analyzed how this process affects their expression of FcγRs and molecules involved in antigen presentation. Hence, dendritic-like and macrophage-like cells were incubated with HEK293-A cells expressing human MOG-EGFP in the presence of anti-MOG antibody negative or positive serum for 2 h and 18 h. Two time points were chosen to assess short- and long-term effects in myeloid APCs. Subsequently, the protein ingestion as well as the expression of FcγRs, CD40, CD80, CD86 and MHCII on human APCs was determined. As reported in chapter 3.1.4.2, the addition of serum containing anti-MOG antibodies strongly enhanced the internalization of human MOG by APCs after 2 h. However, this effect was vanished after 18 h (Fig. 10A). On dendritic-like cells, neither the expression of FcγRs nor of molecules involved in antigen presentation was altered by anti-MOG antibody positive serum (Fig. 10B, C). By contrast, macrophage-like cells displayed a significantly reduced detectability of FcγR III in the presence of anti-MOG antibody positive serum after 2 h and 18 h (Fig. 10B). Moreover, the expression of FcγR I and II was also diminished in the presence of serum containing MOG-specific antibodies (Fig. 10B). The addition of MOGAD patient-derived serum further reduced the expression of CD40 and MHCII on macrophage-like cells after 18 h (Fig. 10C). In summary, these findings suggest that macrophage-like cells potentially recognize and internalize MOG opsonized by anti-MOG antibodies via FcγR III.

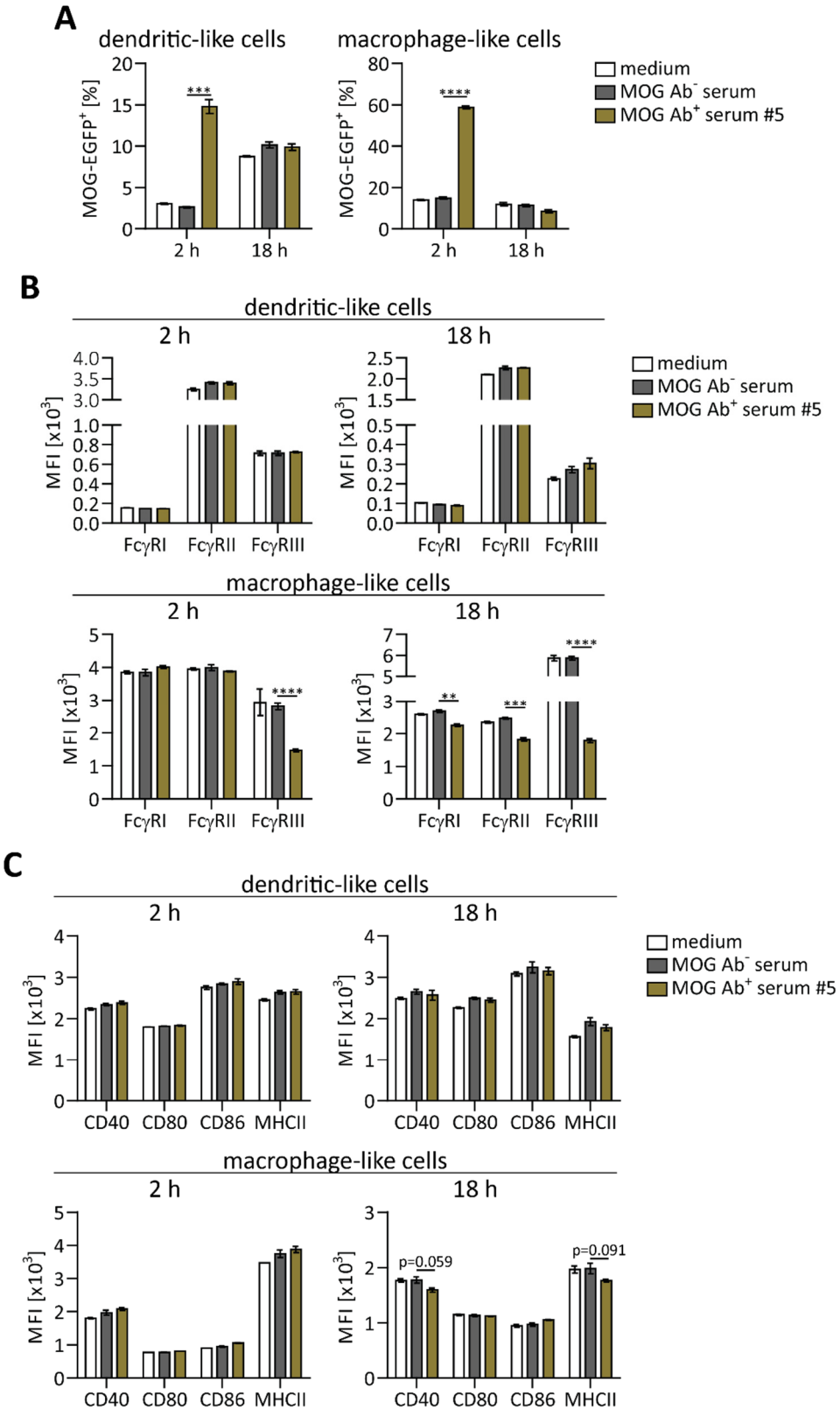

Figure 10: *In vitro* generated macrophage-like cells are assumed to recognize MOG opsonized by anti-MOG antibodies via FcγR III. Dendritic-like and macrophage-like cells were incubated with HEK293-A cells expressing human MOG-EGFP on the cell surface in the presence of anti-MOG antibody (Ab) negative/positive serum for 2 h and 18 h, respectively. The **(A)** phagocytosis rate of the generated cells as well as the expression of **(B)** FcγRs and **(C)** molecules involved in antigen presentation was determined using flow cytometry. **(A)** Mean frequency of MOG-EGFP$^+$ cells ± SEM and **(B, C)** mean fluorescence intensity (MFI) ± SEM gated on intact CD11c$^+$CD14$^-$ dendritic-like

cells or $CD11c^+CD14^+$ macrophage-like cells; n = 3; representative data of 2 independent experiments; two-sided *t* test of MOG Ab^- serum vs. MOG Ab^+ serum.

3.1.6 Anti-AQP4 antibody-mediated opsonization of membrane-bound AQP4 facilitates its ingestion by human phagocytes

In NMOSD, AQP4-specific antibodies are known to bind AQP4 expressed on astrocytes and trigger astrocyte destruction via CDC and ADCC (Alexopoulos et al. 2015; Phuan et al. 2012; Vincent et al. 2008). However, it is uncertain if opsonization of AQP4 may also represent an effector mechanism of anti-AQP4 antibodies. It was therefore investigated whether patient-derived anti-AQP4 antibodies are capable of opsonizing AQP4, thus fostering its uptake by human APCs. In the first experimental setup, whole IgG were isolated from 3 NMOSD patients and anti-AQP4 antibody seropositivity of the purified IgG samples was confirmed by CBA (Fig. 11A, B). Dendritic-like and macrophage-like cells were incubated with HEK293-A cells expressing human AQP4-EmGFP in the presence of anti-AQP4 antibody negative or positive IgG and internalization of AQP4-EmGFP was subsequently quantified. All IgG samples containing AQP4-specific antibodies enhanced the frequency of AQP4-EmGFP positive cells (Fig. 11C, D). However, the phagocytosis rate of macrophage-like cells was stronger increased than that of dendritic-like cells (Fig. 11D). When applying HEK293-A which expressed human MOG instead of AQP4, the promoting effect of NMOSD patient-derived IgG was zeroed (Fig. 11E).

In a second experimental approach, the effect of anti-AQP4 antibody positive serum on the ingestion activity of human APCs was analyzed. For this purpose, serum from 3 NMOSD patients was isolated and anti-AQP4 antibody seropositivity was confirmed by CBA (Fig. 12A, B). All anti-AQP4 antibody positive serum samples elevated the uptake of human AQP4 expressed on HEK293-A cells by *in vitro* generated APCs, with macrophage-like cells displaying a stronger increase in the ingestion activity compared to dendritic-like cells (Fig. 12C). By contrast, serum containing AQP4-reactive antibodies had no effect on the internalization of membrane-bound MOG-EGFP by human phagocytes, indicating that anti-AQP4 antibodies specifically recognize human AQP4 (Fig. 12D). In conjunction, these findings demonstrate that patient-derived anti-AQP4 antibodies are capable of opsonizing AQP4 und thus promote antigen uptake by human APCs.

A

α-AQP4 Ab$^{-/+}$ IgG	Patient's clinical key feature
AQP4 Ab^{-} IgG	Sjogren's syndrome
AQP4 Ab^{+} IgG #1	LETM
AQP4 Ab^{+} IgG #2	ON
AQP4 Ab^{+} IgG #3	LETM

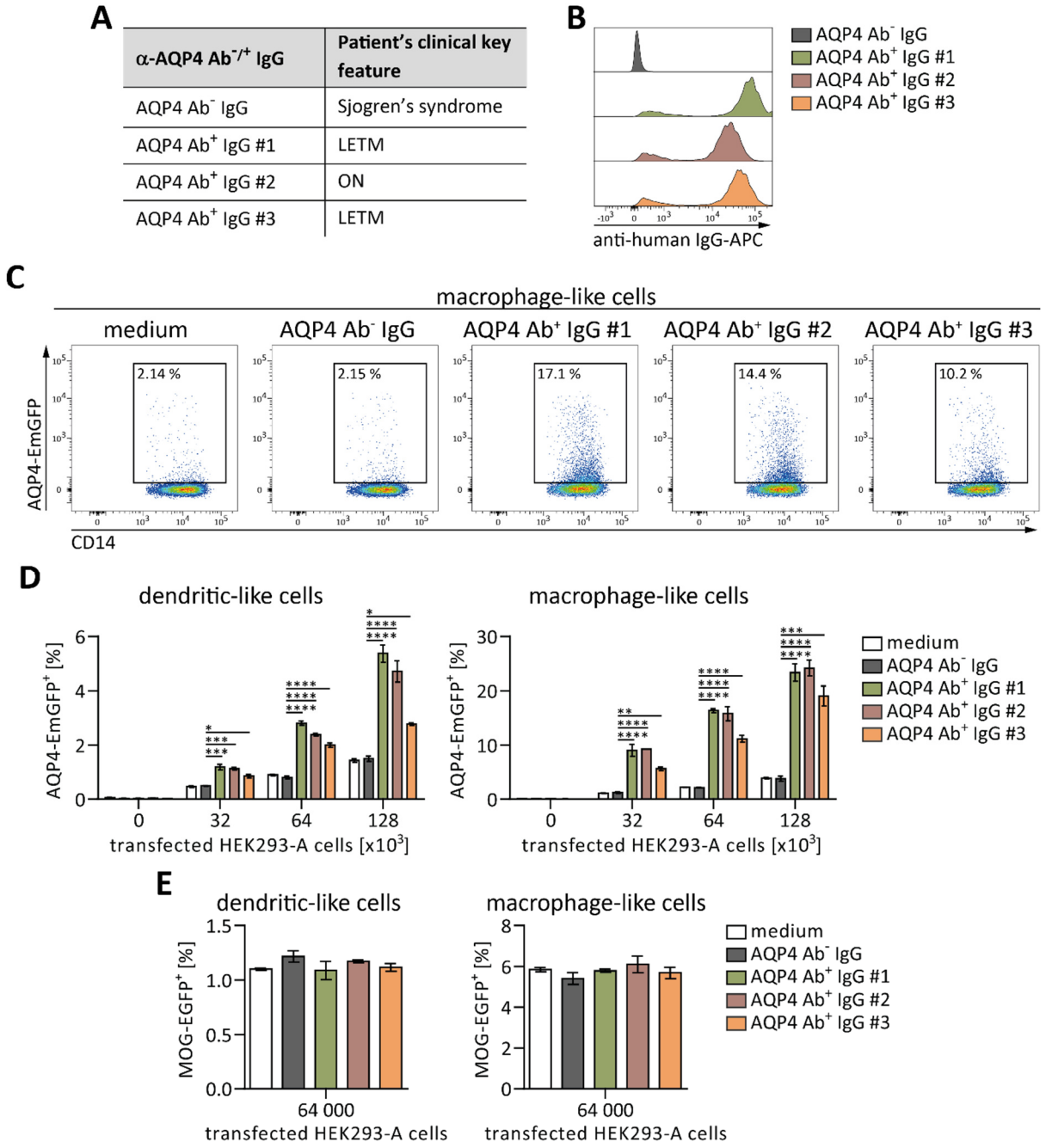

Figure 11: The ingestion of membrane-bound AQP4 is significantly enhanced in the presence of whole IgG purified from NMOSD patients. A) Overview of the purified whole IgG samples from anti-AQP4 antibody (Ab) negative/positive patients and the corresponding clinical features. **B)** Anti-AQP4 antibody positivity of the isolated IgG samples was determined using CBA. HEK293-A cells stably expressing human AQP4 on the cell surface were incubated with whole IgG and bound anti-AQP4 antibodies were detected with APC-labeled anti-human IgG antibody. **C, D)** Generated phagocytes were incubated with HEK293-A cells transiently expressing AQP4-EmGFP in the presence of anti-AQP4 antibody negative or positive whole IgG for 2 h. **C)** Representative flow cytometry plots of macrophage-like cells. **D)** Mean frequency of AQP4-EmGFP^{+} cells ± SEM gated on intact CD11c^{+}CD14^{-} dendritic-like cells or CD11c^{+}CD14^{+} macrophage-like cells; n = 3; representative data of 3 independent experiments; one-way ANOVA with Dunnett's multiple comparison test of AQP4 Ab^{-} IgG vs. AQP4 Ab^{+} IgG samples. **E)** Myeloid APCs were incubated with HEK293-A cells expressing MOG-EGFP and anti-AQP4 antibody negative/positive whole IgG for 2 h. Mean [%] ± SEM gated on intact CD11c^{+}CD14^{-} dendritic-like cells or CD11c^{+}CD14^{+} macrophage-like cells; n = 3; representative data of 2 independent experiments; one-way ANOVA with Dunnett's multiple comparison test of AQP4 Ab^{-} IgG vs. AQP4 Ab^{+} IgG samples.

A

α-AQP4 Ab$^{-/+}$ serum	Patient's clinical key feature
AQP4 Ab^{-} serum	healthy controls
AQP4 Ab^{+} serum #1	ON
AQP4 Ab^{+} serum #2	ON
AQP4 Ab^{+} serum #3	LETM

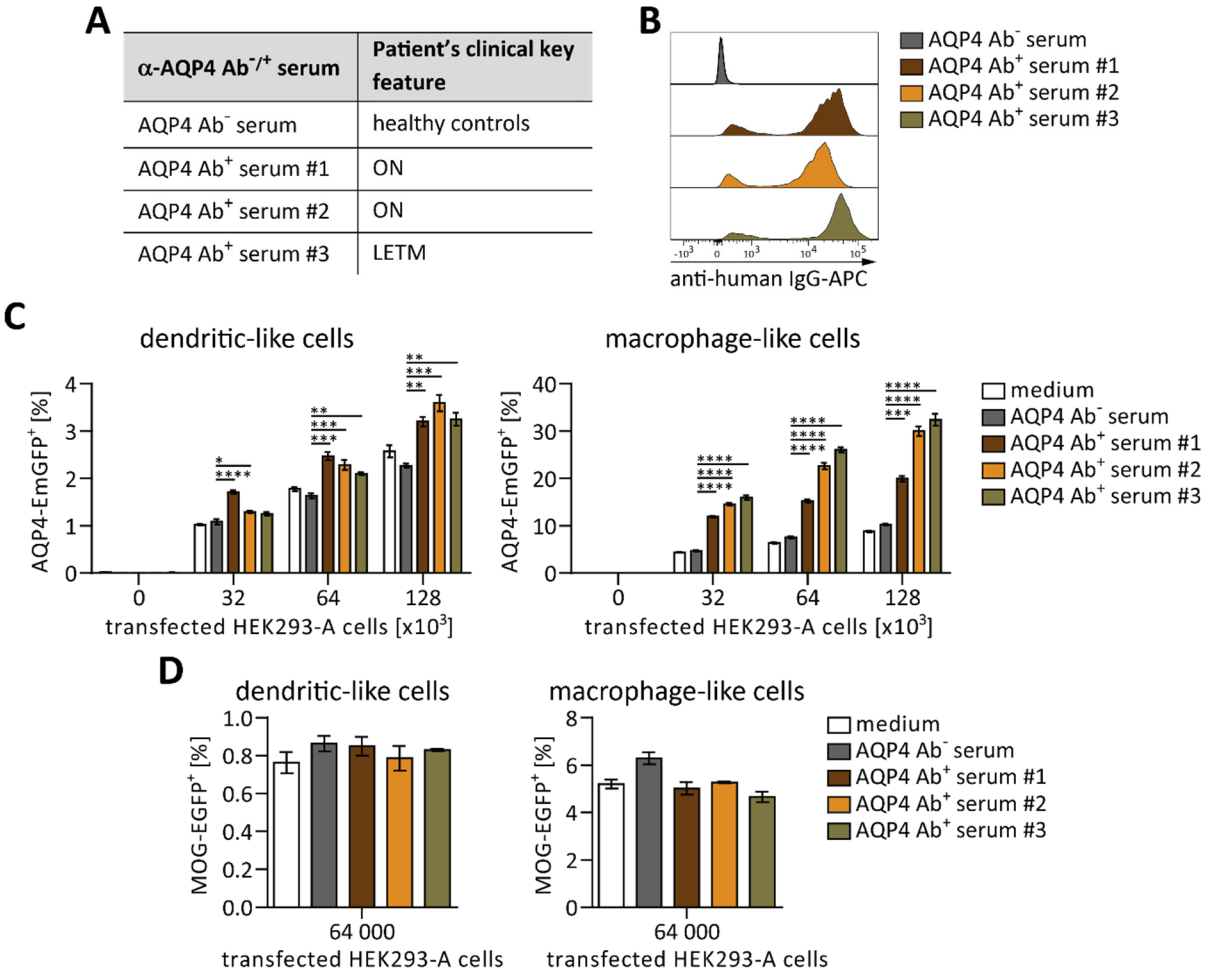

Figure 12: Patient-derived anti-AQP4 antibody positive serum fosters the recognition of membrane-bound AQP4 by human phagocytes. A) Overview of serum samples from healthy controls and anti-AQP4 antibody (Ab) positive patients with the corresponding clinical features. **B)** Anti-AQP4 antibody seropositivity of the isolated serum samples was determined using CBA. HEK293-A cells stably expressing human AQP4 on the cell surface were incubated with serum and bound anti-AQP4 antibodies were detected with APC-labeled anti-human IgG antibody. **C)** Dendritic-like and macrophage-like cells were incubated with HEK293-A cells expressing AQP4-EmGFP on the cell surface in the presence of anti-AQP4 antibody negative or positive serum for 2 h. The frequency of AQP4-EmGFP^{+} cells was quantified by flow cytometry and is depicted as mean ± SEM, gated on intact CD11c^{+}CD14^{-} dendritic-like cells or CD11c^{+}CD14^{+} macrophage-like cells; n = 3; representative data of 2 independent experiments; one-way ANOVA with Dunnett's multiple comparison test of AQP4 Ab^{-} serum vs. AQP4 Ab^{+} serum samples. **D)** Human phagocytes were incubated with HEK293-A cells expressing MOG-EGFP and anti-AQP antibody negative/ positive serum for 2 h. Mean frequency of MOG-EGFP^{+} cells ± SEM gated on intact CD11c^{+}CD14^{-} dendritic-like cells or CD11c^{+}CD14^{+} macrophage-like cells; n = 3; representative data of 2 independent experiments; one-way ANOVA with Dunnett's multiple comparison test of AQP4 Ab^{-} serum vs. AQP4 Ab^{+} serum samples.

3.2 Project 2: Inhibition of Bruton's tyrosine kinase as a therapeutic strategy for anti-MOG antibody-mediated CNS demyelination

The second project of the present study focused on the therapeutic potential of BTK inhibitor evobrutinib in anti-MOG antibody-triggered CNS demyelination. Since BTK is required for FcγR signaling in myeloid cells (Koprulu and Ellmeier 2009; Lopez-Herrera et al. 2014), its inhibition can be a promising strategy to prevent activation of myeloid cells induced by anti-MOG antibody-mediated opsonization. Thus, the effect of evobrutinib on myeloid cells activated by MOG-specific antibodies was investigated *in vitro* and in an anti-MOG antibody-driven EAE model *in vivo*.

3.2.1 *In vitro* differentiated phagocytes express BTK and its inhibition diminishes the anti-MOG antibody-mediated increase in MOG uptake by macrophage-like cells

Before applying BTK inhibitor evobrutinib in the *in vitro* model established in project 1, the intracellular expression of BTK by *in vitro* differentiated phagocytes was determined, showing that both dendritic-like and macrophage-like cells highly expressed BTK (Fig. 13A). Afterwards, it was analyzed how BTK inhibition affects the phagocytosis activity as all as the expression of surface markers by human APCs in the presence of anti-MOG antibody negative and positive serum. For this purpose, the same experimental setup described in chapter 3.1.5 was used. Since anti-MOG antibody-mediated opsonization only promoted protein uptake after an incubation of 2 h (see section 3.1.5), internalization of membrane-bound MOG by human phagocytes is only depicted for this time point in Fig. 13A. Evobrutinib did not alter the phagocytosis rate of dendritic-like cells in the presence of anti-MOG antibody negative or positive serum. In contrast, BTK inhibition diminished the anti-MOG antibody-mediated increase in the ingestion of MOG by macrophage-like cells, without affecting the phagocytosis in the presence of anti-MOG antibody negative serum (Fig. 13B). The expression of FcγRs on dendritic-like cells was not modified by evobrutinib, neither after 2 h nor 18 h (Fig. 13C). However, macrophage-like cells exhibited an increased surface expression of FcγR III in the presence of evobrutinib when serum containing MOG-specific antibodies was applied. This effect was also observed in the presence of anti-MOG antibody negative serum, but only after 18 h (Fig. 13D). As depicted in Fig. 14A and B, the expression of molecules involved in antigen presentation by *in vitro* differentiated APCs was not affected by evobrutinib after 2 h incubation, regardless of the presence of anti-MOG antibody negative or positive serum. After 18 h however, inhibition of BTK resulted in a decreased expression of CD86 on dendritic-like

and macrophage-like cells as well as a significantly reduced CD40 expression by dendritic-like cells in the presence of anti-MOG antibody positive serum (Fig. 14A, B). Taken together, these results indicate that evobrutinib partially blocks the anti-MOG antibody-mediated phagocytosis increase of macrophage-like cells, with simultaneously elevating the surface expression of FcγR III. Furthermore, BTK inhibition reduces the expression of co-stimulatory molecules on human phagocytes in the presence of anti-MOG antibody positive serum.

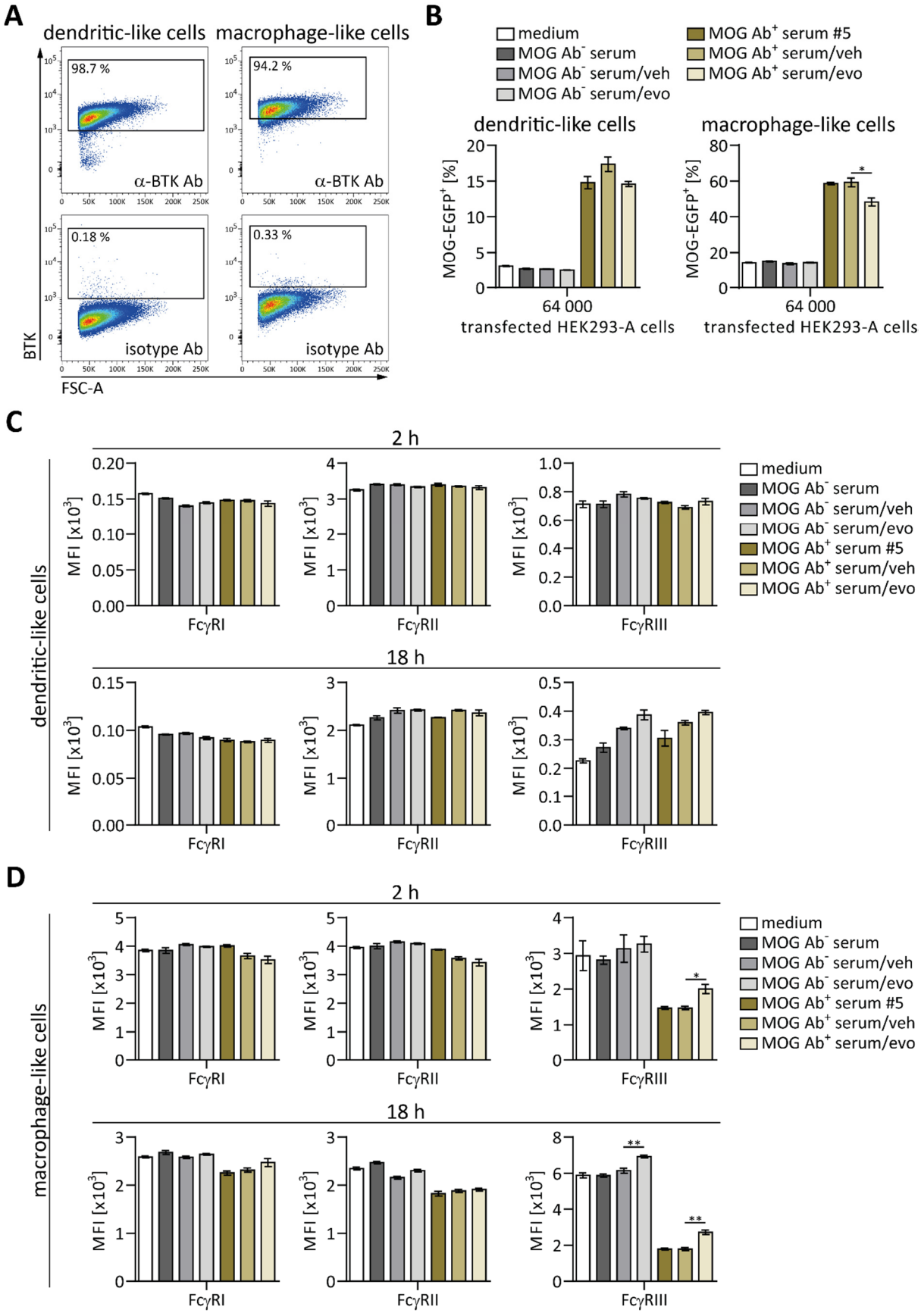
A
dendritic-like cells
macrophage-like cells
98.7 %
94.2 %
α-BTK Ab
0.18 %
0.33 %
isotype Ab
BTK
FSC-A
B
medium
MOG Ab⁻ serum
MOG Ab⁻ serum/veh
MOG Ab⁻ serum/evo
MOG Ab⁺ serum #5
MOG Ab⁺ serum/veh
MOG Ab⁺ serum/evo
dendritic-like cells
macrophage-like cells
MOG-EGFP⁺ [%]
64 000
transfected HEK293-A cells
C
2 h
18 h
dendritic-like cells
MFI [x10³]
FcγRI
FcγRII
FcγRIII
D
macrophage-like cells

Figure 13: BTK inhibitor evobrutinib affects the anti-MOG antibody-mediated increase in phagocytosis and the FcγR III expression of macrophage-like cells. A) The intracellular expression of BTK by dendritic-like and macrophage-like cells was analyzed using Phosflow. Representative flow cytometry plots of 3 independent experiments. **B – D)** Human phagocytes were pre-incubated with evobrutinib (evo) or vehicle (veh, 20 % Kleptose buffer) for 60 min, followed by addition of HEK293-A cells expressing human MOG-EGFP and anti-MOG antibody (Ab) negative or positive serum. The cells were then incubated for 2 h or 18 h and **(B)** the phagocytosis activity and **(C, D)** FcγR expression of the generated cells were assessed by flow cytometry. **B)** Internalization of MOG-EGFP by human APCs after 2 h incubation. Mean frequency of MOG-EGFP$^+$ cells ± SEM gated on intact CD11c$^+$CD14$^-$ dendritic-like cells or CD11c$^+$CD14$^+$ macrophage-like cells; n = 3; two-sided *t* test. **C, D)** Mean fluorescence intensity (MFI) ± SEM gated on intact **(C)** CD11c$^+$CD14$^-$ dendritic-like cells or **(D)** CD11c$^+$CD14$^+$ macrophage-like cells; n = 3; two-sided *t* test of vehicle vs. evobrutinib for MOG Ab$^-$ and Ab$^+$ serum.

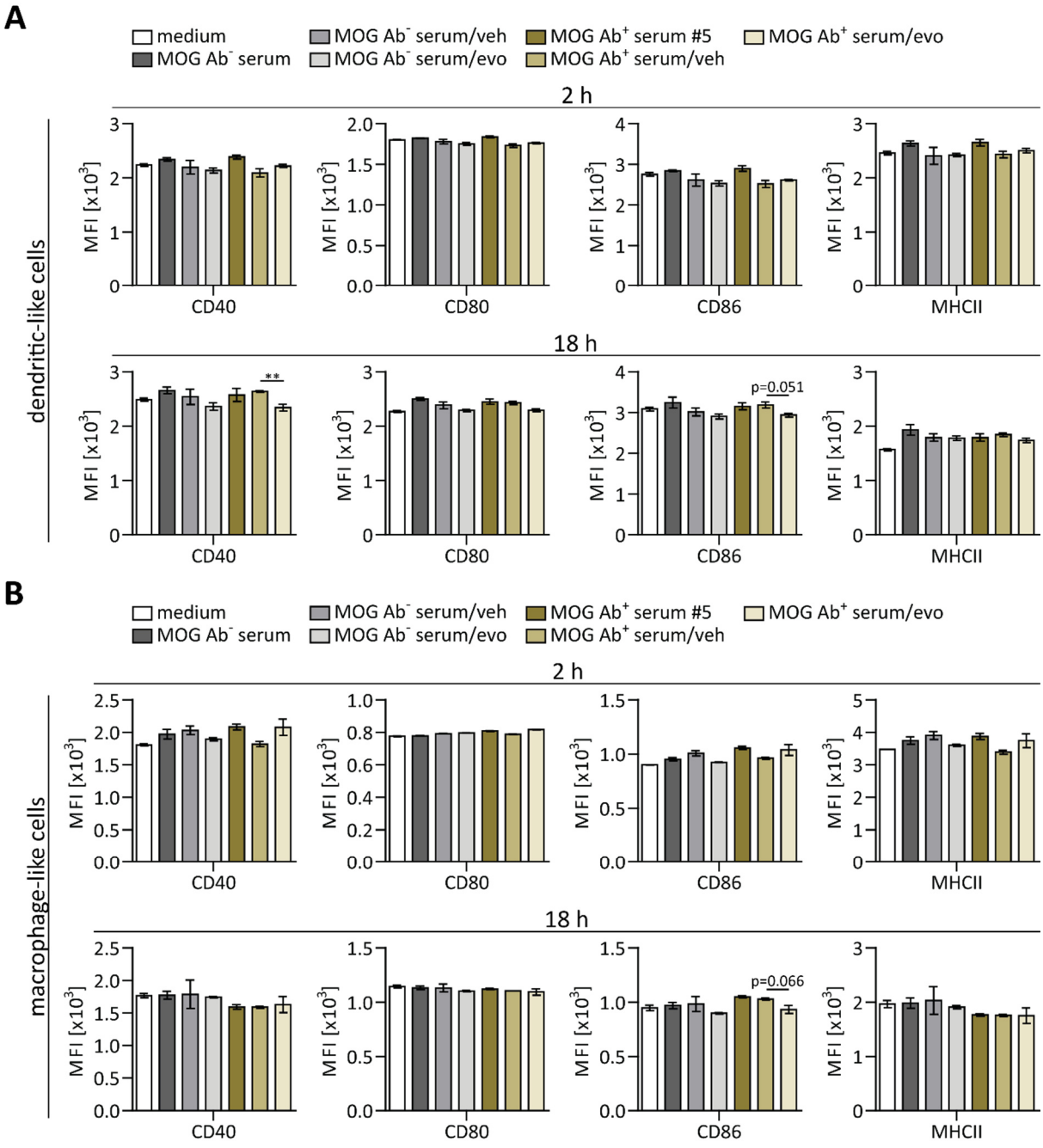

Figure 14: BTK inhibition diminishes the expression of co-stimulatory molecules by human phagocytes only in the presence of anti-MOG antibody positive serum. Generated APCs were pre-incubated with evobrutinib (evo) or vehicle (veh, 20 % Kleptose buffer) for 60 min, and HEK293-A cells expressing human MOG-EGFP plus anti-MOG antibody (Ab) negative or positive serum were subsequently added, followed by an incubation of 2 h or 18 h. The expression of molecules involved in antigen presentation on **(A)** dendritic-like and **(B)** macrophage-like cells was analyzed by flow cytometry and is shown as the mean fluorescence intensity (MFI) ± SEM, gated on intact $CD11c^+CD14^-$ dendritic-like cells or $CD11c^+CD14^+$ macrophage-like cells; n = 3; two-sided *t* test of vehicle vs. evobrutinib for MOG Ab^- and Ab^+ serum.

3.2.2 In wildtype mice, evobrutinib did neither affect the differentiation nor the phenotype of myeloid cells

In the first *in vivo* setting, the impact of BTK inhibition on B lymphocytes, myeloid cells and T cells in the absence of inflammation was assessed. For this purpose, non-transgenic 2D2 mice (termed WT mice) were treated with evobrutinib or vehicle and immune cells from spleen, inguinal and cervical lymph nodes were subsequently analyzed. To verify that evobrutinib treatment was effective, the maturation of B lymphocytes was examined, since Torke and colleagues demonstrated that evobrutinib inhibits B cell maturation by specifically blocking the development of follicular I B cells (Torke et al. 2020). In accordance with the aforementioned study, an accumulation of follicular II B cells and a simultaneous reduction of follicular I B lymphocytes was observed in all analyzed compartments upon treatment with evobrutinib, indicating that evobrutinib treatment was successful (Fig. 15A, B). Next, the effect of BTK inhibition on the immune cell composition was investigated, revealing that BTK inhibition did not specifically alter the frequency of B cells and T lymphocytes in the analyzed organs. However, evobrutinib slightly reduced the frequency of $CD11b^+$ cells in the spleen (Fig. 15C). To determine the effect of evobrutinib on $CD11b^+$ myeloid cells more in detail, they were divided into neutrophils, eosinophils and monocytes/macrophages. The latter population was further subdivided into inflammatory and resident cells (Fig. 15D). As depicted in Fig. 15E and F, evobrutinib did not alter the differentiation of myeloid cells in general nor of monocytes and macrophages. Since we assume that monocytes and macrophages represent the most involved myeloid cell types in the pathogenesis of anti-MOG antibody-driven EAE, it was further investigated how evobrutinib influences the phenotype of these cells. BTK inhibition had no effect on the expression of FcγRs or molecules involved in activation and antigen presentation, respectively (Fig. 15G, 16A). Finally, the impact of evobrutinib on the composition and activation of T cells was examined. Although T lymphocytes do not express BTK (Neys et al. 2021; Torke and Weber 2020), evobrutinib increased the frequency of $CD4^+$ T cells in cervical lymph nodes (Fig. 16B). In addition, it diminished the expression of CD95 on $CD4^+$ T lymphocytes isolated from spleen (Fig. 16C). In summary, these findings show that in the absence of inflammation, evobrutinib potently inhibits B cell maturation but does not affect the differentiation or phenotype of myeloid cells in regard to the analyzed parameters. Furthermore, evobrutinib was found to alter the T cell

composition and the expression of CD95 on $CD4^+$ T cells, which may be due to off-target effects or secondary effects mediated by other immune cells.

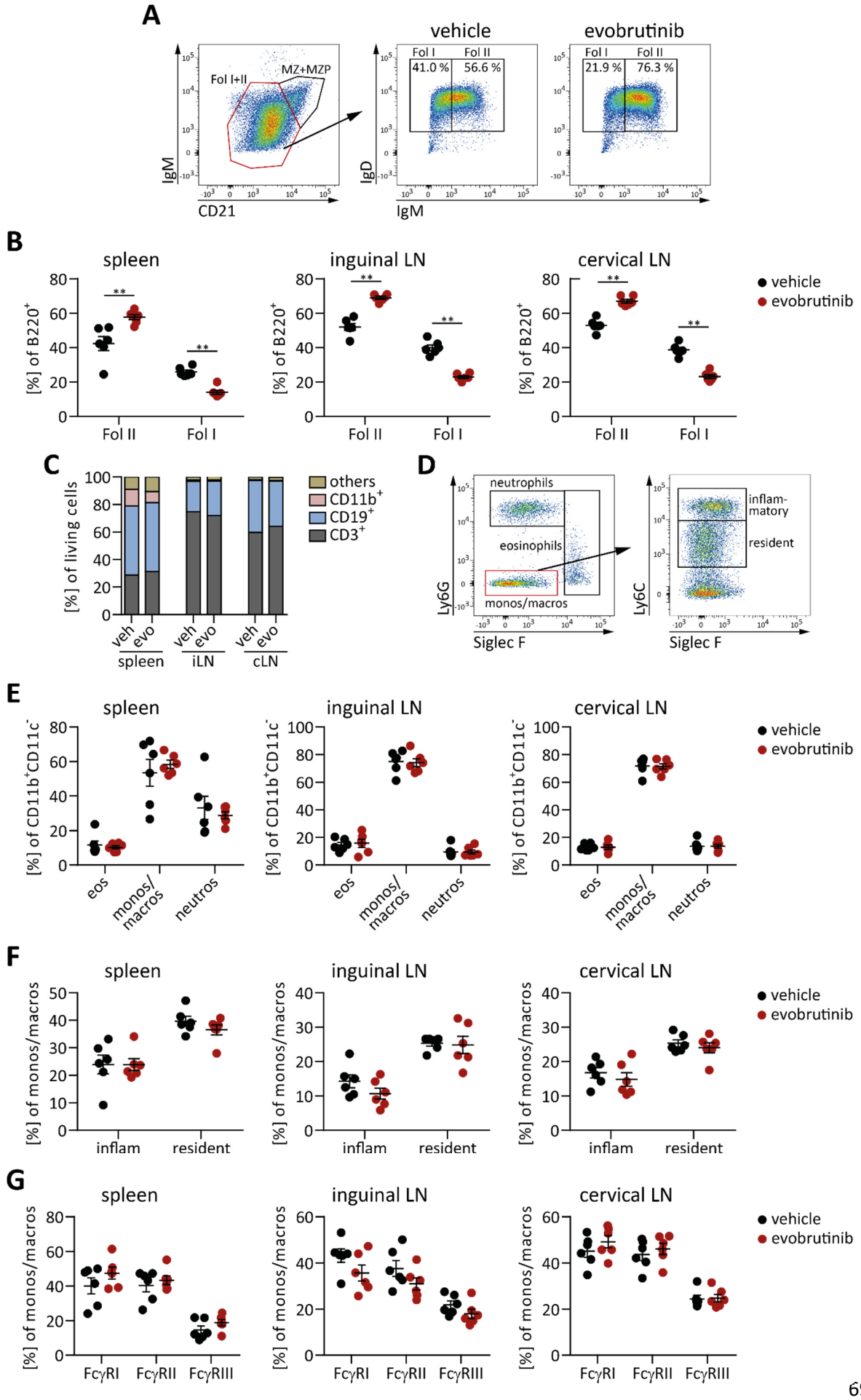
A
vehicle
evobrutinib
Fol I+II
MZ+MZP
IgM
CD21
Fol I
Fol II
41.0 %
56.6 %
21.9 %
76.3 %
IgD
IgM
B
spleen
inguinal LN
cervical LN
[%] of B220+
Fol II
Fol I
vehicle
evobrutinib
C
[%] of living cells
others
CD11b+
CD19+
CD3+
veh
evo
spleen
iLN
cLN
D
neutrophils
eosinophils
monos/macros
Ly6G
Siglec F
inflam-matory
resident
Ly6C
E
[%] of CD11b+CD11c-
eos
monos/ macros
neutros
F
[%] of monos/macros
inflam
resident
G
FcγRI
FcγRII
FcγRIII

Figure 15: Evobrutinib alters the maturation of B cells but not the phenotype of myeloid cells in WT mice. Non-transgenic 2D2 mice (= WT mice) were treated daily with vehicle (veh) or evobrutinib (evo) for 21 days. Subsequently, immune cells from spleen, inguinal and cervical lymph nodes (LN) were isolated and analyzed by flow cytometry; n = 6 mice/group; Mann-Whitney U test. **A)** Gating strategy to identify follicular B cells. $B220^+$ cells were separated into $CD19^+$ and $CD19^-$ cells (gating not shown). $CD19^+$ cells were divided into follicular (Fol) cells and marginal zone (MZ) + marginal zone precursor (MZP) cells. Follicular B cells were further subdivided into Fol I and Fol II cells. **B)** Mean [%] Fol II and Fol I cells of $B220^+$ cells ± SEM. **C)** Composition of immune cells, depicted as mean [%] of living cells; iLN = inguinal lymph node, cLN = cervical lymph node. **D)** Gating strategy to identify subtypes of myeloid cells. $CD11b^+CD11c^-$ cells were divided into neutrophils, eosinophils and monocytes/macrophages (monos/macros). Monocytes/macrophages were further subdivided into inflammatory and resident populations. **E)** Mean frequency of eosinophils (eos), monocytes/macrophages (monos/macros) and neutrophils (neutros) ± SEM gated on $CD11b^+CD11c^-$ cells. **F)** Mean [%] inflammatory (inflam) and resident monocytes of monocytes/macrophages population ± SEM. **G)** Expression of FcγRs on monocytes and macrophages, indicated in mean [%] ± SEM.

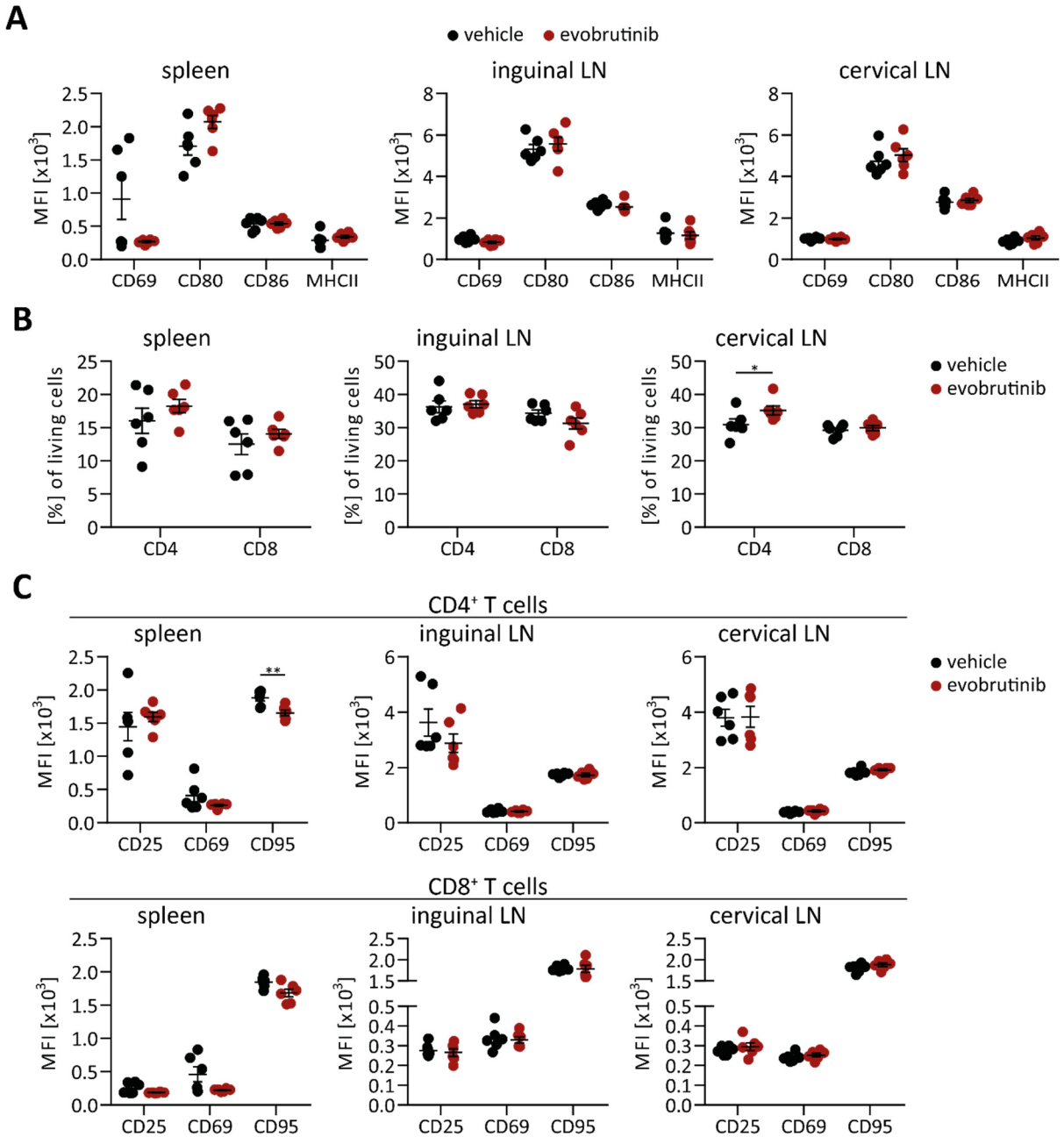

Figure 16: The T cell composition and the expression of CD95 on CD4⁺ T cells is affected by evobrutinib. Non-transgenic 2D2 mice (= WT mice) were treated daily with vehicle or evobrutinib for 21 days. Subsequently, immune cells from spleen, inguinal and cervical lymph nodes (LN) were isolated and analyzed by flow cytometry; n = 6 mice/group; Mann-Whitney U test. **A)** Mean fluorescence intensity (MFI) ± SEM of molecules involved in activation and antigen presentation, gated on monocytes/macrophages. **B)** Composition of T cells, depicted in mean [%] of living cells ± SEM. **C)** Expression of activation markers on CD4⁺ and CD8⁺ T cells, shown as mean fluorescence intensity ± SEM.

3.2.3 Evobrutinib inhibits anti-MOG antibody-triggered EAE

Next, the effect of BTK inhibition was analyzed in an inflammatory *in vivo* setting. For this purpose, evobrutinib was applied in an anti-MOG antibody-driven EAE model established by Kinzel and colleagues (Kinzel et al. 2016). In detail, transgenic 2D2 mice containing MOG-

specific T cells were treated with evobrutinib and EAE was induced by repetitive injections of the anti-MOG antibody clone 8.18C5 (Fig. 17A). The impact of evobrutinib on the clinical and histological outcome as well as on the phenotype of immune cells from spleen, inguinal and cervical lymph nodes was determined.

3.2.3.1 BTK inhibitor evobrutinib significantly reduces anti-MOG antibody-mediated CNS inflammation

To first verify that evobrutinib treatment did not affect the serum level of the applied 8.18C5 antibody and thus interfere with disease induction per se, serum was isolated from 2D2 mice on day 18 and 39 after the first antibody transfer and anti-MOG antibody levels were determined by MOG ELISA. Indicated in Fig. 17B, vehicle and evobrutinib mice receiving 8.18C5 antibody exhibited equal anti-MOG antibody titer. However, no MOG-specific antibodies were detected in the blood of control mice receiving isotype antibody (clone MOPC-21).

In total, 4 out of 18 vehicle-treated mice receiving 8.18C5 antibody developed clinical signs of EAE, with an average maximal EAE score of 3.9 (Fig. 17C, D; Table 20). By contrast, none of 18 8.18C5 antibody recipients treated with evobrutinib developed EAE. Moreover, none of isotype antibody recipients treated with vehicle or evobrutinib exhibited clinical symptoms of EAE (Fig. 17C; Table 20). These findings were further supported by histological analyses of the spinal cord. 9 out of 18 vehicle treated mice receiving 8.18C5 antibody revealed inflammatory CNS demyelination, whereas only 2 out of 18 8.18C5 recipients treated with evobrutinib showed CNS inflammation (Fig. 18A, B; Table 20). In the majority of 8.18C5/vehicle mice with CNS demyelination, inflammation was characterized by a pronounced infiltration of T cells and macrophages. In contrast, the degree of immune cell infiltration was significantly diminished in 8.18C5 recipients treated with evobrutinib (Fig. 18C, D). However, mice receiving isotype antibody did not exhibit inflammatory CNS demyelination nor immune cell infiltration (Fig. 18 A – D; Table 20), which is in accordance with experimental observations by Kinzel and colleagues (Kinzel et al. 2016). In conjunction, these findings demonstrate that BTK inhibition by evobrutinib potently reduces inflammatory CNS demyelination caused by anti-MOG antibodies, thus preventing clinical symptoms of EAE.

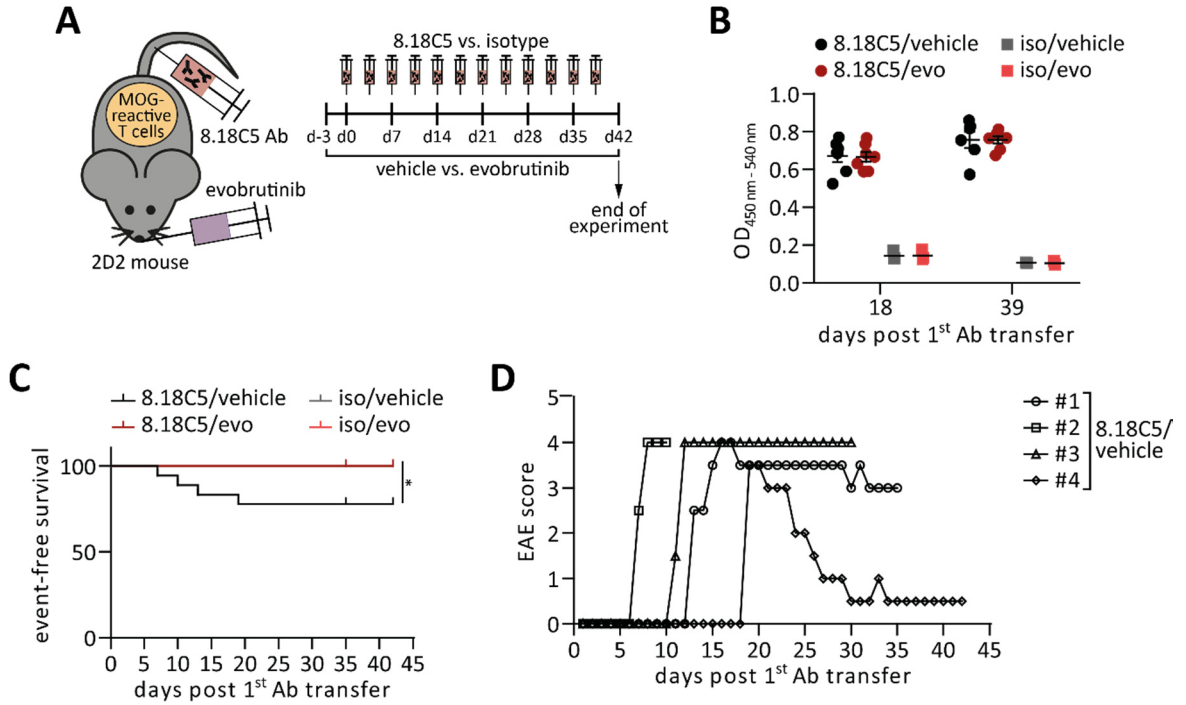

Figure 17: Inhibition of BTK prevents the development of anti-MOG antibody-mediated EAE in 2D2 mice. Transgenic 2D2 mice were treated daily with vehicle or evobrutinib (evo) starting 3 days before the first antibody (Ab) transfer. They received repetitive injections of anti-MOG antibody 8.18C5 or isotype control (iso). **A)** Overview of the experimental setup. **B)** To monitor the anti-MOG antibody titer in the blood of 2D2 mice, serum was isolated on day 18 and 39 after the first antibody (Ab) transfer and anti-MOG antibodies were detected by MOG ELISA. 1:4500 dilution; n = 3 – 7 mice/group; representative data of 3 independent experiments; OD = optical density. **C)** The incidence of 2D2 mice developing clinical symptoms of EAE was plotted in a Kaplan-Meier curve. An event is defined as the day of EAE onset; n = 6 – 18 mice/group; Mantel-Cox logrank test. **D)** Individual EAE scores of 2D2 mice receiving 8.18C5 antibody and Kleptose buffer (vehicle).

Table 20: Summary of clinical and histological findings of treated 2D2 mice

Group	Number of animals with clinical symptoms	Mean max. EAE severity	Range EAE onset (days post 1st Ab transfer)	Number of animals with CNS demyelination
8.18C5/vehicle	4/18	3.9	7 – 19	9/18
8.18C5/evo	0/18	-	-	2/18
isotype/vehicle	0/7	-	-	0/7
isotype/evo	0/6	-	-	0/6

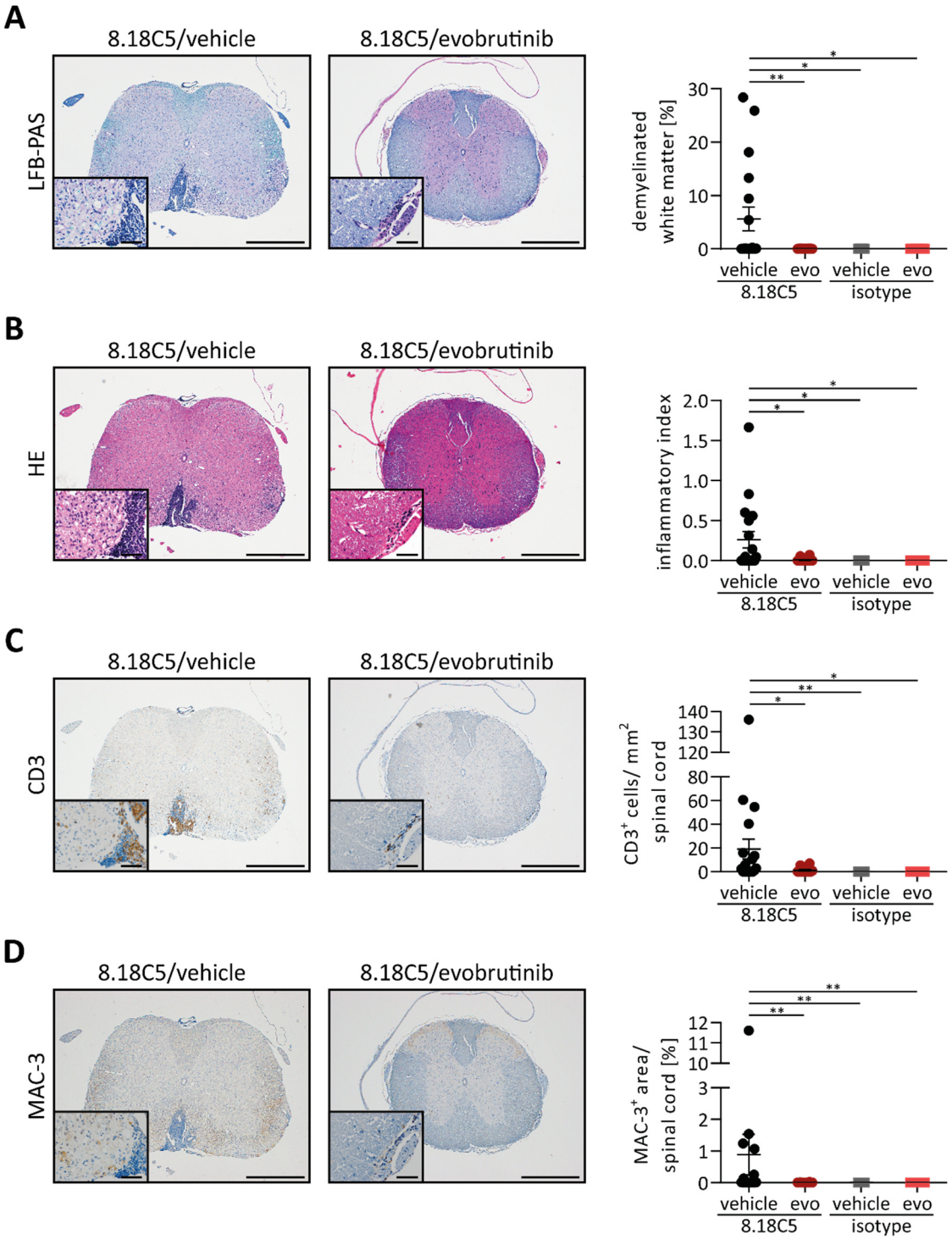

Figure 18: Evobrutinib significantly diminishes anti-MOG antibody-triggered CNS inflammation. Transgenic 2D2 mice were treated daily with vehicle or evobrutinib (evo) starting 3 days before the first antibody transfer. They received repetitive injections of anti-MOG antibody 8.18C5 or isotype control (iso). 42 days after the first antibody injection, histological analysis of the spinal cord was performed. Representative sections of mice receiving 8.18C5 and vehicle or evobrutinib are shown on the left side. Scale bar overview = 500 µm, scale bar inlay = 50 µm; n = 6 – 18 mice/group; Kruskal-Wallis test with Dunn's post hoc test between all groups. **A)** Demyelination of the spinal cord was visualized by LFB-PAS staining. Mean [%] of demyelinated white matter ± SEM. **B)** Inflammation of the spinal cord was visualized by HE staining. Mean inflammatory index ± SEM; 0 = no inflammation, 1 = slight inflammation, 2 = moderate inflammation, 3 = strong inflammation. **C)** Infiltration of T cells into the spinal cord was visualized by CD3 immunostaining. Mean $CD3^+$ cells/ mm^2 spinal cord ± SEM. **D)** Infiltration of macrophages into the spinal cord was visualized by MAC-3 immunostaining. Mean [%] of $MAC\text{-}3^+$ area/ spinal cord ± SEM.

3.2.3.2 Monocytes and macrophages display an activated phenotype in mice with CNS demyelination – a feature which may be prevented by evobrutinib

To identify the underlying mechanisms of EAE inhibition mediated by evobrutinib, immune cells from spleen, inguinal and cervical lymph nodes were analyzed. By determining the frequency of follicular I and II B cells, it was first verified that evobrutinib treatment was effective in 2D2 mice (see chapter 3.2.2.1). As depicted in Fig. 19A, evobrutinib blocked the maturation of follicular I B cells in all examined compartments of mice receiving 8.18C5 or isotype antibody, indicating that evobrutinib treatment was successful. Next, the immune cell composition in the analyzed organs was investigated, showing that neither BTK inhibition nor 8.18C5 antibody administration specifically altered the frequency of T cells, B lymphocytes and myeloid cells (Fig. 19B). Also, the differentiation of myeloid cells into eosinophils, monocytes/macrophages and neutrophils was not modified by evobrutinib or 8.18C5 antibody administration (Fig. 19C). However, a trend towards a reduced frequency of inflammatory monocytes/macrophages in the spleen of 8.18C5 antibody recipients was observed upon evobrutinib treatment (Fig. 19D). Interestingly, 8.18C5/vehicle mice that exhibited CNS demyelination (highlighted in purple) showed an increased frequency of inflammatory monocytes/macrophages and a corresponding reduced frequency of resident cells in the spleen compared to 8.18C5 recipients without CNS inflammation (Fig. 19D).

Next, the impact of evobrutinib on the phenotype of monocytes and macrophages was analyzed. BTK inhibition significantly diminished the expression of FcγR II by monocytes/macrophages in the spleen of 2D2 mice receiving anti-MOG antibodies (Fig. 20A). Similar findings were obtained for the expression of FcγR I on monocytes and macrophages, but a statistically significant difference was only achieved for the analysis of animals with signs of CNS demyelination (Fig. 20A, B). The expression of FcγR III on monocytes and macrophages in the spleen was not affected by BTK inhibition. Moreover, neither evobrutinib nor 8.18C5 antibody administration altered the expression of FcγRs on monocytes/macrophages in inguinal and cervical lymph nodes (Fig. 20A).

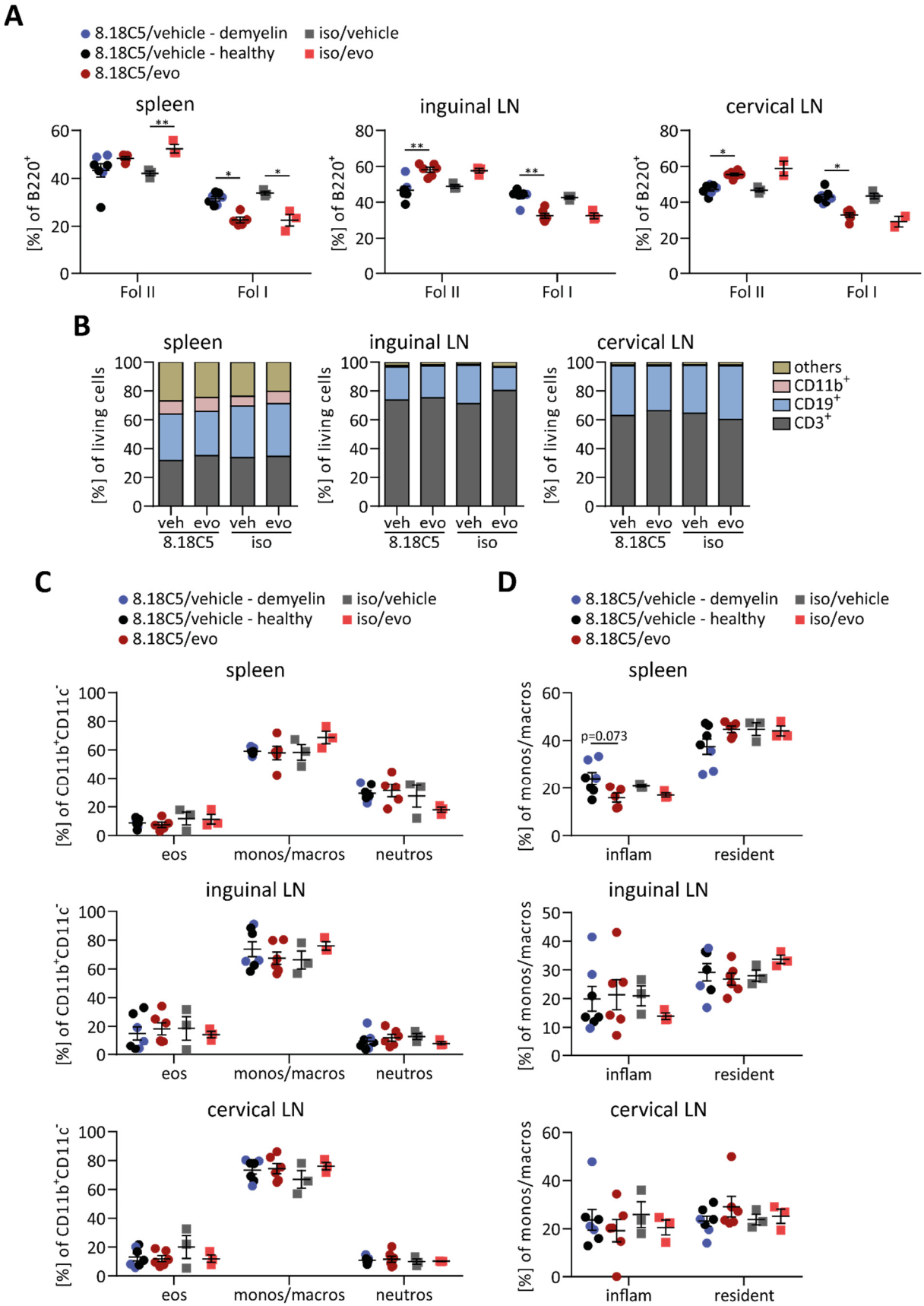
A
8.18C5/vehicle - demyelin
8.18C5/vehicle - healthy
8.18C5/evo
iso/vehicle
iso/evo
spleen
inguinal LN
cervical LN
[%] of B220+
Fol II
Fol I
B
spleen
inguinal LN
cervical LN
[%] of living cells
others
CD11b+
CD19+
CD3+
veh evo veh evo
8.18C5
iso
C
spleen
inguinal LN
cervical LN
[%] of CD11b+CD11c-
eos
monos/macros
neutros
D
spleen
inguinal LN
cervical LN
[%] of monos/macros
p=0.073
inflam
resident

Figure 19: Inhibition of BTK results in a reduction of inflammatory macrophages and monocytes in the spleen. Transgenic 2D2 mice were treated daily with vehicle (veh) or evobrutinib (evo) starting 3 days before the first antibody transfer. They received repetitive injections of anti-MOG antibody 8.18C5 or isotype control (iso). 42 days after the first antibody injection, immune cells from spleen, inguinal and cervical lymph nodes (LN) were isolated and analyzed by flow cytometry. 8.18C5/vehicle mice with CNS demyelination are highlighted in purple; n = 3 – 7 mice/group; representative data of 3 independent experiments; Kruskal-Wallis test with Dunn's multiple comparison test between all groups. **A)** Mean [%] Fol II and Fol I cells of $B220^+$ cells ± SEM. **B)** Composition of immune cells, depicted as mean [%] of living cells. **C)** Mean frequency of eosinophils (eos), monocytes/macrophages (monos/macros) and neutrophils (neutros) ± SEM gated on $CD11b^+CD11c^-$ cells. **D)** Mean [%] inflammatory (inflam) and resident cells of monocytes/ macrophages population ± SEM.

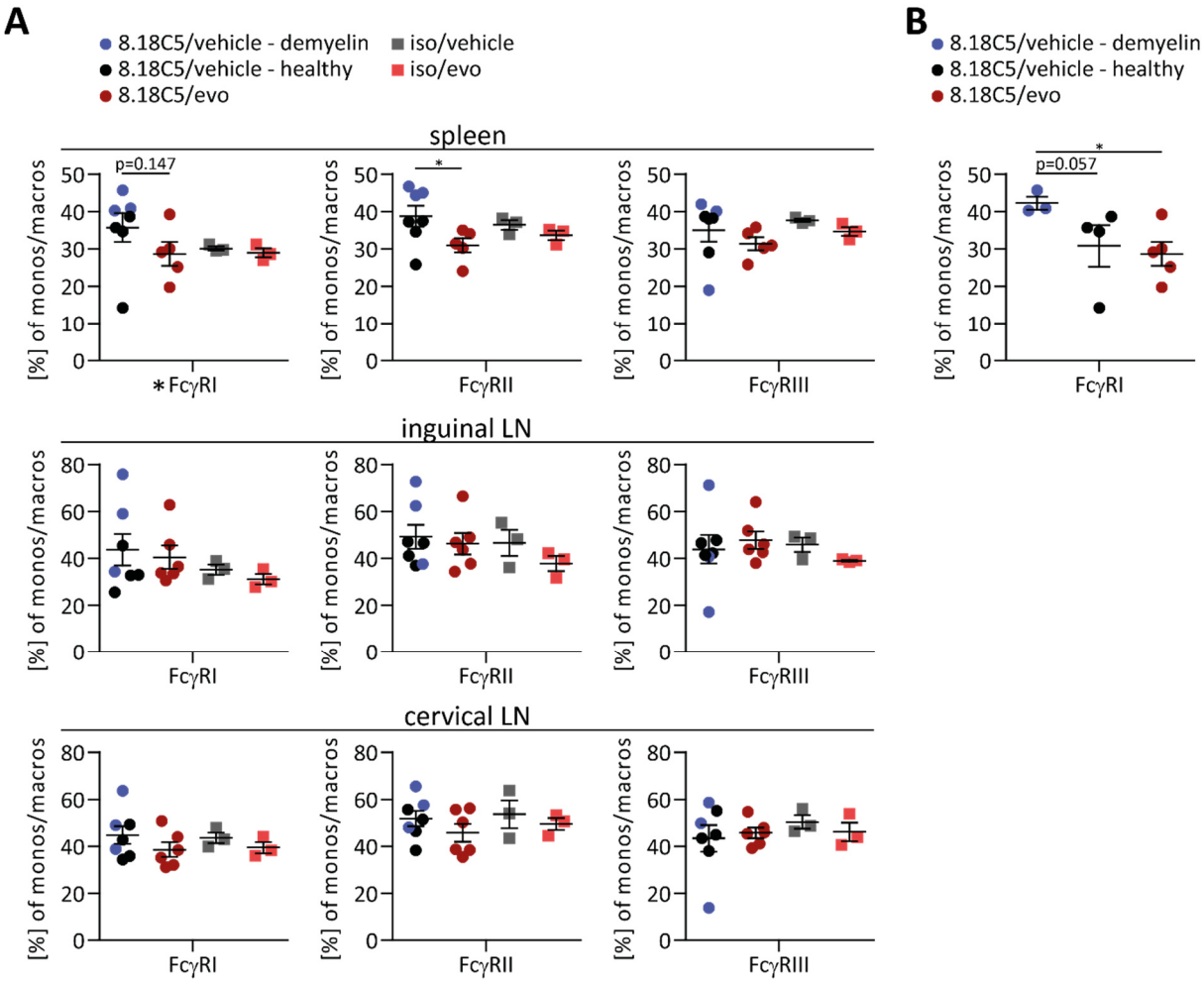

Figure 20: Evobrutinib diminishes the expression of FcγRs on monocytes and macrophages in mice receiving anti-MOG antibodies. Transgenic 2D2 mice were treated daily with vehicle or evobrutinib (evo) starting 3 days before the first antibody transfer. They received repetitive injections of anti-MOG antibody 8.18C5 or isotype control (iso). 42 days after the first antibody injection, immune cells from spleen, inguinal and cervical lymph nodes (LN) were isolated and analyzed by flow cytometry. 8.18C5/vehicle mice with CNS demyelination are highlighted in purple; n = 3 – 7 mice/group; representative data of 3 independent experiments; Kruskal-Wallis test with Dunn's multiple comparison test between all groups. **A, B)** Expression of FcγRs on monocytes and macrophages (monos/macros), indicated in mean [%] ± SEM. The FcγRI data set of the spleen (marked with an asterisk) was further split into demyelinated (demyelin) and healthy 8.18C5/vehicle mice and 8.18C5/evobrutinib mice, depicted in **(B)**.

Further phenotype analyses revealed that in all examined compartments, the expression of CD69, CD80, CD86 and MHCII on monocytes/macrophages was not significantly modified by evobrutinib treatment nor 8.18C5 antibody administration (Fig. 21A). Notably, monocytes and macrophages in the spleen of 2D2 mice with CNS inflammation did not only display an increased expression of FcγRs (Fig. 20A), they also exhibited a significantly higher expression of CD86 and MHCII than monocytes/macrophages of healthy 8.18C5/vehicle and 8.18C5/evobrutinib mice (Fig. 21A, B). In addition, the MHCII expression of monocytes and macrophages in cervical lymph nodes of demyelinated 8.18C5 antibody recipients was also strongly enhanced.

In summary, these findings indicate that in 2D2 mice with CNS demyelination, monocytes and macrophages are characterized by an inflammatory and activated phenotype. By reducing the expression of FcγRs on monocytes/macrophages, evobrutinib may prevent the pro-inflammatory activation of these cells in mice receiving anti-MOG antibodies.

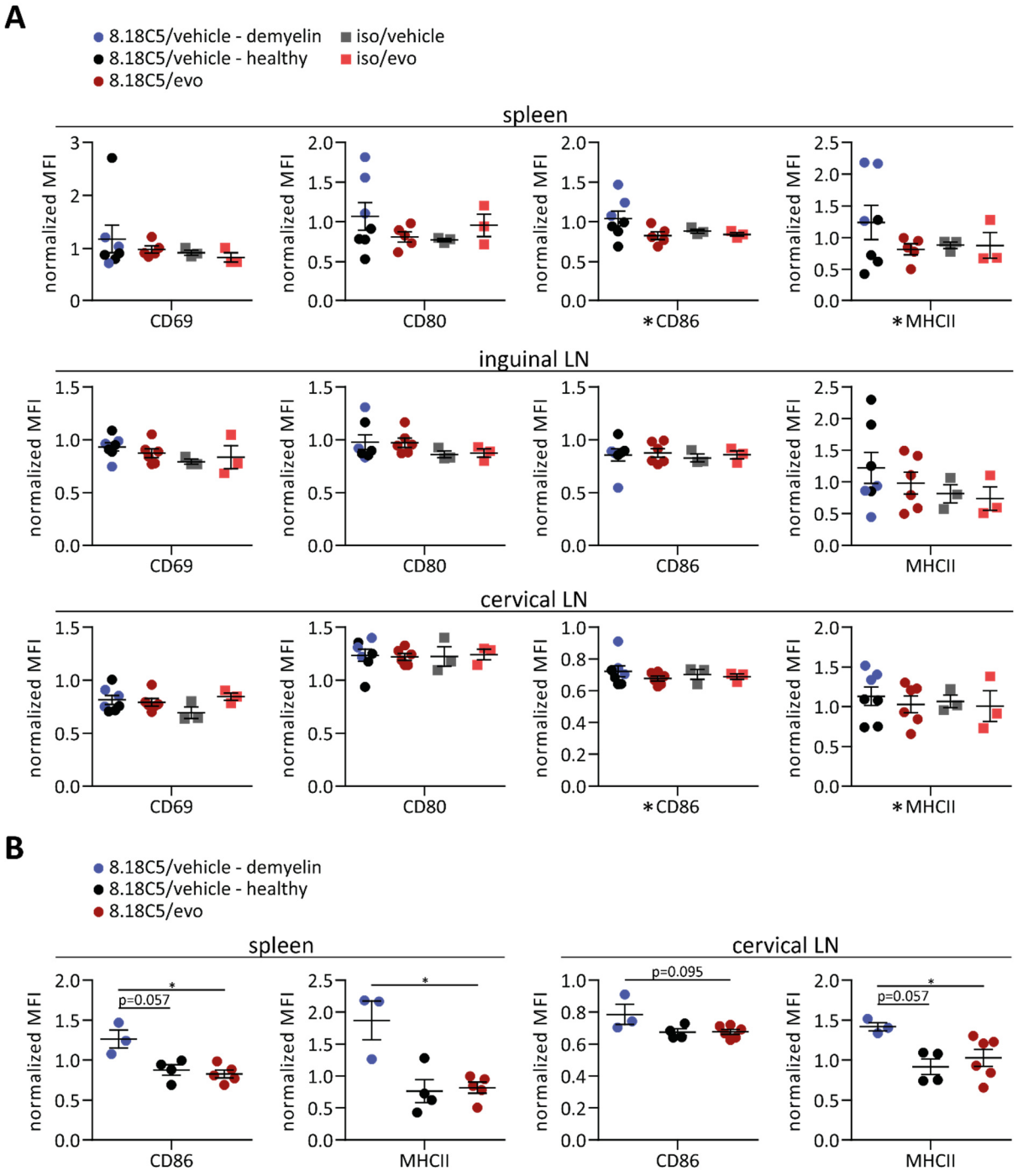

Figure 21: 2D2 mice with CNS inflammation display a higher expression of molecules involved in antigen presentation than healthy mice. Transgenic 2D2 mice were treated daily with vehicle or evobrutinib (evo) starting 3 days before the first antibody transfer. They received repetitive injections of anti-MOG antibody 8.18C5 or isotype control (iso). 42 days after the first antibody injection, immune cells from spleen, inguinal and cervical lymph nodes (LN) were isolated and analyzed by flow cytometry. 8.18C5/vehicle mice with CNS demyelination are highlighted in purple; n = 3 – 7 mice/group; representative data of 3 independent experiments; Kruskal-Wallis test with Dunn's multiple comparison test between all groups. **A, B)** Normalized mean fluorescence intensity (MFI) ± SEM of molecules involved in activation and antigen presentation, gated on monocytes/macrophages. CD86 and MHCII data sets of the spleen and cervical lymph nodes (marked with an asterisk) were further split into demyelinated (demyelin) and healthy 8.18C5/vehicle mice and 8.18C5/evobrutinib mice, shown in **(B)**.

3.2.3.3 Evobrutinib does not affect the composition and activation of T cells in secondary lymphoid tissue

After demonstrating that BTK inhibition alters the phenotype of myeloid cells, the impact of evobrutinib on T lymphocytes in secondary peripheral organs was investigated. As a first parameter, the composition of T cells was examined, indicating that neither anti-MOG antibody administration nor evobrutinib treatment affected the frequency of $CD4^+$ or $CD8^+$ T cells in the analyzed compartments (Fig. 22A). Similar findings were obtained for the activation of T lymphocytes in treated mice receiving 8.18C5 or isotype antibody, with $CD4^+$ and $CD8^+$ T cells showing no significantly differences in the expression of CD25, CD69 and CD95 (Fig. 22B, 23). Interestingly, the expression of CD25 and CD69 on $CD4^+$ T cells was strongly elevated in cervical lymph nodes in 2 out of 3 mice with CNS demyelination (Fig. 22B). Since $CD4^+$ T cells in inguinal lymph nodes and $CD8^+$ T cells in general did not exhibit such an increase (Fig. 22B, 23), this observation may be an indication for the involvement of cervical lymph nodes in the development of anti-MOG antibody driven EAE. Taken together, these results show that in the chronic phase of EAE, BTK inhibitor evobrutinib does not affect the composition and activation of T lymphocytes in secondary lymphoid organs.

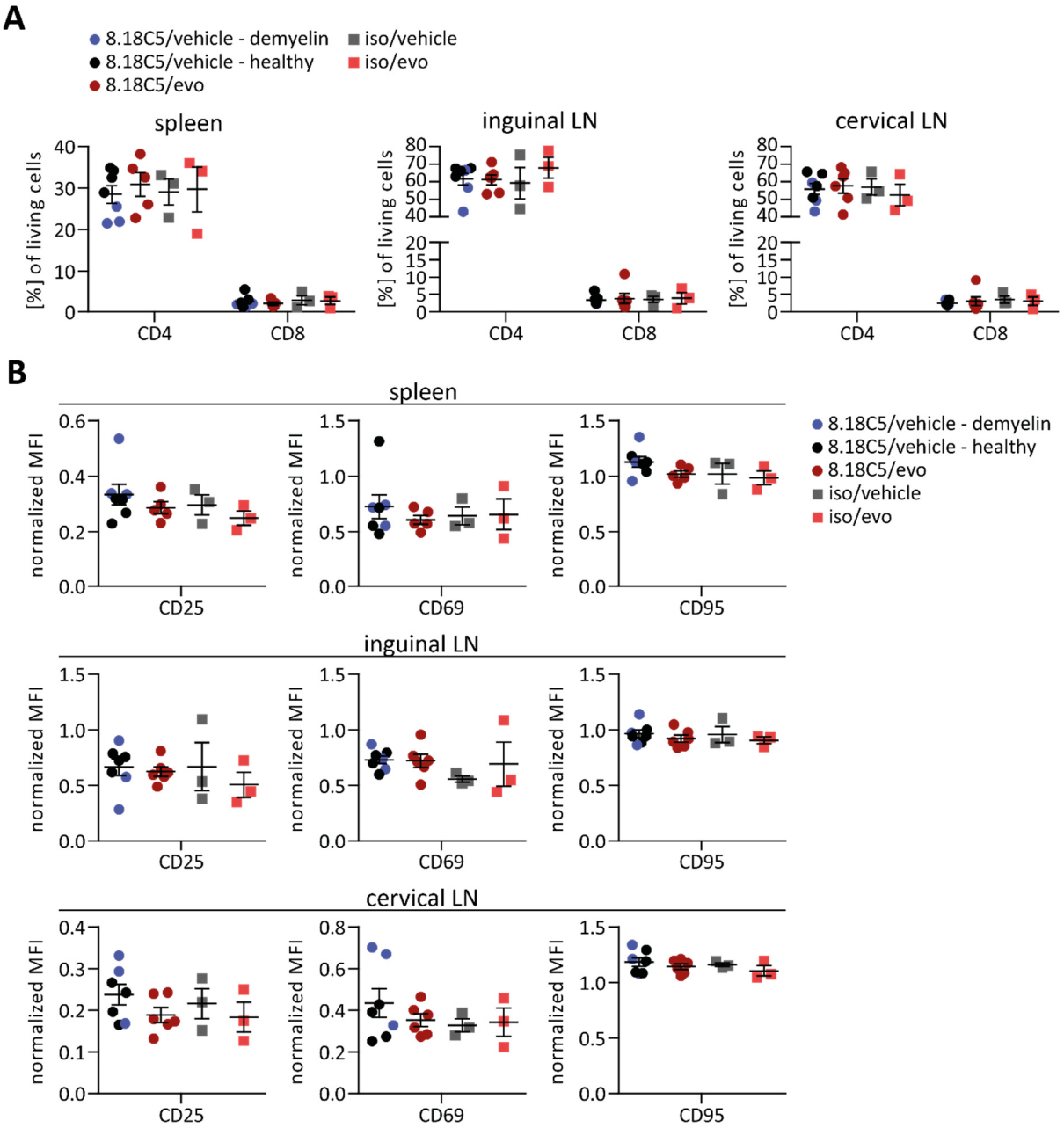

Figure 22: Evobrutinib has neither an impact on the T cell composition nor on the activation of CD4⁺ T cells. Transgenic 2D2 mice were treated daily with vehicle or evobrutinib (evo) starting 3 days before the first antibody transfer. They received repetitive injections of anti-MOG antibody 8.18C5 or isotype control (iso). 42 days after the first antibody injection, immune cells from spleen, inguinal and cervical lymph nodes (LN) were isolated and analyzed by flow cytometry. 8.18C5/vehicle mice with CNS demyelination are highlighted in purple; n = 3 – 7 mice/group; representative data of 3 independent experiments; Kruskal-Wallis test with Dunn's multiple comparison test between all groups. **A)** Frequency of CD4⁺ and CD8⁺ T cells in mean [%] of living cells ± SEM. **B)** Normalized mean fluorescence intensity of activation markers expressed on CD4⁺ T cells ± SEM.

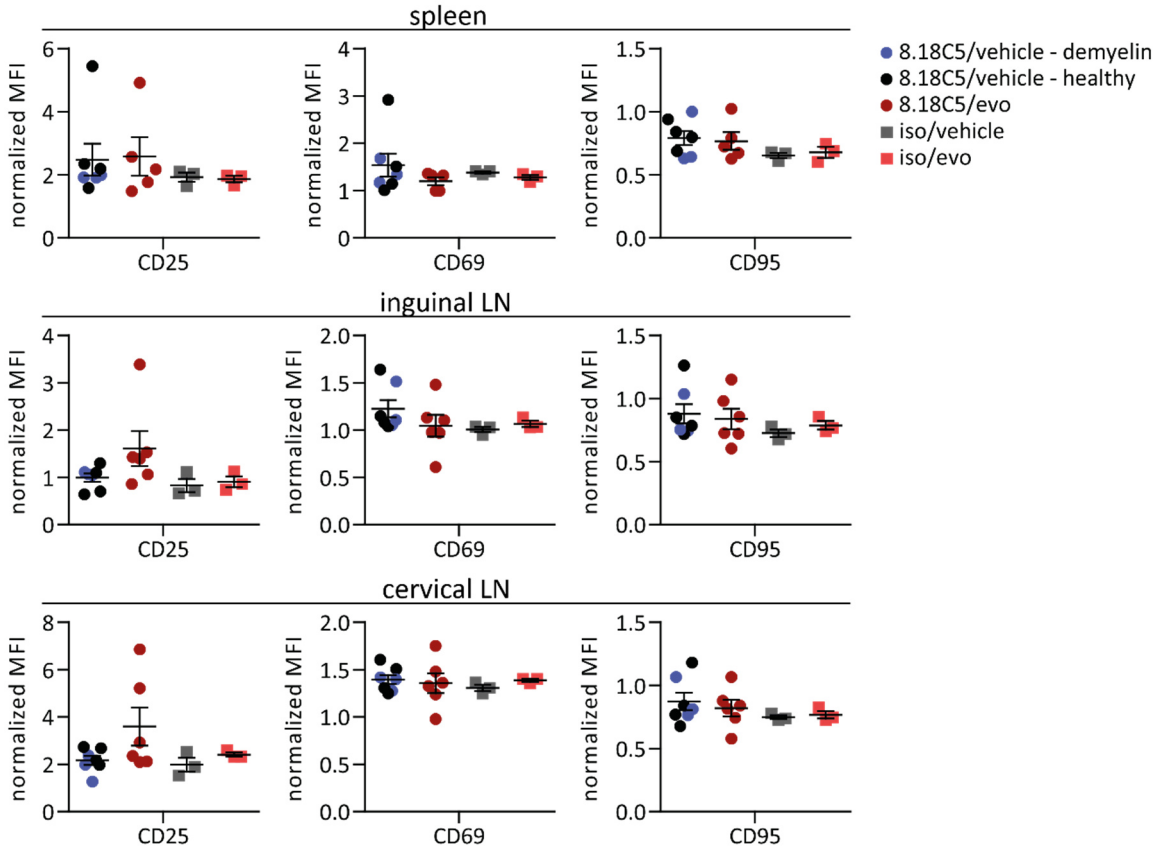

Figure 23: Inhibition of BTK does not affect the activation state of CD8⁺ T cells in secondary lymphoid tissue. Transgenic 2D2 mice were treated daily with vehicle or evobrutinib (evo) starting 3 days before the first antibody transfer. They received repetitive injections of anti-MOG antibody 8.18C5 or isotype control (iso). 42 days after the first antibody injection, immune cells from spleen, inguinal and cervical lymph nodes (LN) were isolated and analyzed by flow cytometry. Expression of activation markers on CD8⁺ T cells, depicted as normalized mean fluorescence intensity ± SEM. 8.18C5/vehicle mice with CNS demyelination are highlighted in purple; n = 3 – 7 mice/group; representative data of 3 independent experiments; Kruskal-Wallis test with Dunn's multiple comparison test between all groups.

4 DISCUSSION

Over many years, NMOSD and MOGAD were considered to be variants of the most common CNS demyelinating disorder, MS. However, their distinct clinical and pathological features and, in particular, the discovery of peripheral autoantibodies against AQP4 and MOG, respectively, have resulted in their delineation as separate disease entities. The role of anti-AQP4 antibodies in NMOSD is well defined, indicating that these antibodies bind to AQP4 on astrocytes and induce astrocyte destruction through different effector mechanisms, including CDC and ADCC (Alexopoulos et al. 2015; Phuan et al. 2012; Vincent et al. 2008). By contrast, the pathogenic relevance of anti-MOG antibodies for initiation and progression of MOGAD is widely unknown. In this regard, it was previously proposed that anti-MOG antibody-mediated opsonization of endogenous MOG can trigger inflammatory CNS demyelination in mice (Kinzel et al. 2016). However, it remains elusive if this may also occur in MOGAD patients. Hence, in the first part of the present study, it was investigated if peripheral autoantibodies from MOGAD patients are capable of opsonizing MOG. Using an *in vitro* setting with human myeloid APCs, it was demonstrated that patient-derived anti-MOG antibodies opsonized soluble and membrane-bound MOG, thus fostering antigen uptake by human APCs presumable via FcγR III. These results support the hypothesis that anti-MOG antibody-mediated opsonization may represent a disease-triggering mechanism in MOGAD patients.

Based on the aforementioned findings, peripheral anti-MOG antibodies and their effector mechanisms may serve as potential targets for new therapy options. Since BTK is crucially involved in FcγR signaling in myeloid cells (Koprulu and Ellmeier 2009; Lopez-Herrera et al. 2014), its inhibition can be a promising strategy to prevent FcγR-mediated activation of myeloid cells induced by anti-MOG antibodies. Thus, the second project of the study addressed the therapeutic potential of BTK inhibitor evobrutinib in anti-MOG antibody-driven EAE. Evobrutinib was found to prevent the clinical manifestation of EAE by significantly reducing inflammatory CNS demyelination in the spinal cord. Analysis of immune cells in secondary lymphoid organs revealed that BTK inhibition diminished the expression of FcγRs on monocytes and macrophages, but did not affect the phenotype of T lymphocytes in the chronic phase of EAE. These findings indicate that BTK inhibition by evobrutinib can be a promising strategy to counteract anti-MOG antibody-triggered CNS demyelination, although the underlying immunological mechanisms should be further investigated.

4.1 Patient-derived anti-MOG antibodies facilitate MOG internalization by human antigen-presenting cells via opsonization

In MOGAD, it is still unknown if peripheral autoantibodies against MOG harbor pathogenic functions. This may be due to the low prevalence of MOGAD accounting for only 1 – 6 % of all major demyelinating disorders in adults (Marignier et al. 2021), in conjunction with the circumstance that MOGAD has been just recently defined as an own disease entity. Nevertheless, several studies already addressed the potential pathogenic role of MOG-specific antibodies in animal models, revealing that they are capable of trigger CNS demyelination (Flach et al. 2016; Kinzel et al. 2016; Spadaro et al. 2018). However, how these findings are applicable to MOGAD patients has not been clarified yet. Hence, the first part of the study on hand aimed at elucidating the pathomechanism of anti-MOG antibodies in an *in vitro* setting with human APCs. It was investigated if peripheral anti-MOG antibodies from MOGAD patients are able to opsonize human MOG, thus promoting its ingestion by myeloid APCs.

To assess the opsonizing capacity of anti-MOG antibodies, an *in vitro* setting with human myeloid APCs was first established. Since macrophages are tissue-resident cells and DCs just rarely occur in the blood (<0.1 % of mononuclear cells), their sampling is difficult and requires large amounts of tissue or blood (Haniffa et al. 2015). In the 1990s, it was found that blood monocytes are able to differentiate into dendritic-like cells or macrophage-like cells under the influence of distinct cytokines, such as GM-CSF, IL-4 or M-CSF (Becker et al. 1987; Kasinrerk et al. 1993; Sallusto and Lanzavecchia 1994). Based on these findings, in the present study, human $CD14^+$ monocytes were differentiated into dendritic-like cells in the presence of GM-CSF, IL-4, IL-1β, IL-6, TNF-α and PGE_2, or macrophage-like cells using M-CSF, IFN-γ and human serum. The *in vitro* differentiated human APCs displayed specific phenotypes, which were primarily affected by the cytokines applied in the generation process. Dendritic-like cells exhibited high expression levels of FcγR II and molecules involved in antigen presentation but minimal or no expression of FcγR I and III. This is in accordance with literature showing that GM-CSF and IL-4 upregulate CD80 and CD86 (GM-CSF) and downregulate FcγR I (IL-4) in human cultures (Ambarus et al. 2012; Boruchov et al. 2005; te Velde et al. 1992). Macrophage-like cells, however, highly expressed FcγRs as well as molecules involved in antigen presentation on the surface. This observation is consistent with the work of Ambarus and colleagues demonstrating that M-CSF and IFN-γ increase the expression of FcγR I, FcγR III, CD80 and CD86 (Ambarus et al. 2012). Since dendritic-like as well as macrophage-like cells

expressed common features of APCs, we supposed that both cell types are suitable to investigate the opsonizing capacity of MOG-specific antibodies. However, due to their distinct FcγR expression patterns, dendritic-like and macrophage-like cells may be differentially affected by anti-MOG antibodies.

After confirming that *in vitro* differentiated APCs are capable of internalizing soluble and membrane-bound human MOG, it was examined if the MOG uptake can be fostered by humanized anti-MOG antibody 8.18C5. Interestingly, the addition of h8.18C5 only enhanced the ingestion of membrane-bound but not of soluble human MOG, being the first indication that the protein structure may play a crucial role in anti-MOG antibody-mediated opsonization of MOG. This hypothesis is further supported by the observation that whole IgG from 3 different MOGAD patients significantly increased the phagocytosis of membrane-bound MOG by human APCs, whereas only 1 of these samples facilitated recognition of soluble human MOG. The obtained findings collectively suggest that a particular domain of membrane-bound MOG is essential for recognition by MOG-specific antibodies. In this regard, Macrini et al. recently demonstrated that most patient-derived anti-MOG antibodies require the intramembranous second hydrophobic domain of membrane-bound MOG for antigen binding (Macrini et al. 2021). However, a few MOGAD patients also recognized the extracellular part of MOG in its soluble form, which is in line with the present study. Macrini and colleagues further showed that anti-MOG antibodies preferentially bound human MOG in a bivalent manner. Thus, they propose that the intracellular part of MOG facilitates a suitable distance between two MOG monomers, which allows bivalent binding by MOG-specific antibodies (Macrini et al. 2021).

In the study on hand, whole IgG as well as serum from MOGAD patients potently increased the ingestion of membrane-bound MOG by *in vitro* differentiated dendritic-like and macrophage-like cells. These findings reveal that peripheral MOG-specific antibodies are capable of opsonizing human MOG and thus facilitate its recognition by myeloid APCs. This mechanism may represent the initial step in a potential humoral immune response against MOG, leading to disease and/or relapse induction in MOGAD patients. However, up to now, it has not been investigated if the ingestion of opsonized MOG by human APCs results in the activation of naïve T cells, which is a limitation of our *in vitro* model. Instead, the phenotype of the *in vitro* differentiated APCs in regard to antigen presentation was examined. As it is known that co-stimulatory molecules are upregulated on professional APCs upon activation

(Kambayashi and Laufer 2014), we expected an increased expression of these molecules on dendritic-like and macrophage-like cells in the presence of anti-MOG antibody positive serum. However, analysis of molecules involved in antigen presentation 18 h post opsonization initiation revealed that in the presence of anti-MOG antibodies, the expression of CD40 and MHCII was slightly reduced on macrophage-like cells, whereas dendritic-like cells did not show an altered expression of these molecules in comparison to anti-MOG antibody negative serum. Since the generated APCs already exhibited a high expression of co-stimulatory molecules and MHCII by themselves due to pro-inflammatory cytokines in the differentiation process, a further upregulation during antigen processing might not have been possible. However, despite these findings, in further experiments it will be analyzed whether anti-MOG antibody-mediated opsonization of human MOG results in the activation of T cells.

The finding that patient-derived MOG-specific antibodies are capable of opsonizing human MOG supports the hypothesis that anti-MOG antibody-mediated opsonization represents a disease-triggering mechanism in MOGAD patients. However, it also raises the question where these peripheral autoantibodies potentially recognize MOG, given the fact that it is solely expressed in the CNS. A possible site are the deep cervical lymph nodes, where lymphatic vessels continuously drain brain fluid (Aspelund et al. 2015; Louveau et al. 2015). In this regard, traces of myelin have been detected in the cervical lymph nodes of MS patients as well as of EAE mice (Fabriek et al. 2005; Weller et al. 1996). Besides the periphery, anti-MOG antibodies may directly act within the CNS. This assumption is supported by the work of Flach et al., which revealed that peripherally applied anti-MOG antibodies diffused into the CNS and facilitated MOG recognition to CNS-resident antigen-presenting phagocytes, resulting in enhanced tissue destruction by T lymphocytes (Flach et al. 2016). Another study which emphasizes a potential pathogenic role of anti-MOG antibodies in the CNS, although not in the context of opsonization, represents the work of Pellerin and colleagues. They showed that MOG-reactive antibodies induced a proliferative response in brain and spinal cord microglia via FcγRs. However, the ingestion of myelin by microglia was not enhanced in the presence of anti-MOG antibodies (Pellerin et al. 2021).

Besides triggering inflammation via opsonization and subsequent T cell activation, anti-MOG antibodies may also damage the CNS by inducing demyelination via CDC. This assumption is supported by the detection of activated complement deposits within lesions of MOGAD patients (Hoftberger et al. 2020; Weber et al. 2018) and the observation that patient-derived

anti-MOG antibodies were able to cause complement-mediated myelin loss in organotypic brain slices (Peschl et al. 2017b). Along the same line, Spadaro and colleagues further showed that human MOG-specific antibodies in conjunction with myelin basic protein-reactive T cells triggered demyelination associated with complement deposition within the CNS of rats (Spadaro et al. 2018).

While the precise function of anti-MOG antibodies is still under investigation, the pathogenic role of AQP4-specific antibodies isolated from NMOSD patients is characterized more in detail. Anti-AQP4 antibodies bind to AQP4 expressed on astrocytes and trigger astrocyte destruction and subsequent demyelination via CDC and ADCC (Alexopoulos et al. 2015; Phuan et al. 2012; Vincent et al. 2008). However, it has not been investigated yet whether anti-AQP4 antibodies also facilitate antigen recognition by APCs and thus trigger T cell activation, similar to the process suggested for anti-MOG antibodies (Flach et al. 2016; Kinzel et al. 2016). Hence, the opsonizing capacity of patient-derived anti-AQP4 antibodies was analyzed in the here established *in vitro* model. Both IgG and serum isolated from NMOSD patients opsonized membrane-bound AQP4 and thus significantly increased the protein uptake by human APCs. These findings indicate that besides mediating CDC and ADCC, AQP4-specific antibodies are additionally capable of facilitating antigen recognition by APCs via opsonization, thus potentially inducing T cell activation. This assumption is in line with the observation that NMOSD patients contain AQP4-reactive T lymphocytes in the blood (Hofer et al. 2020; Matsuya et al. 2011; Vaknin-Dembinsky et al. 2016). However, Hillebrand and colleagues recently demonstrated that systemically injected anti-AQP4 antibodies can enter the CNS via circumventricular organs and meningeal or parenchymal blood vessels, resulting in the formation of NMOSD-like lesions with AQP4 loss (Hillebrand et al. 2019). This observation suggests that AQP4-specific antibodies may act both in the periphery and the CNS.

In summary, the work on hand showed that patient-derived anti-MOG antibodies are capable of opsonizing human MOG and thus promote its internalization by *in vitro* differentiated APCs, presumable via FcγR III. This mechanism may represent the initial step in a potential humoral immune response against MOG, resulting in inflammatory CNS demyelination in MOGAD patients.

4.2 Inhibition of Bruton's tyrosine kinase represents a promising strategy for targeting anti-MOG antibody-mediated CNS inflammation

As peripheral MOG-specific antibodies are increasingly suggested to fulfill a pathogenic function in MOGAD patients, they and their effector mechanisms may serve as potential targets for new therapeutic options. Due to the crucial involvement of BTK in FcγR signaling in myeloid cells (Koprulu and Ellmeier 2009; Lopez-Herrera et al. 2014), its inhibition can be a promising strategy to prevent FcγR-mediated activation of myeloid cells triggered by anti-MOG antibodies and thus counteract anti-MOG antibody-induced CNS demyelination. Hence, the second project of the present study addressed the therapeutic potential of BTK inhibitor evobrutinib in anti-MOG antibody-driven CNS demyelination. It was investigated *in vitro* and *in vivo* how evobrutinib affects the function and phenotype of myeloid cells activated by anti-MOG antibody-mediated opsonization.

Since BTK was found to be involved in FcγR-mediated phagocytosis (Amoras et al. 2003; Jongstra-Bilen et al. 2008), it was first analyzed whether BTK inhibition modifies the anti-MOG antibody-mediated increase in the phagocytosis activity of human APCs using the already established *in vitro* setup. Indeed, evobrutinib diminished the anti-MOG antibody-mediated enhancement of MOG uptake by macrophage-like cells, whereas it did not alter FcγR-independent protein internalization. This was further accompanied by an elevated expression of FcγR III on macrophage-like cells, regardless of the presence of anti-MOG antibodies or control antibodies. These findings are in line with published data of Amoras and colleagues. They showed that monocytes isolated from XLA patients, which are characterized by mutations in the BTK gene (Lopez-Herrera et al. 2014), exhibited a decreased FcγR-mediated phagocytosis in comparison to healthy controls (Amoras et al. 2003). Moreover, monocytes from XLA patients showed a significantly higher expression of FcγR III compared to control monocytes (Amoras et al. 2007). The expression of FcγR I and II was not altered, correlating with the findings observed for macrophage-like cells in the present study. However, Ren et al. demonstrated that BTK inhibitor ibrutinib did not affect FcγR-mediated phagocytosis of human monocytes (Ren et al. 2016), indicating that the role of BTK in FcγR-mediated phagocytosis is not fully understood yet. In contrast to macrophage-like cells, evobrutinib did not modify the phagocytosis activity nor the expression of FcγRs on dendritic-like cells, which may be due to the very low expression of FcγR I and FcγR III. It was further investigated whether evobrutinib affects the expression of molecules involved in antigen presentation on

human APCs and thus potentially alters their ability to activate T cells. In the presence of anti-MOG antibodies, BTK inhibition reduced the expression of CD40 and CD86 on dendritic-like cells as well as the expression of CD86 on macrophage-like cells after an incubation of 18 h, which may result in an impaired capacity of the APCs to stimulate T lymphocytes. These findings are in contrast to other studies demonstrating that the expression of molecules involved in antigen presentation on monocyte-derived DCs was equivalent between XLA patients and healthy controls upon stimulation (Gagliardi et al. 2003; Liu et al. 2012). However, the authors applied LPS and influenza virus, respectively, as stimulation and therefore targeted toll-like receptors (TLR) (Murphy 2012). This may have a different effect on the expression of co-stimulatory molecules and MHCII in comparison to FcγR-mediated activation of dendritic-like cells.

While the impact of BTK inhibition on B lymphocytes has been well-described in mice (Bame et al. 2021; Haselmayer et al. 2019; Torke et al. 2020), less is known about the effects in myeloid cells. Hence, it was examined how BTK inhibitor evobrutinib affects the phenotype of myeloid cells in WT mice (non-transgenic 2D2 mice) in the absence of inflammation. It was observed that BTK inhibition neither affected the differentiation of myeloid cells nor the phenotype of monocytes and macrophages in spleen, inguinal and cervical lymph nodes. This finding may be a result of the lacking stimulation of myeloid cells. Supporting this assumption, Gabhann and colleagues found in BTK deficient mice that the recruitment of pro-inflammatory M1 macrophages was reduced upon LPS administration. *Ex vivo* experiments further demonstrated an impaired ability of BTK deficient macrophages to polarize into M1 phenotype in response to LPS/IFN-γ stimulation, instead expressing anti-inflammatory M2-associated markers (Ni Gabhann et al. 2014). In the study on hand, it was further analyzed how BTK inhibition affects the composition and activation of T lymphocytes. Mice treated with evobrutinib showed an increased frequency of $CD4^+$ T cells in cervical lymph nodes and a reduced expression of CD95 on $CD4^+$ T lymphocytes in the spleen compared to vehicle-treated mice. Since BTK is not expressed in T lymphocytes (Neys et al. 2021; Torke and Weber 2020), the observed findings may be explained by off-target effects or secondary effects mediated by other immune cells, such as B lymphocytes. A possible explanation for the increased frequency of $CD4^+$ T cells in cervical lymph is the concurrent decline of B cells in this compartment, which is likely caused by an impaired B cell maturation induced by evobrutinib.

The reduced expression of CD95 on $CD4^+$ T lymphocytes in the spleen implies a diminished activation of these cells, as CD95 is known to be upregulated on activated T cells (Paulsen and Janssen 2011). However, the observation that other activation markers (CD25 and CD69) did not exhibit a reduced expression in the presence of evobrutinib contradicts this assumption. Since most regulatory T cells are characterized by a constitutive expression of CD95 (Fritzsching et al. 2005), it is also possible that BTK inhibition decreased the number of regulatory T cells.

It was already revealed that BTK inhibitor evobrutinib significantly diminishes inflammatory CNS demyelination in MS patients (Montalban et al. 2019) and in the animal model EAE (Torke et al. 2020). We assume that evobrutinib may be likewise effective in anti-MOG antibody-driven EAE. As anti-MOG antibody-triggered CNS demyelination was shown to be FcγR-dependent (Kinzel et al. 2016), evobrutinib may inhibit FcγR signaling and thus counteract inflammatory CNS demyelination. It was therefore assessed whether evobrutinib can reduce or even prevent CNS inflammation in an anti-MOG antibody-driven EAE model. Remarkably, evobrutinib inhibited the clinical manifestation of EAE by significantly diminishing anti-MOG antibody-induced CNS demyelination in comparison to vehicle treated 2D2 mice. This was accompanied by a strongly decreased infiltration of T cells and macrophages within the CNS. To identify the underlying mechanism of the observed effect, immune cells from spleen, inguinal and cervical lymph nodes were analyzed. Since we assume that anti-MOG antibodies recognize endogenous MOG in the deep cervical lymph nodes, this compartment was of particular interest. While BTK inhibition did not affect the differentiation of myeloid cells, it reduced the frequency of inflammatory monocytes and macrophages in the spleen of mice receiving 8.18C5 antibody. This finding is in accordance with a recent study of Purvis et al., which demonstrated that BTK inhibitor ibrutinib impeded the recruitment of inflammatory monocytes/macrophages to the peritoneum in a zymosan-induced peritonitis model (Purvis et al. 2021). In the present study, it was further revealed that evobrutinib significantly diminished the expression of FcγR II and slightly reduced the FcγR I expression on monocytes/ macrophages in the spleen of mice receiving 8.18C5 antibody. These results are in contrast to data of Pellerin and colleagues, demonstrating that the expression of FcγRs on microglia is not altered by BTK inhibition in mice receiving anti-MOG antibodies (Pellerin et al. 2021). Notably, in the work on hand, 8.18C5/vehicle mice with CNS demyelination exhibited a particular high expression of FcγRs and molecules involved in antigen presentation on monocytes and

macrophages in the spleen, indicating a more activated phenotype of these cells compared to healthy 8.18C5/vehicle as well as 8.18C5/evobrutinib mice. The obtained findings may suggest that anti-MOG antibody-mediated activation of myeloid cells only occurred in mice with CNS demyelination, not in all 8.18C5/vehicle. However, it is also possible that the detected phenotypical changes of monocytes and macrophages are just a result of inflammatory processes in 2D2 mice with CNS demyelination. Interestingly, 8.18C5/vehicle mice with CNS inflammation also showed an increased MHCII expression on monocytes/macrophages as well as an elevated activation of $CD4^+$ T cells in the cervical lymph nodes, being the first indication that anti-MOG antibody-mediated opsonization may occur in this compartment. However, neither the cell composition nor the activation of T lymphocytes was affected by evobrutinib in mice receiving 8.18C5 antibody and isotype antibody, respectively. Taken together, the underlying immunological mechanisms of the observed decline of CNS demyelination mediated by evobrutinib have not been completely deciphered yet. There can be various conceivable reasons for this result. First, immune cells from 2D2 mice were analyzed in the chronic phase of disease. Since anti-MOG antibody-triggered activation of myeloid cells and T lymphocytes is expected to occur before disease onset, an earlier analysis of immune cells, e.g. at disease onset, is very recommendable. Furthermore, the chosen immunological readout may not assess all effect mechanisms of evobrutinib. In this regard, it was revealed that BTK inhibition suppressed the production of TNF-α in monocytes upon FcγR-mediated stimulation (Bame et al. 2021; Ren et al. 2016). A reduction of the cytokine production may be particularly effective in MOGAD patients, as they are characterized by elevated levels of cytokines, including IL-6, IFN-γ and GM-CSF, in the CSF compared to MS patients (Hofer et al. 2019; Kaneko et al. 2018). Moreover, it is possible that evobrutinib not only affects peripheral but also CNS-resident APCs, as it was found to be able to cross the BBB (Piasecka-Stryczynska et al. 2021). In this context, Pellerin et al. demonstrated that BTK inhibitor ibrutinib partially blocked the proliferation of microglia induced by anti-MOG antibodies (Pellerin et al. 2021).
Taken together, it was shown that BTK inhibition did not affect the phenotype of myeloid cells in the absence of disease but during experimental CNS inflammation. Evobrutinib was found to prevent the clinical manifestation of anti-MOG antibody-driven EAE by significantly reducing inflammatory CNS demyelination in the spinal cord. These results indicate that BTK inhibition by evobrutinib can be a promising strategy to counteract anti-MOG antibody-mediated CNS demyelination.

4.3 Outlook

4.3.1 Project 1: Investigation of the opsonizing capacity of patient-derived anti-MOG antibodies

The first project of the present study focused on the potential pathogenic role of peripheral MOG-specific antibodies. It was shown that anti-MOG antibodies in IgG and serum samples from MOGAD patients are capable of opsonizing human MOG, thus fostering antigen recognition and uptake by *in vitro* differentiated human APCs. However, it remains elusive if the internalized MOG is processed by the APCs and subsequently presented to T cells, which may then proliferate and differentiate in an encephalitogenic manner. Such a mechanism has been already proposed to trigger inflammatory CNS demyelination in mice (Kinzel et al. 2016). To address this question, freshly isolated T lymphocytes from MOGAD patients should be applied in the established *in vitro* model. However, since it was previously demonstrated that peripheral T cells from MOGAD patients do not exhibit autoreactive responses against MOG (Hofer et al. 2020), a humanized MOG-reactive T cell line (Chou et al. 2004) might be used instead.

Besides FcγRs, phagocytes can also recognize and ingest opsonized protein via complement receptors when complement proteins bind to the antigen-antibody complexes (Aderem and Underhill 1999). As the used serum samples from MOGAD patients contain complement proteins, the phagocytosis of opsonized MOG by *in vitro* differentiated APCs may be increased by these proteins. Thus, it should be investigated if the inactivation of complement factors, e.g. by heat, results in a diminished internalization of opsonized MOG.

Finally, the finding that patient-derived anti-MOG antibodies can opsonize human MOG raises the question where these autoantibodies potentially recognize CNS antigen in MOGAD patients. A possible site represent the deep cervical lymph nodes, where lymphatic vessels continuously drain brain fluid (Aspelund et al. 2015; Louveau et al. 2015). To address this assumption, the function of deep cervical lymph nodes should be examined in the anti-MOG antibody-driven EAE model established by Kinzel and colleagues (Kinzel et al. 2016).

4.3.2 Project 2: Inhibition of Bruton's tyrosine kinase as a therapeutic strategy for anti-MOG antibody-mediated CNS demyelination

The second project addressed the therapeutic potential of BTK inhibitor evobrutinib in anti-MOG antibody-driven EAE. Evobrutinib was found to prevent the clinical manifestation of EAE by significantly reducing inflammatory CNS demyelination in the spinal cord. Analysis of

immune cells in secondary lymphoid organs showed that BTK inhibition diminished the expression of FcγRs on monocytes and macrophages, but did not alter the phenotype of T cells in the chronic phase of EAE. To further evaluate the underlying immunological mechanisms, an earlier analysis of immune cells, e.g. at disease onset, is highly recommendable, since anti-MOG antibody-triggered activation of myeloid cells and T lymphocytes is expected to occur before disease onset. In addition, the effect of evobrutinib on other immune cell functions, including the production of pro- and anti-inflammatory cytokines, should be studied. As evobrutinib was recently shown to be able to cross the BBB (Piasecka-Stryczynska et al. 2021), it is possible that BTK inhibition also influences CNS-resident APCs, such as microglia. Thus, the impact of evobrutinib on the phenotype and function of microglia in anti-MOG antibody-driven EAE should be analyzed as well.

Besides evobrutinib, other BTK inhibitors, inluding tolebrutinib or fenebrutinib, have been recently shown to be effective in treatment of MS (Garcia-Merino 2021; Reich et al. 2021). Since all inhibitors exhibit distinct molecular properties, such as the BTK binding mechanism or size, they may act differently in the anti-MOG antibody-driven EAE model. Thus, it should be investigated how other BTK inhibitors affect anti-MOG antibody-mediated CNS demyelination in mice.

5 BIBLIOGRAPHY

Aderem A, Underhill DM (1999): Mechanisms of phagocytosis in macrophages. Annu Rev Immunol 17, 593-623

Alankus YB, Grenningloh R, Haselmayer P, Bender AT, Bruttger J: Inhibition of Bruton's tyrosine kinase prevents inflammatory macrophage differentiation: a potential role in multiple sclerosis. hrsg. 2018

Alexopoulos H, Kampylafka EI, Fouka P, Tatouli I, Akrivou S, Politis PK, Moutsopoulos HM, Tzioufas AG, Dalakas MC (2015): Anti-aquaporin-4 autoantibodies in systemic lupus erythematosus persist for years and induce astrocytic cytotoxicity but not CNS disease. J Neuroimmunol 289, 8-11

Ambarus CA, Krausz S, van Eijk M, Hamann J, Radstake TR, Reedquist KA, Tak PP, Baeten DL (2012): Systematic validation of specific phenotypic markers for in vitro polarized human macrophages. J Immunol Methods 375, 196-206

Ambrosius W, Michalak S, Kozubski W, Kalinowska A (2020): Myelin Oligodendrocyte Glycoprotein Antibody-Associated Disease: Current Insights into the Disease Pathophysiology, Diagnosis and Management. Int J Mol Sci 22

Amoras AL, Kanegane H, Miyawaki T, Vilela MM (2003): Defective Fc-, CR1- and CR3-mediated monocyte phagocytosis and chemotaxis in common variable immunodeficiency and X-linked agammaglobulinemia patients. J Investig Allergol Clin Immunol 13, 181-188

Amoras AL, da Silva MT, Zollner RL, Kanegane H, Miyawaki T, Vilela MM (2007): Expression of Fc gamma and complement receptors in monocytes of X-linked agammaglobulinaemia and common variable immunodeficiency patients. Clin Exp Immunol 150, 422-428

Aspelund A, Antila S, Proulx ST, Karlsen TV, Karaman S, Detmar M, Wiig H, Alitalo K (2015): A dural lymphatic vascular system that drains brain interstitial fluid and macromolecules. J Exp Med 212, 991-999

Bame E, Tang H, Burns JC, Arefayene M, Michelsen K, Ma B, Marx I, Prince R, Roach AM, Poreci U, et al. (2021): Next-generation Bruton's tyrosine kinase inhibitor BIIB091 selectively and potently inhibits B cell and Fc receptor signaling and downstream functions in B cells and myeloid cells. Clin Transl Immunology 10, e1295

Banchereau J, Briere F, Caux C, Davoust J, Lebecque S, Liu YJ, Pulendran B, Palucka K (2000): Immunobiology of dendritic cells. Annu Rev Immunol 18, 767-811

Becker S, Warren MK, Haskill S (1987): Colony-stimulating factor-induced monocyte survival and differentiation into macrophages in serum-free cultures. J Immunol 139, 3703-3709

Bennett JL, Lam C, Kalluri SR, Saikali P, Bautista K, Dupree C, Glogowska M, Case D, Antel JP, Owens GP, et al. (2009): Intrathecal pathogenic anti-aquaporin-4 antibodies in early neuromyelitis optica. Ann Neurol 66, 617-629

Berger T, Rubner P, Schautzer F, Egg R, Ulmer H, Mayringer I, Dilitz E, Deisenhammer F, Reindl M (2003): Antimyelin antibodies as a predictor of clinically definite multiple sclerosis after a first demyelinating event. N Engl J Med 349, 139-145

Bettelli E, Pagany M, Weiner HL, Linington C, Sobel RA, Kuchroo VK (2003): Myelin oligodendrocyte glycoprotein-specific T cell receptor transgenic mice develop spontaneous autoimmune optic neuritis. J Exp Med 197, 1073-1081

Bonnan M, Valentino R, Olindo S, Mehdaoui H, Smadja D, Cabre P (2009): Plasma exchange in severe spinal attacks associated with neuromyelitis optica spectrum disorder. Mult Scler 15, 487-492

Boruchov AM, Heller G, Veri MC, Bonvini E, Ravetch JV, Young JW (2005): Activating and inhibitory IgG Fc receptors on human DCs mediate opposing functions. J Clin Invest 115, 2914-2923

Bournazos S, Ravetch JV (2017): Diversification of IgG effector functions. Int Immunol 29, 303-310

Bruhns P (2012): Properties of mouse and human IgG receptors and their contribution to disease models. Blood 119, 5640-5649

Caldwell RD, Qiu H, Askew BC, Bender AT, Brugger N, Camps M, Dhanabal M, Dutt V, Eichhorn T, Gardberg AS, et al. (2019): Discovery of Evobrutinib: An Oral, Potent, and Highly Selective, Covalent Bruton's Tyrosine Kinase (BTK) Inhibitor for the Treatment of Immunological Diseases. J Med Chem 62, 7643-7655

Carnero Contentti E, Correale J (2020): Bruton's tyrosine kinase inhibitors: a promising emerging treatment option for multiple sclerosis. Expert Opin Emerg Drugs 25, 377-381

Carnero Contentti E, Correale J (2021): Neuromyelitis optica spectrum disorders: from pathophysiology to therapeutic strategies. J Neuroinflammation 18, 208

Chang BY, Huang MM, Francesco M, Chen J, Sokolove J, Magadala P, Robinson WH, Buggy JJ (2011): The Bruton tyrosine kinase inhibitor PCI-32765 ameliorates autoimmune arthritis by inhibition of multiple effector cells. Arthritis Res Ther 13, R115

Chen JJ, Flanagan EP, Bhatti MT, Jitprapaikulsan J, Dubey D, Lopez Chiriboga ASS, Fryer JP, Weinshenker BG, McKeon A, Tillema JM, et al. (2020): Steroid-sparing maintenance immunotherapy for MOG-IgG associated disorder. Neurology 95, e111-e120

Chihara N, Aranami T, Sato W, Miyazaki Y, Miyake S, Okamoto T, Ogawa M, Toda T, Yamamura T (2011): Interleukin 6 signaling promotes anti-aquaporin 4 autoantibody production from plasmablasts in neuromyelitis optica. Proc Natl Acad Sci U S A 108, 3701-3706

Chou YK, Culbertson N, Rich C, LaTocha D, Buenafe AC, Huan J, Link J, Wands JM, Born WK, Offner H, et al. (2004): T-cell hybridoma specific for myelin oligodendrocyte glycoprotein-35-55 peptide produced from HLA-DRB1*1501-transgenic mice. J Neurosci Res 77, 670-680

Collin M, McGovern N, Haniffa M (2013): Human dendritic cell subsets. Immunology 140, 22-30

Colonna M, Trinchieri G, Liu YJ (2004): Plasmacytoid dendritic cells in immunity. Nat Immunol 5, 1219-1226

Conley ME, Rohrer J, Rapalus L, Boylin EC, Minegishi Y (2000): Defects in early B-cell development: comparing the consequences of abnormalities in pre-BCR signaling in the human and the mouse. Immunol Rev 178, 75-90

Etemadifar M, Nasr Z, Khalili B, Taherioun M, Vosoughi R (2015): Epidemiology of neuromyelitis optica in the world: a systematic review and meta-analysis. Mult Scler Int 2015, 174720

Fabriek BO, Zwemmer JN, Teunissen CE, Dijkstra CD, Polman CH, Laman JD, Castelijns JA (2005): In vivo detection of myelin proteins in cervical lymph nodes of MS patients using ultrasound-guided fine-needle aspiration cytology. J Neuroimmunol 161, 190-194

Fanger NA, Wardwell K, Shen L, Tedder TF, Guyre PM (1996): Type I (CD64) and type II (CD32) Fc gamma receptor-mediated phagocytosis by human blood dendritic cells. J Immunol 157, 541-548

Flach AC, Litke T, Strauss J, Haberl M, Gomez CC, Reindl M, Saiz A, Fehling HJ, Wienands J, Odoardi F, et al. (2016): Autoantibody-boosted T-cell reactivation in the target organ triggers manifestation of autoimmune CNS disease. Proc Natl Acad Sci U S A 113, 3323-3328

Fletcher JM, Lalor SJ, Sweeney CM, Tubridy N, Mills KH (2010): T cells in multiple sclerosis and experimental autoimmune encephalomyelitis. Clin Exp Immunol 162, 1-11

Flores M, Desai DD, Downie M, Liang B, Reilly MP, McKenzie SE, Clynes R (2009): Dominant expression of the inhibitory FcgammaRIIB prevents antigen presentation by murine plasmacytoid dendritic cells. J Immunol 183, 7129-7139

Forthal DN (2014): Functions of Antibodies. Microbiol Spectr 2, 1-17

Fritzsching B, Oberle N, Eberhardt N, Quick S, Haas J, Wildemann B, Krammer PH, Suri-Payer E (2005): In contrast to effector T cells, CD4+CD25+FoxP3+ regulatory T cells are highly susceptible to CD95 ligand- but not to TCR-mediated cell death. J Immunol 175, 32-36

Gagliardi MC, Finocchi A, Orlandi P, Cursi L, Cancrini C, Moschese V, Miyawaki T, Rossi P (2003): Bruton's tyrosine kinase defect in dendritic cells from X-linked agammaglobulinaemia patients does not influence their differentiation, maturation and antigen-presenting cell function. Clin Exp Immunol 133, 115-122

Garcia-Merino A (2021): Bruton's Tyrosine Kinase Inhibitors: A New Generation of Promising Agents for Multiple Sclerosis Therapy. Cells 10

Geissmann F, Manz MG, Jung S, Sieweke MH, Merad M, Ley K (2010): Development of monocytes, macrophages, and dendritic cells. Science 327, 656-661

Genain CP, Cannella B, Hauser SL, Raine CS (1999): Identification of autoantibodies associated with myelin damage in multiple sclerosis. Nat Med 5, 170-175

Gilmore CP, Donaldson I, Bo L, Owens T, Lowe J, Evangelou N (2009): Regional variations in the extent and pattern of grey matter demyelination in multiple sclerosis: a comparison between the cerebral cortex, cerebellar cortex, deep grey matter nuclei and the spinal cord. J Neurol Neurosurg Psychiatry 80, 182-187

Gold R, Linington C, Lassmann H (2006): Understanding pathogenesis and therapy of multiple sclerosis via animal models: 70 years of merits and culprits in experimental autoimmune encephalomyelitis research. Brain 129, 1953-1971

Gold SM, Willing A, Leypoldt F, Paul F, Friese MA (2019): Sex differences in autoimmune disorders of the central nervous system. Semin Immunopathol 41, 177-188

Green AJ, McQuaid S, Hauser SL, Allen IV, Lyness R (2010): Ocular pathology in multiple sclerosis: retinal atrophy and inflammation irrespective of disease duration. Brain 133, 1591-1601

Guilliams M, Bruhns P, Saeys Y, Hammad H, Lambrecht BN (2014): The function of Fcgamma receptors in dendritic cells and macrophages. Nat Rev Immunol 14, 94-108

Haniffa M, Bigley V, Collin M (2015): Human mononuclear phagocyte system reunited. Semin Cell Dev Biol 41, 59-69

Haselmayer P, Camps M, Liu-Bujalski L, Nguyen N, Morandi F, Head J, O'Mahony A, Zimmerli SC, Bruns L, Bender AT, et al. (2019): Efficacy and Pharmacodynamic Modeling of the BTK Inhibitor Evobrutinib in Autoimmune Disease Models. J Immunol 202, 2888-2906

Hauser SL, Oksenberg JR (2006): The neurobiology of multiple sclerosis: genes, inflammation, and neurodegeneration. Neuron 52, 61-76

Hauser SL, Cree BAC (2020): Treatment of Multiple Sclerosis: A Review. Am J Med 133, 1380-1390 e1382

Hauser SL, Waubant E, Arnold DL, Vollmer T, Antel J, Fox RJ, Bar-Or A, Panzara M, Sarkar N, Agarwal S, et al. (2008): B-cell depletion with rituximab in relapsing-remitting multiple sclerosis. N Engl J Med 358, 676-688

Hauser SL, Bar-Or A, Comi G, Giovannoni G, Hartung HP, Hemmer B, Lublin F, Montalban X, Rammohan KW, Selmaj K, et al. (2017): Ocrelizumab versus Interferon Beta-1a in Relapsing Multiple Sclerosis. N Engl J Med 376, 221-234

Hemmer B, Archelos JJ, Hartung HP (2002): New concepts in the immunopathogenesis of multiple sclerosis. Nat Rev Neurosci 3, 291-301

Hendriks RW, Yuvaraj S, Kil LP (2014): Targeting Bruton's tyrosine kinase in B cell malignancies. Nat Rev Cancer 14, 219-232

Hillebrand S, Schanda K, Nigritinou M, Tsymala I, Bohm D, Peschl P, Takai Y, Fujihara K, Nakashima I, Misu T, et al. (2019): Circulating AQP4-specific auto-antibodies alone can induce neuromyelitis optica spectrum disorder in the rat. Acta Neuropathol 137, 467-485

Hinson SR, Pittock SJ, Lucchinetti CF, Roemer SF, Fryer JP, Kryzer TJ, Lennon VA (2007): Pathogenic potential of IgG binding to water channel extracellular domain in neuromyelitis optica. Neurology 69, 2221-2231

Hinson SR, Romero MF, Popescu BF, Lucchinetti CF, Fryer JP, Wolburg H, Fallier-Becker P, Noell S, Lennon VA (2012): Molecular outcomes of neuromyelitis optica (NMO)-IgG binding to aquaporin-4 in astrocytes. Proc Natl Acad Sci U S A 109, 1245-1250

Hofer LS, Ramberger M, Gredler V, Pescoller AS, Rostasy K, Sospedra M, Hegen H, Berger T, Lutterotti A, Reindl M (2020): Comparative Analysis of T-Cell Responses to Aquaporin-4 and Myelin Oligodendrocyte Glycoprotein in Inflammatory Demyelinating Central Nervous System Diseases. Front Immunol 11, 1188

Hofer LS, Mariotto S, Wurth S, Ferrari S, Mancinelli CR, Delogu R, Monaco S, Gajofatto A, Schwaiger C, Rostasy K, et al. (2019): Distinct serum and cerebrospinal fluid cytokine and chemokine profiles in autoantibody-associated demyelinating diseases. Mult Scler J Exp Transl Clin 5, 2055217319848463

Hoftberger R, Guo Y, Flanagan EP, Lopez-Chiriboga AS, Endmayr V, Hochmeister S, Joldic D, Pittock SJ, Tillema JM, Gorman M, et al. (2020): The pathology of central nervous system inflammatory demyelinating disease accompanying myelin oligodendrocyte glycoprotein autoantibody. Acta Neuropathol 139, 875-892

Horwood NJ, Mahon T, McDaid JP, Campbell J, Mano H, Brennan FM, Webster D, Foxwell BM (2003): Bruton's tyrosine kinase is required for lipopolysaccharide-induced tumor necrosis factor alpha production. J Exp Med 197, 1603-1611

Horwood NJ, Page TH, McDaid JP, Palmer CD, Campbell J, Mahon T, Brennan FM, Webster D, Foxwell BM (2006): Bruton's tyrosine kinase is required for TLR2 and TLR4-induced TNF, but not IL-6, production. J Immunol 176, 3635-3641

Jarius S, Wildemann B (2013): The history of neuromyelitis optica. J Neuroinflammation 10, 8

Jarius S, Paul F, Aktas O, Asgari N, Dale RC, de Seze J, Franciotta D, Fujihara K, Jacob A, Kim HJ, et al. (2018): MOG encephalomyelitis: international recommendations on diagnosis and antibody testing. J Neuroinflammation 15, 134

Johns TG, Bernard CC (1999): The structure and function of myelin oligodendrocyte glycoprotein. J Neurochem 72, 1-9

Joller N, Weber SS, Oxenius A (2011): Antibody-Fc receptor interactions in protection against intracellular pathogens. Eur J Immunol 41, 889-897

Jongstra-Bilen J, Puig Cano A, Hasija M, Xiao H, Smith CI, Cybulsky MI (2008): Dual functions of Bruton's tyrosine kinase and Tec kinase during Fcgamma receptor-induced signaling and phagocytosis. J Immunol 181, 288-298

Junker F, Gordon J, Qureshi O (2020): Fc Gamma Receptors and Their Role in Antigen Uptake, Presentation, and T Cell Activation. Front Immunol 11, 1393

Kambayashi T, Laufer TM (2014): Atypical MHC class II-expressing antigen-presenting cells: can anything replace a dendritic cell? Nat Rev Immunol 14, 719-730

Kaneko K, Sato DK, Nakashima I, Ogawa R, Akaishi T, Takai Y, Nishiyama S, Takahashi T, Misu T, Kuroda H, et al. (2018): CSF cytokine profile in MOG-IgG+ neurological disease is similar to AQP4-IgG+ NMOSD but distinct from MS: a cross-sectional study and potential therapeutic implications. J Neurol Neurosurg Psychiatry 89, 927-936

Kapingidza AB, Kowal K, Chruszcz M (2020): Antigen-Antibody Complexes. Subcell Biochem 94, 465-497

Kasinrerk W, Baumruker T, Majdic O, Knapp W, Stockinger H (1993): CD1 molecule expression on human monocytes induced by granulocyte-macrophage colony-stimulating factor. J Immunol 150, 579-584

Kinzel S, Lehmann-Horn K, Torke S, Hausler D, Winkler A, Stadelmann C, Payne N, Feldmann L, Saiz A, Reindl M, et al. (2016): Myelin-reactive antibodies initiate T cell-mediated CNS autoimmune disease by opsonization of endogenous antigen. Acta Neuropathol 132, 43-58

Koprulu AD, Ellmeier W (2009): The role of Tec family kinases in mononuclear phagocytes. Crit Rev Immunol 29, 317-333

Kroepfl JF, Viise LR, Charron AJ, Linington C, Gardinier MV (1996): Investigation of myelin/oligodendrocyte glycoprotein membrane topology. J Neurochem 67, 2219-2222

Kuhlmann T, Ludwin S, Prat A, Antel J, Bruck W, Lassmann H (2017): An updated histological classification system for multiple sclerosis lesions. Acta Neuropathol 133, 13-24

Laemmli UK (1970): Cleavage of structural proteins during the assembly of the head of bacteriophage T4. Nature 227, 680-685

Lassmann H (2018): Multiple Sclerosis Pathology. Cold Spring Harb Perspect Med 8

Lehmann CHK, Baranska A, Heidkamp GF, Heger L, Neubert K, Luhr JJ, Hoffmann A, Reimer KC, Bruckner C, Beck S, et al. (2017): DC subset-specific induction of T cell responses upon antigen uptake via Fcgamma receptors in vivo. J Exp Med 214, 1509-1528

Lennon VA, Kryzer TJ, Pittock SJ, Verkman AS, Hinson SR (2005): IgG marker of optic-spinal multiple sclerosis binds to the aquaporin-4 water channel. J Exp Med 202, 473-477

Lennon VA, Wingerchuk DM, Kryzer TJ, Pittock SJ, Lucchinetti CF, Fujihara K, Nakashima I, Weinshenker BG (2004): A serum autoantibody marker of neuromyelitis optica: distinction from multiple sclerosis. Lancet 364, 2106-2112

Liu Y, Wu Y, Lam KT, Lee PP, Tu W, Lau YL (2012): Dendritic and T cell response to influenza is normal in the patients with X-linked agammaglobulinemia. J Clin Immunol 32, 421-429

Lopez-Herrera G, Vargas-Hernandez A, Gonzalez-Serrano ME, Berron-Ruiz L, Rodriguez-Alba JC, Espinosa-Rosales F, Santos-Argumedo L (2014): Bruton's tyrosine kinase--an integral protein of B cell development that also has an essential role in the innate immune system. J Leukoc Biol 95, 243-250

Louveau A, Smirnov I, Keyes TJ, Eccles JD, Rouhani SJ, Peske JD, Derecki NC, Castle D, Mandell JW, Lee KS, et al. (2015): Structural and functional features of central nervous system lymphatic vessels. Nature 523, 337-341

Lublin FD, Reingold SC, Cohen JA, Cutter GR, Sorensen PS, Thompson AJ, Wolinsky JS, Balcer LJ, Banwell B, Barkhof F, et al. (2014): Defining the clinical course of multiple sclerosis: the 2013 revisions. Neurology 83, 278-286

Lucchinetti C, Bruck W, Parisi J, Scheithauer B, Rodriguez M, Lassmann H (2000): Heterogeneity of multiple sclerosis lesions: implications for the pathogenesis of demyelination. Ann Neurol 47, 707-717

Macrini C, Gerhards R, Winklmeier S, Bergmann L, Mader S, Spadaro M, Vural A, Smolle M, Hohlfeld R, Kumpfel T, et al. (2021): Features of MOG required for recognition by patients with MOG antibody-associated disorders. Brain 144, 2375-2389

Marignier R, Hacohen Y, Cobo-Calvo A, Pröbstel A-K, Aktas O, Alexopoulos H, Amato M-P, Asgari N, Banwell B, Bennett J, et al. (2021): Myelin-oligodendrocyte glycoprotein antibody-associated disease. The Lancet Neurology 20, 762-772

Matiello M, Schaefer-Klein J, Sun D, Weinshenker BG (2013): Aquaporin 4 expression and tissue susceptibility to neuromyelitis optica. JAMA Neurol 70, 1118-1125

Matsuya N, Komori M, Nomura K, Nakane S, Fukudome T, Goto H, Shiraishi H, Wandinger KP, Matsuo H, Kondo T (2011): Increased T-cell immunity against aquaporin-4 and proteolipid protein in neuromyelitis optica. Int Immunol 23, 565-573

Montalban X, Arnold DL, Weber MS, Staikov I, Piasecka-Stryczynska K, Willmer J, Martin EC, Dangond F, Syed S, Wolinsky JS, et al. (2019): Placebo-Controlled Trial of an Oral BTK Inhibitor in Multiple Sclerosis. N Engl J Med 380, 2406-2417

Morrow MJ, Wingerchuk D (2012): Neuromyelitis optica. J Neuroophthalmol 32, 154-166

Murphy K: Janeway's Immunobiology 8th Edition; Garland Science 2012

Neys SFH, Hendriks RW, Corneth OBJ (2021): Targeting Bruton's Tyrosine Kinase in Inflammatory and Autoimmune Pathologies. Front Cell Dev Biol 9, 668131

Ni Gabhann J, Hams E, Smith S, Wynne C, Byrne JC, Brennan K, Spence S, Kissenpfennig A, Johnston JA, Fallon PG, et al. (2014): Btk regulates macrophage polarization in response to lipopolysaccharide. PLoS One 9, e85834

Obermeier B, Mentele R, Malotka J, Kellermann J, Kumpfel T, Wekerle H, Lottspeich F, Hohlfeld R, Dornmair K (2008): Matching of oligoclonal immunoglobulin transcriptomes and proteomes of cerebrospinal fluid in multiple sclerosis. Nat Med 14, 688-693

Papadopoulos MC, Verkman AS (2012): Aquaporin 4 and neuromyelitis optica. Lancet Neurol 11, 535-544

Park JK, Byun JY, Park JA, Kim YY, Lee YJ, Oh JI, Jang SY, Kim YH, Song YW, Son J, et al. (2016): HM71224, a novel Bruton's tyrosine kinase inhibitor, suppresses B cell and monocyte activation and ameliorates arthritis in a mouse model: a potential drug for rheumatoid arthritis. Arthritis Res Ther 18, 91

Paulsen M, Janssen O (2011): Pro- and anti-apoptotic CD95 signaling in T cells. Cell Commun Signal 9, 7

Pellerin K, Rubino SJ, Burns JC, Smith BA, McCarl CA, Zhu J, Jandreski L, Cullen P, Carlile TM, Li A, et al. (2021): MOG autoantibodies trigger a tightly-controlled FcR and BTK-driven microglia proliferative response. Brain 144, 2361-2374

Peschl P, Bradl M, Hoftberger R, Berger T, Reindl M (2017a): Myelin Oligodendrocyte Glycoprotein: Deciphering a Target in Inflammatory Demyelinating Diseases. Front Immunol 8, 529

Peschl P, Schanda K, Zeka B, Given K, Bohm D, Ruprecht K, Saiz A, Lutterotti A, Rostasy K, Hoftberger R, et al. (2017b): Human antibodies against the myelin oligodendrocyte glycoprotein can cause complement-dependent demyelination. J Neuroinflammation 14, 208

Phuan PW, Ratelade J, Rossi A, Tradtrantip L, Verkman AS (2012): Complement-dependent cytotoxicity in neuromyelitis optica requires aquaporin-4 protein assembly in orthogonal arrays. J Biol Chem 287, 13829-13839

Piasecka-Stryczynska K, Rejdak K, Dyroff M, Hyvert Y, Holmberg K, Mandel M, Cunha C, Mitchell D, Martin E, Montalban X (2021): Concentration of evobrutinib, a BTK inhibitor, in cerebrospinal fluid during treatment of patients with relapsing multiple sclerosis in a phase 2 study. Multiple Sclerosis and Related Disorders 51

Purvis GSD, Aranda-Tavio H, Channon KM, Greaves DR (2021): Bruton's TK regulates myeloid cell recruitment during acute inflammation. Br J Pharmacol

Reich DS, Arnold DL, Vermersch P, Bar-Or A, Fox RJ, Matta A, Turner T, Wallstrom E, Zhang X, Mares M, et al. (2021): Safety and efficacy of tolebrutinib, an oral brain-penetrant BTK inhibitor, in relapsing multiple sclerosis: a phase 2b, randomised, double-blind, placebo-controlled trial. Lancet Neurol 20, 729-738

Ren L, Campbell A, Fang H, Gautam S, Elavazhagan S, Fatehchand K, Mehta P, Stiff A, Reader BF, Mo X, et al. (2016): Analysis of the Effects of the Bruton's tyrosine kinase (Btk) Inhibitor Ibrutinib on Monocyte Fcgamma Receptor (FcgammaR) Function. J Biol Chem 291, 3043-3052

Roesner S, Appel R, Gbadamosi J, Martin R, Heesen C (2012): Treatment of steroid-unresponsive optic neuritis with plasma exchange. Acta Neurol Scand 126, 103-108

Sallusto F, Lanzavecchia A (1994): Efficient presentation of soluble antigen by cultured human dendritic cells is maintained by granulocyte/macrophage colony-stimulating factor plus interleukin 4 and downregulated by tumor necrosis factor alpha. J Exp Med 179, 1109-1118

Sato DK, Callegaro D, Lana-Peixoto MA, Waters PJ, de Haidar Jorge FM, Takahashi T, Nakashima I, Apostolos-Pereira SL, Talim N, Simm RF, et al. (2014): Distinction between MOG antibody-positive and AQP4 antibody-positive NMO spectrum disorders. Neurology 82, 474-481

Schmidt NW, Thieu VT, Mann BA, Ahyi AN, Kaplan MH (2006): Bruton's tyrosine kinase is required for TLR-induced IL-10 production. J Immunol 177, 7203-7210

Schroeder HW, Jr., Cavacini L (2010): Structure and function of immunoglobulins. J Allergy Clin Immunol 125, S41-52

Songthammawat T, Srisupa-Olan T, Siritho S, Kittisares K, Jitprapaikulsan J, Sathukitchai C, Prayoonwiwat N (2020): A pilot study comparing treatments for severe attacks of neuromyelitis optica spectrum disorders: Intravenous methylprednisolone (IVMP) with add-on plasma exchange (PLEX) versus simultaneous ivmp and PLEX. Mult Scler Relat Disord 38, 101506

Sospedra M, Martin R (2005): Immunology of multiple sclerosis. Annu Rev Immunol 23, 683-747

Spadaro M, Winklmeier S, Beltran E, Macrini C, Hoftberger R, Schuh E, Thaler FS, Gerdes LA, Laurent S, Gerhards R, et al. (2018): Pathogenicity of human antibodies against myelin oligodendrocyte glycoprotein. Ann Neurol 84, 315-328

Stadelmann C, Wegner C, Bruck W (2011): Inflammation, demyelination, and degeneration - recent insights from MS pathology. Biochim Biophys Acta 1812, 275-282

Steinman RM (1991): The dendritic cell system and its role in immunogenicity. Annu Rev Immunol 9, 271-296

te Velde AA, de Waal Malefijt R, Huijbens RJ, de Vries JE, Figdor CG (1992): IL-10 stimulates monocyte Fc gamma R surface expression and cytotoxic activity. Distinct regulation of antibody-dependent cellular cytotoxicity by IFN-gamma, IL-4, and IL-10. J Immunol 149, 4048-4052

Torke S, Weber MS (2020): Inhibition of Bruton s tyrosine kinase as a novel therapeutic approach in multiple sclerosis. Expert Opin Investig Drugs 29, 1143-1150

Torke S, Pretzsch R, Hausler D, Haselmayer P, Grenningloh R, Boschert U, Bruck W, Weber MS (2020): Inhibition of Bruton's tyrosine kinase interferes with pathogenic B-cell development in inflammatory CNS demyelinating disease. Acta Neuropathol 140, 535-548

Vaknin-Dembinsky A, Brill L, Kassis I, Petrou P, Ovadia H, Ben-Hur T, Abramsky O, Karussis D (2016): T-cell responses to distinct AQP4 peptides in patients with neuromyelitis optica (NMO). Mult Scler Relat Disord 6, 28-36

Vincent T, Saikali P, Cayrol R, Roth AD, Bar-Or A, Prat A, Antel JP (2008): Functional consequences of neuromyelitis optica-IgG astrocyte interactions on blood-brain barrier permeability and granulocyte recruitment. J Immunol 181, 5730-5737

von Budingen HC, Gulati M, Kuenzle S, Fischer K, Rupprecht TA, Goebels N (2010): Clonally expanded plasma cells in the cerebrospinal fluid of patients with central nervous system autoimmune demyelination produce "oligoclonal bands". J Neuroimmunol 218, 134-139

Walton C, King R, Rechtman L, Kaye W, Leray E, Marrie RA, Robertson N, La Rocca N, Uitdehaag B, van der Mei I, et al. (2020): Rising prevalence of multiple sclerosis worldwide: Insights from the Atlas of MS, third edition. Mult Scler 26, 1816-1821

Waters P, Fadda G, Woodhall M, O'Mahony J, Brown RA, Castro DA, Longoni G, Irani SR, Sun B, Yeh EA, et al. (2020): Serial Anti-Myelin Oligodendrocyte Glycoprotein Antibody Analyses and Outcomes in Children With Demyelinating Syndromes. JAMA Neurol 77, 82-93

Weber MS, Derfuss T, Metz I, Bruck W (2018): Defining distinct features of anti-MOG antibody associated central nervous system demyelination. Ther Adv Neurol Disord 11, 1756286418762083

Weber MS, Menge T, Lehmann-Horn K, Kronsbein HC, Zettl U, Sellner J, Hemmer B, Stuve O (2012): Current treatment strategies for multiple sclerosis - efficacy versus neurological adverse effects. Curr Pharm Des 18, 209-219

Weller RO, Engelhardt B, Phillips MJ (1996): Lymphocyte targeting of the central nervous system: a review of afferent and efferent CNS-immune pathways. Brain Pathol 6, 275-288

Wingerchuk DM, Lennon VA, Lucchinetti CF, Pittock SJ, Weinshenker BG (2007): The spectrum of neuromyelitis optica. Lancet Neurol 6, 805-815

Wingerchuk DM, Banwell B, Bennett JL, Cabre P, Carroll W, Chitnis T, de Seze J, Fujihara K, Greenberg B, Jacob A, et al. (2015): International consensus diagnostic criteria for neuromyelitis optica spectrum disorders. Neurology 85, 177-189

ACKNOWLEDGMENT

First and foremost, I would like to thank my supervisor Prof. Dr. Martin S. Weber for his continuous support and motivation. I am very grateful for the trust he put in me and his valuable advice, which substantially contributed to the successful outcome of this work.

Furthermore, I would like to thank my thesis committee members Prof. Dr. Holger Reichardt and Dr. Sebastian Kügler for the fruitful discussions and their supportive critique during the progress report meetings.

I would also like to express my gratitude to Prof. Dr. Christine Stadelmann-Nessler for giving me the opportunity to work on my PhD project in the Department of Neuropathology.

I am particularly thankful to Dr. Silke Häusser-Kinzel who supported me in all matters and problems regarding my experiments. Thank you very much for sharing your scientific expertise with me and proof-reading my thesis.

Moreover, I would like to thank Katja, Julian and Mira for providing excellent technical help and creating a nice and friendly atmosphere in the lab.

I am very grateful for the professional and emotional support from Adriane, Anastasia, Darius, Jacqueline, Jasmin, Leila, Sarah and Sebastian. I enjoyed the great time we spent together inside and outside the lab and their support kept me motivated even when the times were tough.

I would also like to thank Stefan, Jonas and all the other colleagues at the Department of Neuropathology for their help and the pleasant working atmosphere.

Special thanks to my wonderful family and friends for always believing in me and for their unconditional support. I would not have been able to overcome the challenges of my life without them.

Finally, I would like to thank Lukas for being at my side and for his endless patience and support.

LIST OF CONGRESS ABSTRACTS

Freier M., Häusser-Kinzel S., Weber M.S.

The role of peripheral autoreactive antibodies in initiation and propagation of central nervous system demyelinating disorders

8th Joint meeting of the European Committee for Treatment and Research in Multiple Sclerosis and Americas Committee for Treatment and Research in Multiple Sclerosis (MSVirtual 2020), September 11th – 13th 2020, Poster presentation

Freier M., Häusser-Kinzel S., Weber M.S.

The role of peripheral autoreactive antibodies in initiation and propagation of central nervous system demyelinating disorders

37th Congress of the European Committee for Treatment and Research in Multiple Sclerosis, October 13th – 15th 2021, Oral presentation

Freier M., Häusser-Kinzel S., Weber M.S.

Investigation of the opsonizing capacity of patient-derived anti-MOG antibodies

15th Congress of the International Society of Neuroimmunology, November 8th – 12th 2021, Oral presentation